TAILORED FORCE FIELDS FOR FLEXIBLE FABRICATION

A Dissertation
Presented to
The Academic Faculty

by

Sameh Sadarous Wanis

In Partial Fulfillment
of the Requirements for the Degree
Doctor of Philosophy in Aerospace Engineering

Georgia Institute of Technology
May 2006

TAILORED FORCE FIELDS FOR FLEXIBLE FABRICATION

Approved by:

Dr. Narayanan Komerath, Advisor
School of Aerospace Engineering
Georgia Institute of Technology

Dr. Andrew Peterson
School of Electrical & Computer Engineering
Georgia Institute of Technology

Dr. Erian Armanios
School of Aerospace Engineering
Georgia Institute of Technology

Dr. Sheila Thibeault
NASA Langley Research Center

Dr. Robert Braun
School of Aerospace Engineering
Georgia Institute of Technology

Date Approved: March 30, 2006

To my God and Savior Jesus Christ

And

His faithful servant Pope Shenouda III

“And you shall know the truth and the truth shall set you free”
John 8:32

ACKNOWLEDGEMENTS

I wish to thank my advisor Professor Komerath, whose leadership and guidance throughout my undergraduate and graduate years have been integral to my career and success at Georgia Tech. Professor Sankar and professor Armanios' support and advice throughout my years here are invaluable. I wish to thank all my friends that I have made over the last ten years that I spent in Atlanta. I thank Mina Zaki for his sacrifice of time and comfort to help me with last minute formatting problems and late-night discussions on a wide variety of subjects. I wish to thank Randy for his unwavering support and friendship all the years we spent as friends and roommates. I thank my family for their unconditional love and continued support without which I could not have completed this thesis. I finally would like to thank my Lord Jesus Christ for His love, grace, and sacrifice all of which are at the heart of my being.

TABLE OF CONTENTS

LIST OF TABLES

LIST OF FIGURES

NOMENCLATURE

A	Pressure Amplitude
a	Particle Radius
c	Sound (Light) Speed in Particle
c_o	Sound (Light) Speed in Host Medium
d	Separation Distance Between Two Particles
E	Electric Field
E_o	Electric Field Amplitude
ε_o	Permittivity of Free Space
ε	Dielectric Constant of Particle
f	Frequency
ϕ	Field Potential
j	$\sqrt{-1}$
k	Wave Number
$\vec{P}$	Dipole Moment
U	Potential energy
ρ	Density of Particle
ρ_o	Density of Host Fluid

SUMMARY

By their nature as waves, sound and electromagnetic fields carry energy and momentum with no net mass transport. These waves are used to create force fields which are proposed as a flexible fabrication tool. The fields are created within appropriate resonators such that standing waves are set up, whereby stable surfaces can be formed. The shape of the stable surfaces is tailored by exciting different resonant modes.

Acoustic experiments in the audible range showed that randomly placed particles within a resonant cavity formed stable surfaces. Straight and curved walls were created out of a wide variety of material types. The surface produced was always single-particle-thick irrespective of the size of the particles. The particles were observed to attract each other enabling continuous surfaces to be formed with gaps being filled. These interparticle forces were attributed to secondary scattering. The pressure field was predicted to first order using the solution to the 3D unforced Helmholtz equation with rigid boundary conditions. Pressure-sensitive-paint (PSP) was used to capture the actual pressure field across one of the chambers side walls. This was a first demonstration of porous PSP applied to acoustic fields. The inclusion of the second harmonic in the solution was found to give pressure field solutions that agreed better with the PSP data.

For the application of constructing large space structures long wavelength electromagnetic waves are sought as an alternative to acoustics since they are able to propagate through the vacuum of space. The theory of electromagnetic manipulation of nanoparticles using laser beams was found to be analogous to the theory of acoustic shaping. Alternating electric fields such as those in a microwave or radio wave were studied in the context of utilizing them to induce scattering and gradient forces on electrically-neutral particles. A neutral dielectric particle in the Rayleigh regime will

become polarized in response to the external electric field setup across it. In the electrostatic limit, i.e. Rayleigh regime, this polarization causes the particle to appear as an electric dipole. The well known field radiated by a dipole is used to model the behavior of particles in a standing electromagnetic wave field. The forces onto a particle in response to the imposed external field are called primary forces. Secondary forces arise from the interaction of the particles with each other and results in regions of attraction and repulsion. Both primary and secondary forces are found to be analogous to the forces in acoustics. The analogy between acoustics and electromagnetics is found to be through the force expressions dependency on wavelength; scattering particle radius; separation distance; energy density of the field; impedance mismatch with the host medium; and field intensity. Experiments on secondary forces in acoustic resonators, single particles in microwave resonators, and chain formation using neutral cells at the micro-scale, all validate the generalized formulation and understanding of force field tailoring.

The acoustics-electromagnetics analogy permits conceptual design of an architecture to build the first large-scale space stations large enough to shield occupants against space radiation for long-term habitation. The surface formation process in electromagnetics is found to be different from that in acoustics in the secondary force behavior. While walls can be formed in acoustics in one mode, chains are formed in electromagnetic resonant modes. These chains would then be assembled together to form complete walls by exciting another orthogonal mode.

CHAPTER 1

INTRODUCTION

1.1 Background

To build massive structures in the depths of outer space, or to build nanostructures in the microscopic world, the ideal manufacturing architecture would be one where objects of many shapes can be built with the same tooling; the construction is performed by non-contact means; and the process can be performed automatically. In this thesis, a way to generate and adjust force fields generated by acoustic and electromagnetic waves to accomplish such construction is proposed and studied. Tailored force fields (TFF) is a flexible, non-contact construction technique suitable for microgravity environments. The possible applications of TFF span a wide range of sizes, material properties and types of force fields. A unification of these areas is sought through a generalization of the various theories provided in the literature applicable for each area. Once unified, experiments performed in one field can be used to predict behavior in another.

Many people are familiar with the idea that light absorbed by or reflected off a surface exerts a unidirectional force on the surface, attributed to “radiation pressure.” Many other types of wave motion also exhibit this phenomenon. Surface waves on a liquid, transverse wave on an elastic string (Meyer 1972), electromagnetic waves, and sound waves all exert some sort of radiation force on targets in their path (Torr 1984). Indeed, the phenomenon goes much beyond unidirectional force.

A force field is defined as a region where the force on a target object varies with position only. This implies that the force field is conservative. Examples include inviscid flow fields, gravitational fields, and electrostatic fields. In this thesis, attention is focused on acoustic and electromagnetic wave fields, and how to use them to create force fields.

The ease of confining and controlling both field types is the factor that makes these attractive for construction and manufacturing.

The magnitude of the forces produced in these types of force fields is relatively small compared to those in conventional fabrication tools involving mechanical contact, used in normal earth-surface gravity (1-G) environments. However, there are two regimes where gravity is not a significant factor. The first is in orbits in space, away from massive celestial objects. Here the primary gravitational force is cancelled out, and "jitter" due to intermittent passage near gravity centers is extremely small. In such an environment, even a small sustained acceleration, on the order of one-millionth of earth gravity, is adequate to move objects slowly into stable locations. The other regime is the micro-world, where objects and distances are so small that local forces can exceed gravity by several orders of magnitude.

Focused beams are used in several applications to manipulate individual particles. However, another way to generate strong forces is to use a resonator, where the steady-state input wave amplitude is much smaller than the amplitude of the waves inside the resonator. In resonators, the forces generated can typically be 3 to 5 orders of magnitude above that of the input wave, and the "stiffness" of the stable locations can be 7 orders of magnitude above that created in a single beam.

Chapter 2 discusses evidence showing acoustic radiation pressure used to shape various geometry surfaces. Chapters 2 - 4 discuss sound induced forces. Chapter 5 addresses electromagnetic force fields. Chapter 6 demonstrates the strong analogy between acoustic and electromagnetic force fields and the hypothesis that generalized equations for the forces can describe both types of force fields. These relations are derived from the fundamental principles of both sound and electromagnetic fields. This stage lays the necessary groundwork for a conceptual space based construction test case that is briefly explained in chapter 7. The primary contribution of

this work is a unified treatment, and application, of radiation pressure in acoustic and electromagnetic force fields.

1.2 Tailored Force Field Development

This section is a summary of the development of TFF. Since it was already known that ultrasonic waves are capable of producing forces on a *single* target that scatters the sound field, evidence was sought on the behavior of a *multitude* of particles. This process was carried out using conventional and inexpensive drivers to extend the acoustic wavelength to audible frequencies. Compression drivers used in police vehicle sirens were selected and a simple rectangular acoustic resonator was built. The concept was then tested in reduced gravity flight tests, and low-density material in spherical granular form was used as the target to be shaped. As a standing wave was set up inside the resonator, the material relocated in an orderly fashion, forming a wall. Several pressure distributions (modes) were tested, and the resulting wall shapes were captured on videotape. Ground experiments confirmed that the wall geometry matched pressure contours of the predicted pressure field distribution. This initial set of experiments and preliminary pressure predictions was concluded by succeeding to use only acoustic forces in a resonator to form a few desired shapes.

The next phase of the research project identified the analogy between acoustic and electromagnetic fields. The basic knowledge in the optical frequency range, in the area of “laser tweezers” for manipulation of micro to nanometer sized objects, allowed extension of the concept to frequencies in the microwave and radio frequency range. Studies of the interaction of electromagnetic waves with dielectric material permitted wavelengths to be extended. Within the Rayleigh scattering regime, the expressions for acoustic and electromagnetic forces on matter were found to be similar through their

dependency on wavelength; scattering particle radius; energy density of the field; impedance mismatch with the host medium; and field intensity.

In the next phase these hypotheses were validated. An identification of all the forces involved in the proof-of-concept acoustic experiments is presented. This is done through several experiments to correlate each observed behavior to forces described in the literature.

The formation of walls is not fully explained by the behavior of isolated particles in a force field. Predictions of the forces due to interaction of two particles in an acoustic resonator indicate that a simple dipole model explains wall formation. Experiments in the acoustic resonator validate this concept, and rule out other nonlinear phenomena that are unique to the acoustic field. Simulations of the field of around dielectric particles in an electromagnetic field show that a similar model applies in electromagnetic fields.

1.3 Relevance to Space Construction

To engineer a space-based construction facility based on the TFF, a unified view of acoustic and electromagnetic force fields is established. Though it is but one application of such force fields, in order to maintain focus, space based construction is used to drive the thesis. The development roadmap is illustrated in the schematic below.

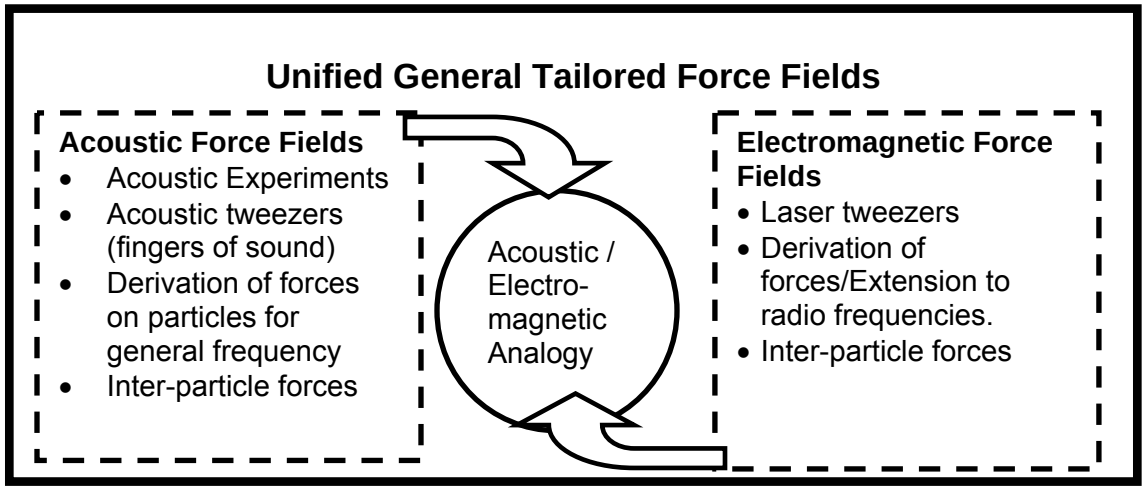

CHAPTER 2

PROOF-OF-CONCEPT STUDY

In 1997 NASA Johnson Space Center announced an opportunity for exploratory experiments in reduced gravity using their KC-135 aircraft. This unique opportunity is what jump-started this investigation and explains why the flight experiments precede much of the detailed theoretical, experimental, and numerical studies of the concept.

The purpose of this chapter is to demonstrate the feasibility of the TFF concept. It contains the genesis of the project which was mainly qualitative experiments that ranged from ground to microgravity tests. The results are shown and followed by simple field calculations that were done in order to understand the basics of the force field. The next two chapters work on refining the prediction capability as knowledge of particle behavior in force fields matured.

2.1 Brief literature review on acoustic levitation and positioning

A brief survey of the literature surrounding acoustic levitation and positioning is presented here. A more thorough literature review on general acoustic forces is provided in Chapter 3. Levitation in the 1-g environment requires powerful acoustic sources placed along the vertical axis, usually in opposition or in a source/reflector configuration. With sufficiently high sound levels, forces induced on particles, including steel spheres in a 183-dB ultrasonic levitator, go towards the nodes (Whymark 1975). The speakers and reflector surfaces were tailored to ensure that there is only one stable point of minimum acoustic force potential for the particle to occupy.

The Patent literature to-date appears to focus on levitation of one or a few particles, and their accurate positioning and manipulation using intense sound fields. Oran et al (1980) described a method and apparatus for shaping and enhancing

acoustical levitation forces in a single-axis acoustic resonance system. They used specially-shaped drivers and reflectors to enhance the levitation force and to better contain fluid substances by means of field shaping. Rey (1981) described multiple reflectors to manipulate and combine levitated materials. Phase variation between two opposed speakers has been used to move levitated particles inside the chamber. Lee (1983) described a system of transducers which propagate acoustic waves along three dimensions of a rectangular chamber to levitate objects and precisely control their rotation. The chamber dimensions are all different to avoid mode degeneracy. Barmatz (1983) described stable levitation of a small object using the convergent field generated from a single acoustic source using a small reflector. The reflector can be located about one-half wavelength from the focal length and can be concavely curved to a radius of about one-half the wavelength to stably support an object one-quarter wavelength away from the reflector. Applications include processes which coat or heat the levitated object(s).

Barmatz et al (1985) described levitation of an object in a sealed chamber with standing waves created by wall vibration, to avoid contamination. They also described a system (Barmatz 1988) that would acoustically levitate an object in a resonant chamber by applying a single frequency from a transducer. The angled walls of the chamber converged above the object. When a standing wave pattern was applied to the top and bottom of the chamber, a curved levitation surface was formed with the lowermost portion near the vertical axis of the cylinder. This employed the force of gravity to keep the object in position and away from the side walls. The authors (Barmatz 1988) described smooth movement of a levitated object and suppression of unwanted modes. A plunger at one end of the chamber moved to change the applied frequency.

Barmatz et al (1990) described rapidly damping oscillations of acoustically levitated objects using acoustic energy at a frequency slightly less than the center

resonant frequency. The restoring force constant of the levitation force is proportional to the square of the oscillation frequency of the object. Danley et al (1989) described horn loading for improved efficiency and thermal protection of a levitation sound source to improve efficiency and protect the source from heat. Ohkawa (1994) described controlling the location and concentration of constituents inside a plasma chamber. A neutral or plasma sound wave with at least a second harmonic component was used. The drift velocity imposed on contaminant particles by Oseen forces moves them away from the work surface being processed by the plasma. This drift velocity vector is controlled by the harmonic content, intensity and phase of the neutral or plasma sound wave. Leung et al (1994) described containerless microgravity processing involving plasma heating of a levitated sample. Goforth et al (1995) described removal of particulates from high temperature industrial exhaust gases using the Oseen forces from an acoustic waveform having a second harmonic content and the appropriate second harmonic phase shift. Guign et al (1996) described a system to position an object using multiple beams of acoustic energy. The wavelength for the acoustic energy in each beam is preferably much less than one-tenth the diameter of the object levitated. This enables efficient momentum transfer of energy to the object.

2.2 Preliminary calculations

Prior to performing any tests basic predictions of the expected outcomes were sought to aid in experiment design. The goal was to test the feasibility of using sound waves to controllably manipulate and position particles in 3 dimensions and then change the shape formed by externally changing the source frequency. The sound field was produced in a rectangular resonator using a low power source where the frequencies used correspond to eigenvalues of the cavity. This meant that standing waves could be varied in 1, 2, or 3 dimensions. The sound field is governed by the wave equation in the

linear approximation. For standing waves, the field is described by the Helmholtz equation for the pressure field, for which solution techniques are well-known and solution surfaces can be easily determined and tailored (Wanis 1998). The boundary conditions specify zero particle velocity, i.e. zero normal derivative of pressure at the wall. The Eigenvalue problem is as follows:

$$p = \psi(\boldsymbol{x}, n) \cdot e^{-i\omega(n)t} \tag{1}$$

where $\psi(\boldsymbol{x},n)$ is the Eigenfunction which satisfies the Helmholtz equation and Neumann boundary conditions given by,

$$\left[\nabla^2 + k^2(n)\right] \cdot \psi(\boldsymbol{x}, n) = 0 \tag{2}$$

$$\nabla \psi(\boldsymbol{x}, n) \cdot n_{out} = 0\,. \tag{3}$$

Using separation of variables we obtain,

$$\psi(\boldsymbol{x}) = X(x)Y(y)Z(z), \tag{4}$$

which yields three linear ordinary differential equations, one for each spatial dimension,

$$X'' + k_x^2 X = 0 \qquad Y'' + k_y^2 Y = 0 \qquad Z'' + k_z^2 Z = 0\,, \tag{5}$$

where the separation constants are related to each other and to the wavenumber k by

$$k_x^2 + k_y^2 + k_z^2 = k^2 \tag{6}$$

After imposing the boundary conditions, we obtain the Eigenfunction solution

$$\psi(x, y, z, n) = A\cos\left(\frac{m\pi x}{L_x}\right)\cos\left(\frac{n\pi x}{L_y}\right)\cos\left(\frac{o\pi x}{L_z}\right) \tag{7}$$

where L_x, L_y, L_z are the dimensions of the cavity and (m, n, o) are the normal mode quantum numbers. Each quantum number designates the number of pressure nodes along its respective direction. For example mode (1, 2, 0) has 1 node in x, 2 in y, and none in z. The Eigenvalues can now be given by

$$k^2 = \pi^2\left[\left(\frac{m}{L_x}\right)^2 + \left(\frac{n}{L_y}\right)^2 + \left(\frac{o}{L_z}\right)^2\right]. \tag{8}$$

The above set of equations assume linear sound waves, perfectly rigid and lossless walls, and no forcing. Despite being an approximation, this turned out to be fairly good for a first order approximation of the pressure field. At this stage of the project only a qualitative understanding of the field was needed. A more refined analysis is discussed in Chapter 4.

2.2.1 Acoustic field in cavity

The focus of this thesis is on manipulating small particles along larger surfaces of interest. The shape of the surface is controlled by changing the source frequency to excite another chamber mode frequency. This excites the corresponding resonant normal mode of the chamber and thus the shape formed is a direct consequence of the mode geometry, i.e. it forms in response to the shape of the acoustic pressure distribution specific to the cavity and frequency. For simplicity, a rectangular cavity was chosen with no equal sides to avoid degenerate modes (i.e. more than one mode having the same frequency). Most of the material tested had impedance far separated from that of the host medium (air) and was regarded as, essentially, rigid. As will be described later in Chapter 3, this results in a force field that drives the particles towards the nodal surfaces.

Cylindrical cavities have also been explored but to a lesser extent. Rectangular resonators allow for sinusoidal dependence of the pressure field, whereas for cylindrical and spherical cavities the equations governing the pressure field are the Bessel and spherical Bessel functions of the first kind, respectively. Figure 1 shows the pressure, potential energy, and the force produced in a cylindrical cavity. Only radial variation in pressure is shown since the axial variation is sinusoidal. It is clear from Figure 1 that the force trap is not symmetrical due to the nature of the Bessel functions, and is thus not as stable as those found in the rectangular geometries (Figure 2-4).

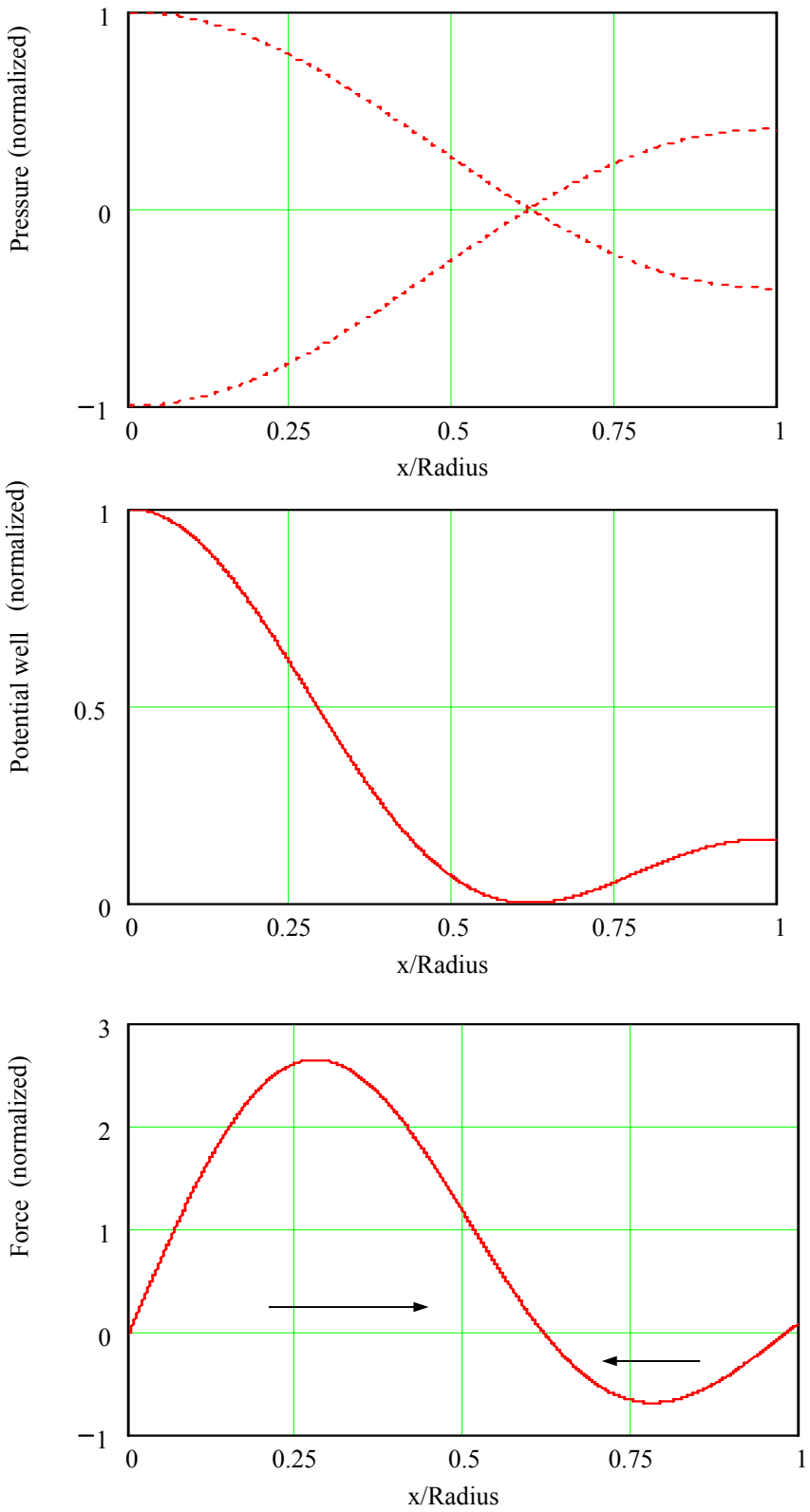

Figure 1 (Top) Radial pressure field in a cylinder due to a Bessel function of the first kind of order 0; (middle) radial potential well setup by the field; and (bottom) radial force generated on particles in the cavity.

The pressure field in a rectangular cavity provides a clue as to where the particle should collect. For a one dimensional wave, the field can be described by Equation 7 with y and z set to zero, from which the potential can be calculated and then the force profile obtained by taking the negative derivative of that potential. This dictates the location where the particles collect.

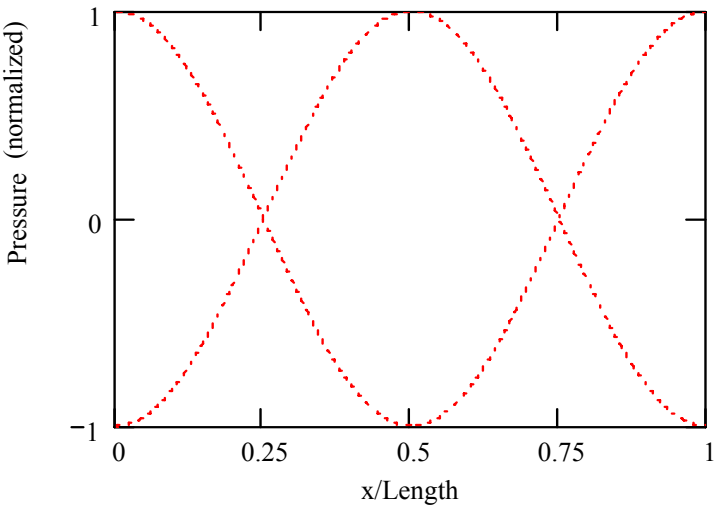

Figure 2 1D Pressure distribution for a standing wave. The spatial dimension corresponds to a full cycle and therefore has 2 pressure nodes spaced one-half wavelength apart. Shown is both the instant where the pressure distribution is at a maximum, and the field 180^{o} later in time.

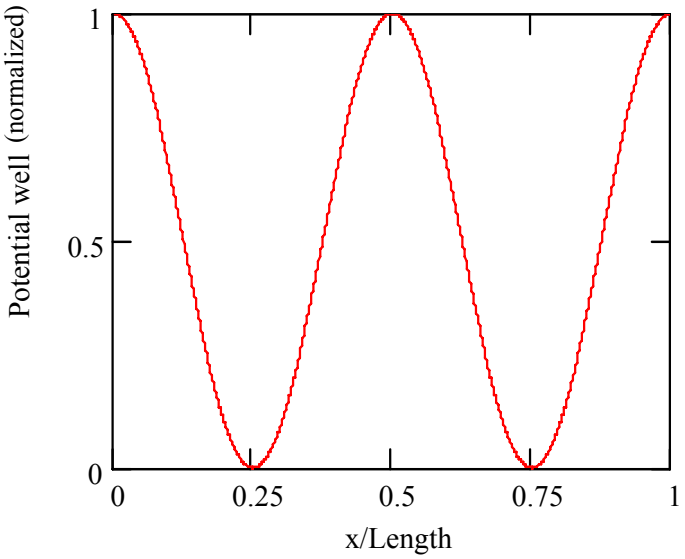

Figure 3 Force potential setup due to alternating pressure field above. Regions of minimum potential correspond to stable pressure nodes.

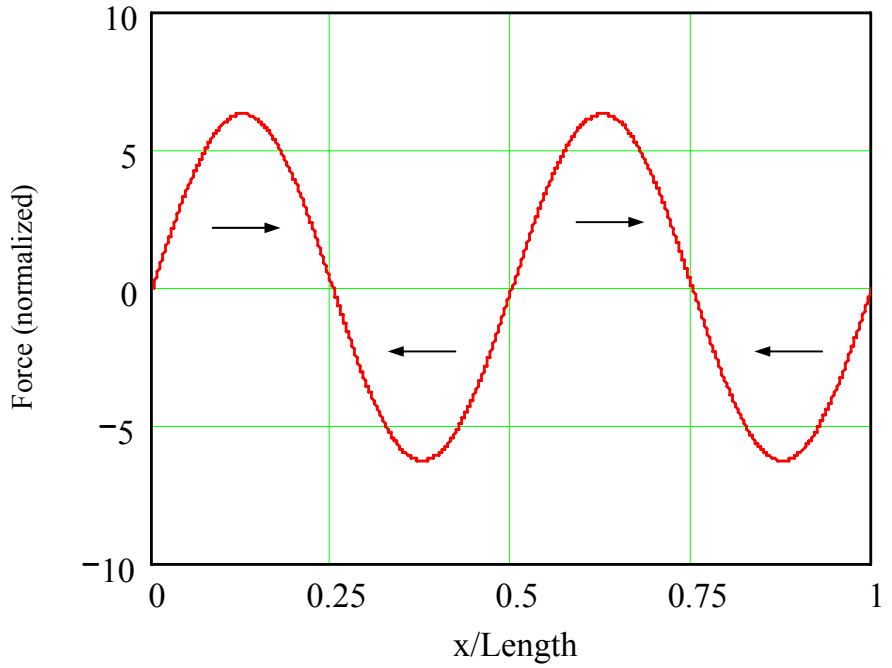

Figure 4 Force profile showing particles of higher characteristic impedance than host medium collect at stable regions that correspond to pressure nodes. Arrows show direction of force on particles.

2.2.2 Simulation of Surface Formation

Initially, a simulation tool was developed in MATLAB to predict the pressure field in the chamber due to the resonant acoustic field. The pressure field was calculated according to Equation 7. Since this is a solution to the Helmholtz equation for a 3D rectangular cavity with perfectly reflecting walls and no source, it is considered to be the ideal pressure field solution. The code is set such that the user inputs the mode number (m,n,o) and the normalized pressure field is calculated. An example ideal pressure field is shown in Figures 5-7 corresponding to modes (1,0,0), (1,1,0) and (2,2,0).

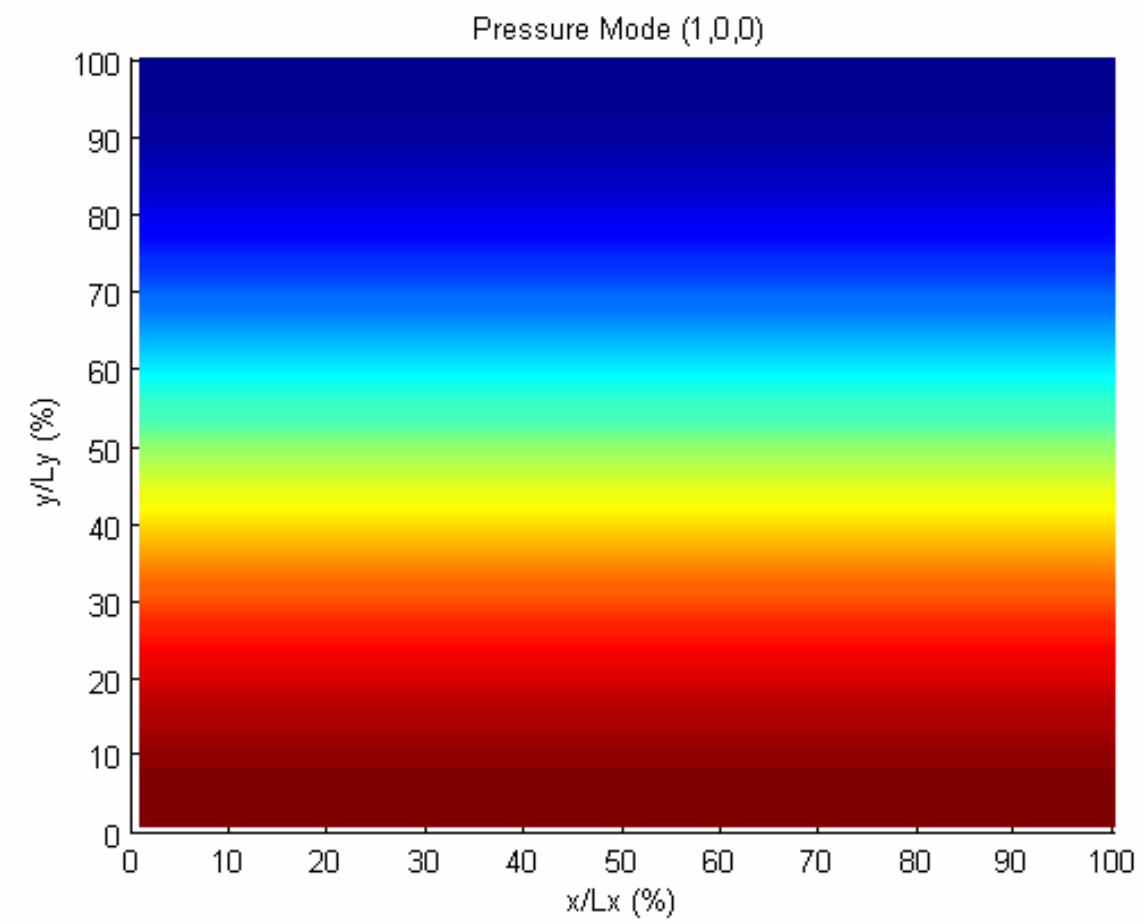

Figure 5 Pressure field for mode (1,0,0)

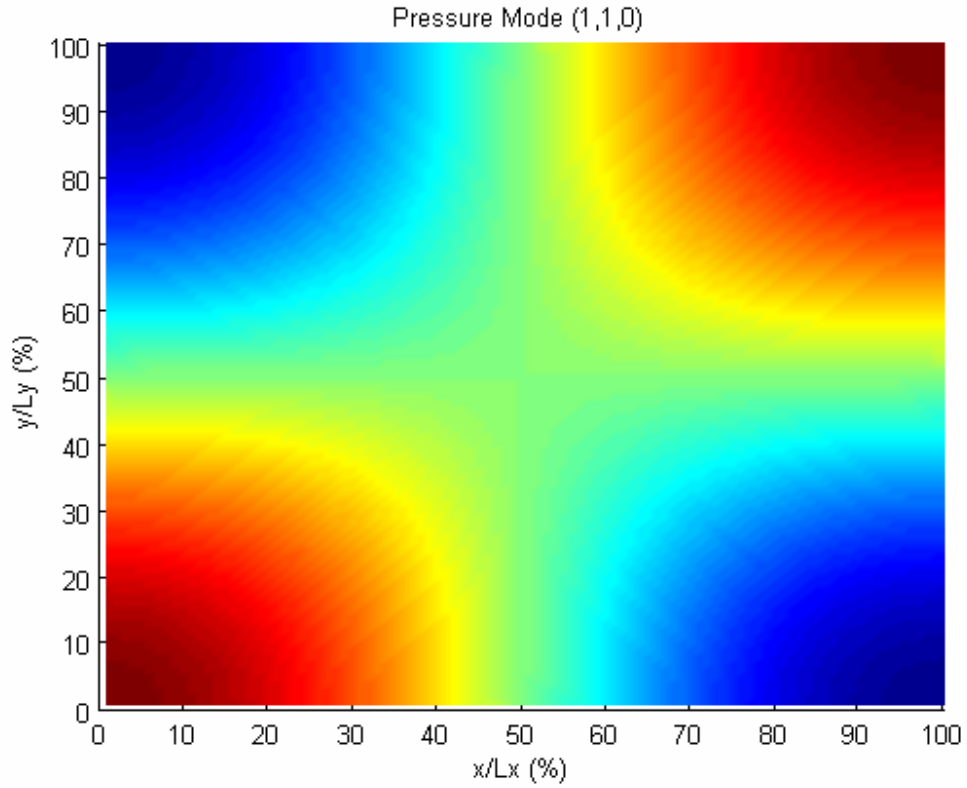

Figure 6 Pressure field for mode (1,1,0)

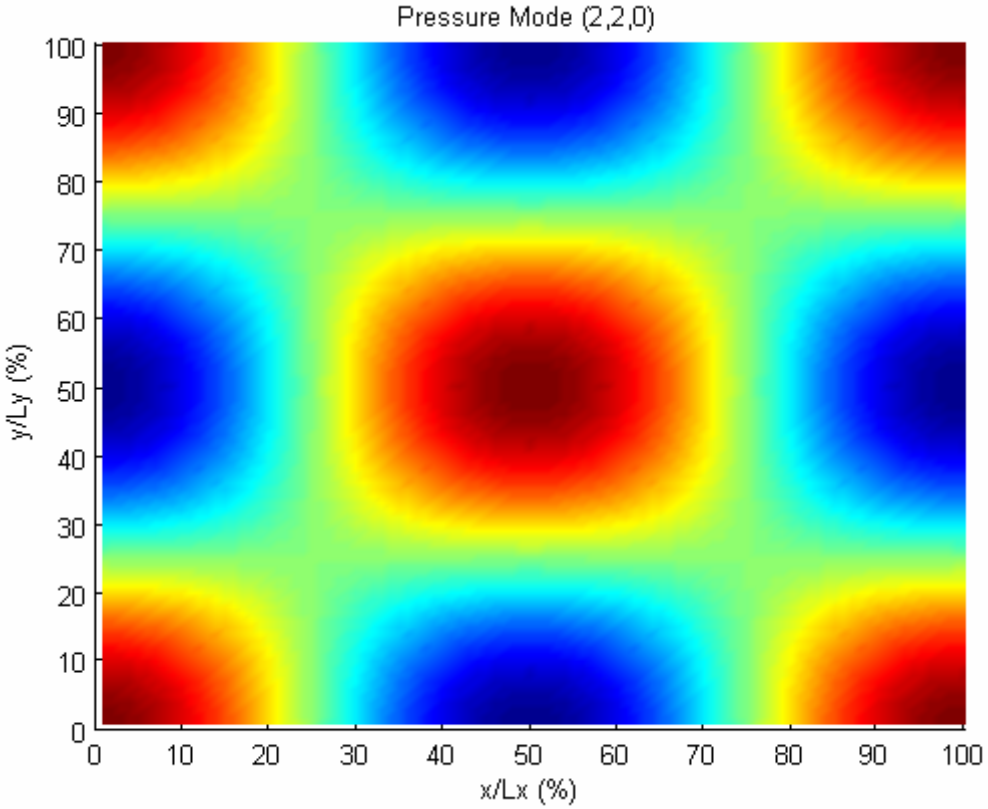

Figure 7 Pressure field for mode (2,2,0)

Even though physical experiments have not been performed with combining modes, it is anticipated that it may be a valid option since these normal modes are a result of orthogonal set of equations (Eigenfunctions) and should not interfere with each other. Moreover, a sound source such as a speaker is capable of emitting more than one frequency concurrently. A few plots showing the pressure field for combined modes are shown below.

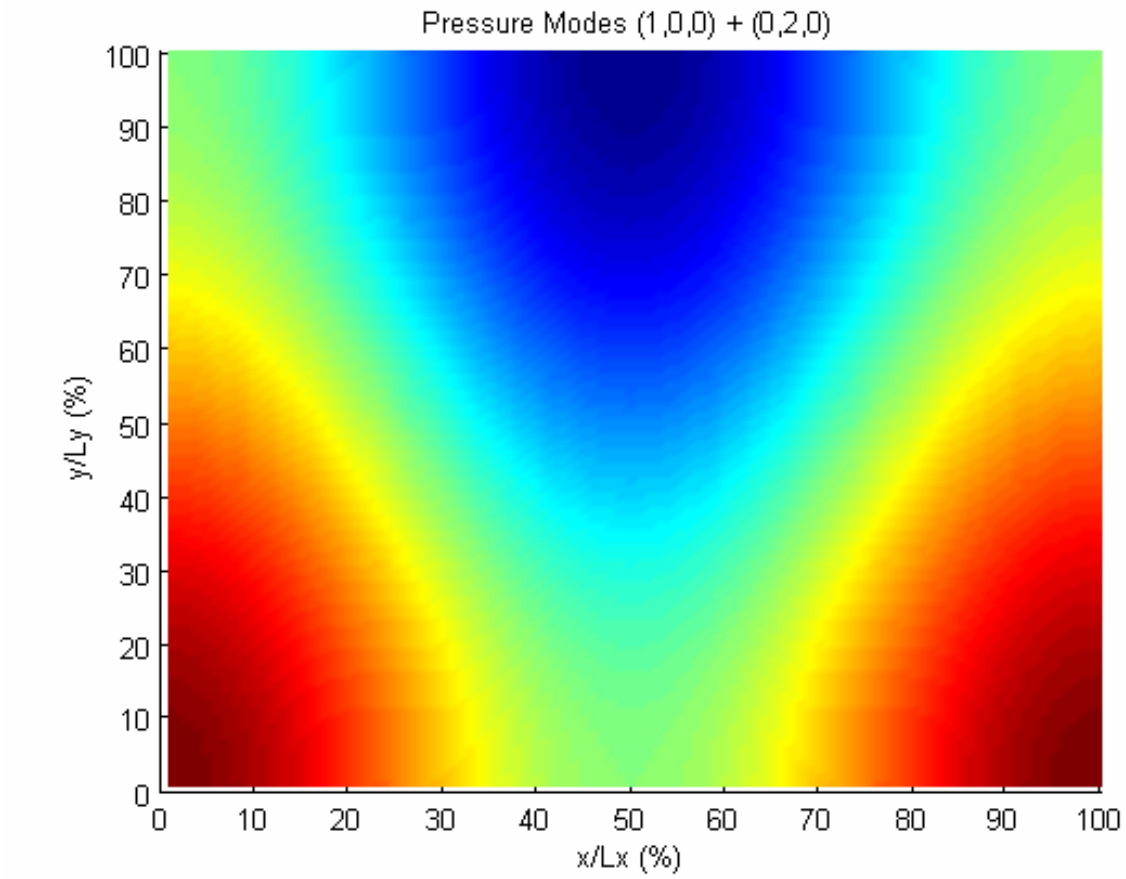

Figure 8 Pressure field for superimposed modes (1,0,0) and (0,2,0)

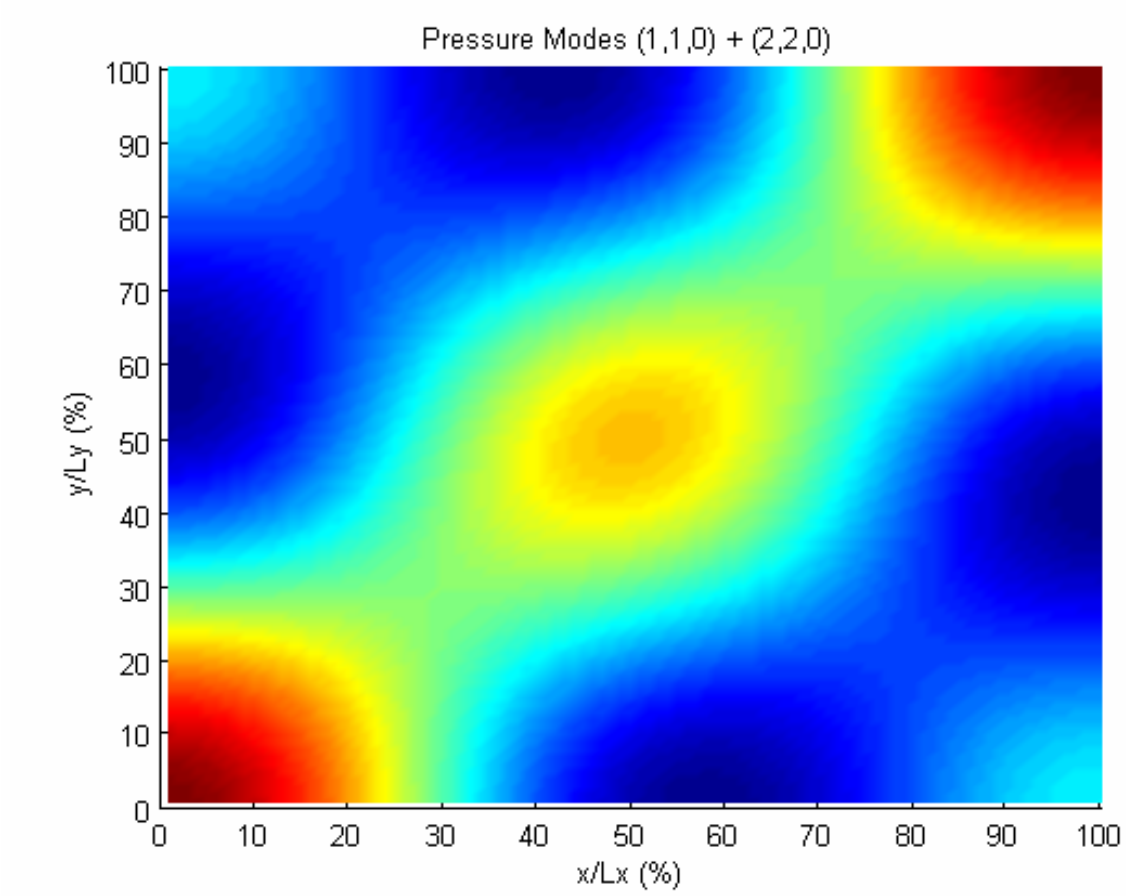

Figure 9 Pressure field for superimposed modes (1,1,0) and (2,2,0)

A few potential energy (proportional to pressure squared) distributions for select modes have been plotted below to aid in visualizing the results in the next section where we discuss predictions of wall formation.

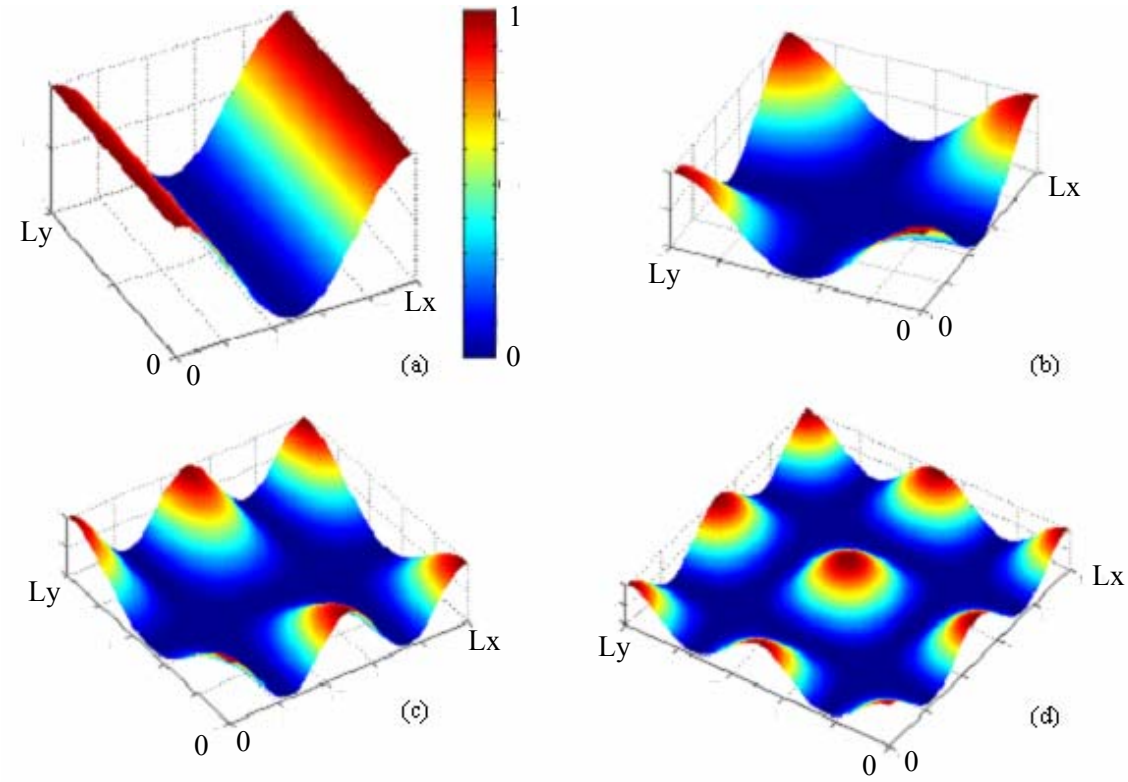

Figure 10 Force-potential field distributions for modes: (a) 1 0 0, (b) 1 1 0, (c) 2 1 0, (d) 2 2 0. Blue regions correspond to minimum potential. Plots produced in MATLAB.

2.3 Microgravity Experiments

The purpose of these experiments was to investigate the possibility of using sound induced forces to form thin sheets of specified shape from a collection of randomly configured particles. The microgravity experiments were aimed at testing the hypothesis of TFF by answering the following questions:

(a) Will a large number of particles arrange themselves evenly along a force equilibrium surface, adjusting position to fill gaps in between themselves, or would the clump together at the global minimum of the

potential field? How does the final surface formed correlate with the predicted pressure field?

(b) Whether particles, especially non-spherical, will experience any spin during the formation process?

(c) How much does the wall formation affect the empty cavity field? If so, can it be large enough to inhibit surface formation?

(d) Can surface shaping occur at frequencies much lower than the typical ultrasound seen in literature? How much power is required?

(e) How sensitive is the shaping process to source location?

The experiments took place aboard NASA's KC135 aircraft (Wanis 1998, 1999). The experimental setup consisted of: (a) an acoustically-hard resonant chamber with interior dimensions: 21 x 17 x 10 cm and 1.25 cm thick acrylic; (b) a compression type speaker mounted flush to the inside walls of the chamber near a corner; (c) home amplifier; (d) function generator; and (e) several particle types to be used in shaping experiments inside the chamber. We experimented with polystyrene pellets, Kellogs Rice Krispies™ cereal, aluminum spheres and aluminum oxide spheres. All particles were much smaller than the wavelength by at least one order of magnitude. The reason this condition was chosen is because it places the scattering phenomena well into the Rayleigh scattering regime. This is helpful in that closed form solutions exist for Rayleigh scattering problems.

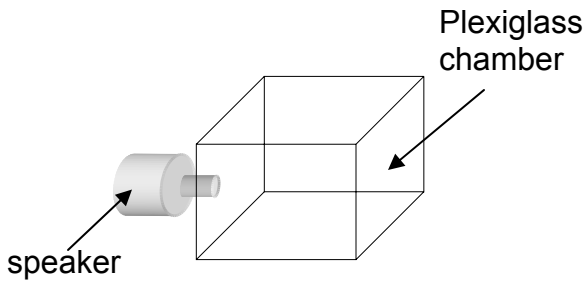

Figure 11 Schematic of experimental setup used for the generation and testing of acoustic force fields

Experiments in microgravity revealed that particles do indeed respond to the imposed acoustic force field and realign themselves into an ordered structure composed of a single particle-thick wall as seen in Figures 12-14. Two video clips from the flight tests are shown in Appendix B showing curved wall formation using mode (1,1,0). For pressure distributions with variations along two dimensions, the formed surfaces did not correspond to the exact nodal surfaces predicted by our back-of-the-envelope calculations. This deviation will be explained in Chapter 4. The geometry of the formed surface changed when the driver frequency changed. The system was driven only at its resonant frequencies as we were not interested in traveling wave dynamics. The various resonant frequencies of the chamber correspond to unique mode shapes, which have different geometries. The entire TFF system is based upon this fundamental aspect.

Figure 12 Styrofoam pellets being shaped in microgravity to form straight walls using a (1,0,0) mode which corresponds to a 800 Hz excitation frequency. Maximum wall height is 10cm.

Figure 13 Rice Krispies™ pellets being shaped in microgravity to form a straight wall using a (1,0,0) mode which corresponds to a 800 Hz excitation frequency. Maximum wall height is 9 cm.

Figure 14 Styrofoam pellets being shaped in microgravity to form curved walls using a (1 1 0) mode which corresponds to a 1250 Hz excitation frequency. Maximum wall height is 9 cm.

2.4 Ground Experiments

Based on the results obtained from microgravity tests, ground tests were conducted in an attempt to answer other questions and those that arose from the microgravity experiments. Results from ground experiments showed similar behavior but did not produce as large a surface as those formed in microgravity. The behavior of water in the chamber was tested out in ground experiments (Wanis 2000). This resulted in wall formation as well about 1.5 cm high. A remarkable feature of using water as the material to be shaped is that the frequency inside the chamber jumps to a higher harmonic upon wall formation. The water wall serving as an added boundary to the field explains this. The location of the surface in relation to the chamber walls determines which harmonic is excited. The water wall was very unstable as it formed and water drops were observed to eject from the top as a fountain. Placing styrofoam pellets on the water layer resulted in larger walls compared to the dry pellet case, as seen in Figure 15. The water layer enhanced the attractive force between the particles because of surface tension.

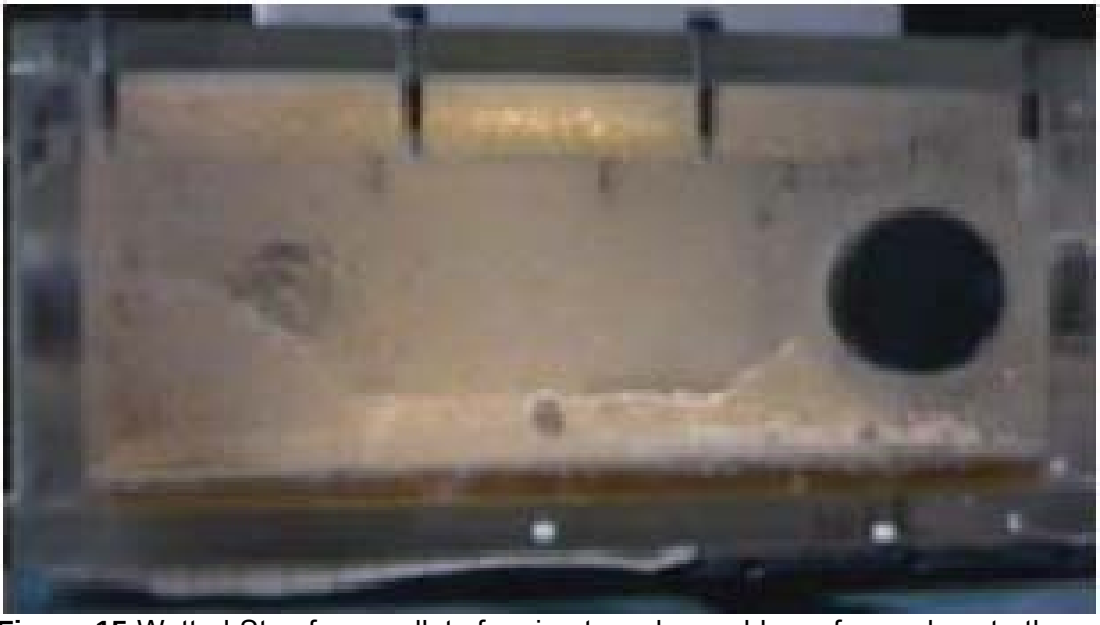

Figure 15 Wetted Styrofoam pellets forming two observable surfaces close to the walls. Side view of chamber.

This provided the basis to perform a hardening experiment where a surface would be formed out of randomly placed particles in the chamber and hardened. Plastic beads from a child's toy were used as the shaping particles due to their bright color for ease of image capturing and low weight. Agarose - an organic liquid in melt form at 60^{o}C and solid at room temperature, was used as the hardener. Liquid agarose was poured into the chamber bottom and the particles were added. The field was switched on and the particles were seen to stand up in a wall. As the wetted particles cooled down they adhered to one another forming a permanent structure. The excitation frequency was adjusted to account for the reduction in speed of sound as the experiment progressed in time. The structure formed is shown in Figure 16 from (Wanis 2000).

Figure 16 Plastic beads formed into a wall and hardened with Agarose. Chamber is open and field is off. Penny is shown for size reference.

With this in mind a wall prediction capability was added to the simulation tool. The resulting shape when running mode 1 1 0 is shown in Figure 17.

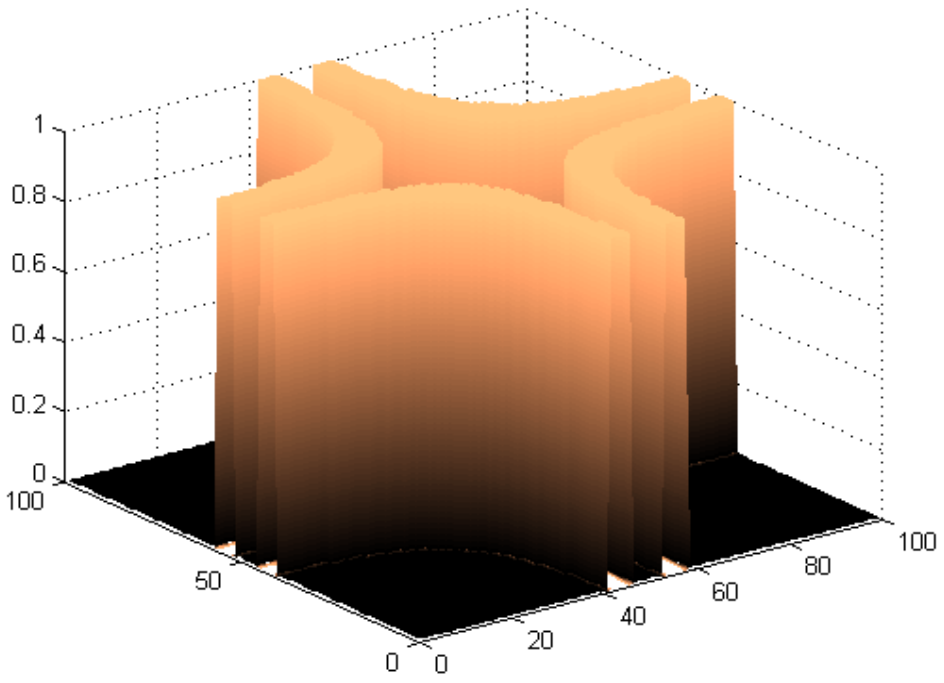

Figure 17 Simulated formed surface in mode (1 1 0). This mode is responsible for the actual surface formed in microgravity flight tests and is shown in Figure 14.

Interesting wall shapes are expected for combination modes as seen in Figure 18 below.

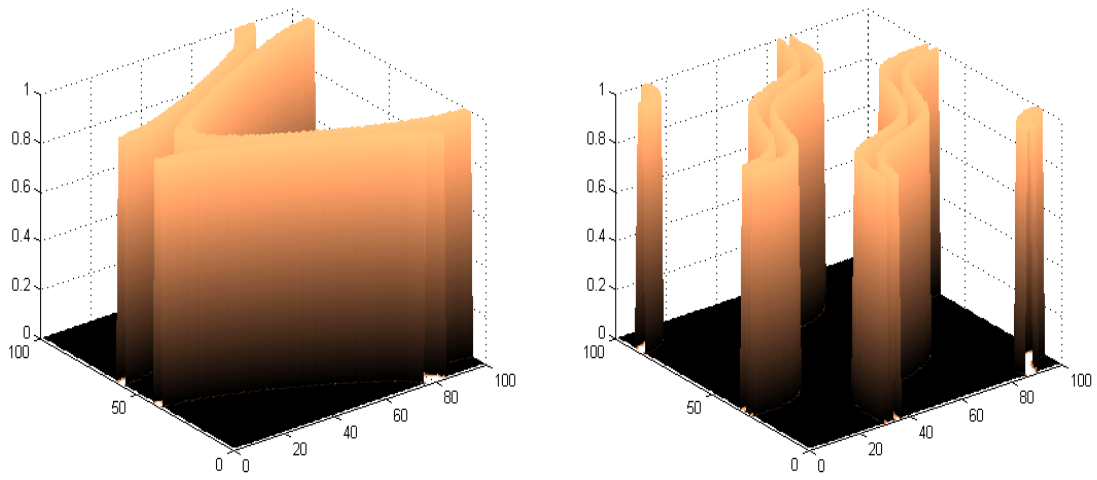

Figure 18 Surface formed due to combination modes; left: modes (1 0 0) and (0 2 0); right: modes (1 1 0) and (2 2 0).

2.5 Results

It was shown that the concept of using standing acoustic fields to create structures of desired geometry is feasible. Forces are generated as a result of the interaction of particles with the field. The force field is adjustable by controlling which resonant cavity modes are excited. In one dimensional fields, the force profile has a spatial frequency that is twice that of the sound field, which means that the force goes to zero at both the pressure nodes and antinodes. However, only the nodes are stable. This is a result of the force profile having a negative gradient at the nodes which means that immediately around that point are restoring forces that create a potential well deep enough to contain the particle.

Surfaces were formed that were both straight and curved. The radius of curvature of the surfaces was much larger than the particle radius. The formation of walls did not seem to affect the field dramatically since the locations of the surfaces formed correspond to pressure fields predicted for an empty cavity. A measurement of

the resonant frequency of the empty cavity, and with particles, could not resolve any systematic difference. This is due to the ratio of aggregate particle volume to total cavity volume remaining small. The power levels used to excite the microgravity tests were minimal ranging from 17 to 42 Watts, which through resonance yielded intensity levels from 0.32 kW/m^2 (145 dB) to 1.3 kW/m^2 (151 dB), i.e. an energy density range from 0.9 to 3.7 J/m^3.

To excite a normal mode of the cavity, we place a low amplitude velocity source at a velocity node of that mode. The result is a large amplitude velocity anti-node ¼ wavelength away. The location of the speaker is optimum at any corner since the corners always correspond to a pressure anti-node for every mode of the chamber. However, limitations on realistically achieving that while still maintaining as close as possible the geometry of the cavity to a perfect rectangular prism forced us to place it flush with one of the interior walls and close to the corner.

Comparisons with flight tests show good agreement for one dimensional modes. For two dimensional modes the walls form along constant pressure lines but not at the exact minimum predicted potential. This alludes to the presence of other forces in the field or a miscalculation in modes with variations along more than one dimension. This is a matter to be discussed in Chapter 4 in the context of secondary forces.

CHAPTER 3

PRIMARY ACOUSTIC FORCE FIELDS

This chapter addresses the underlying physics of sound generated forces. For particles placed randomly in a standing wave field, the forces that push them towards regions of minimum force potential are called *primary forces*. The forces that may exist between the particles themselves, usually effective only at short ranges, are called *secondary forces*. In other words, primary forces are what govern the shape of the structure formed. The secondary forces govern the actual process of formation, and the quality (structural integrity and finishing) of the surface formed. Primary forces are the subject of this chapter, followed by a series of experiments and basic numerical work.

3.1 Introduction

In this section we discuss the principles behind the interaction of a single particle with the primary sound field. A literature search is first presented to provide a frame of reference of the development of this branch of nonlinear physical acoustics. A summary of the widely diverse branches of physics that utilize these forces in different ways is also given to lay the foundations for the hypothesis about flexible, space-based construction.

3.2 Literature Review

Radiation pressure in acoustic fields is a manifestation of a universal phenomenon. All types of wave motion exert some type of unidirectional force on a reflecting and/or absorbing obstacle in their path (Torr 1984). The term radiation pressure was first used in electromagnetics by Maxwell which was then introduced in acoustics by Lord Rayleigh

(1905) as he searched for an acoustic analogue. In acoustic waves, both momentum and energy are carried with no net transport of the medium hosting the wave. As a wave collides with a particle or interface having a different impedance, the momentum and energy of the wave are altered in some fashion dictated by several parameters to be discussed later. In general, we can say that a change in the energy of the wave takes place through any absorption process inside the particle or interface where a dissipation of energy occurs. A change in the momentum of the wave occurs as a result of scattering (i.e. refraction and reflection processes). According to Newton's second law, the force produced on a particle is equal to the rate of change of momentum that occurs due to scattering. Acoustic radiation pressure is the net pressure exerted on a surface, or interface separating two fluids, by an acoustic field (Wang 1998). Nyborg (1967) shows that using the terminology used in the method of successive approximations the pressure in the field can be expressed as follows: $p = p_0 + p_1 + p_2 + \cdots$. The static pressure is given by p_0 which is a zero-order contribution. The first order contribution given by p_1 varies harmonically in space and time at the same frequency of the source and amplitude proportional to the source amplitude. Linear acoustics goes up to only the first-order term, and thus averaging over one wave period results in a zero net pressure. At higher sound intensities nonlinear second-order effects cease to be negligible which is given by p_2. This pressure is time-independent and can therefore induce a net pressure after time averaging, and this is what we call radiation pressure. The magnitude of this second-order term is proportional to the source amplitude squared. The higher order terms include the pressure fields that vary in time and space at multiple integers of the source frequency and with amplitudes proportional to the source amplitude squared. These terms are usually called 1^{st}, 2^{nd}, 3^{rd} harmonic etc.

3.2.1 Rayleigh and Langevin Radiation Pressure Concepts

There are two theories that explain acoustic radiation pressure depending on the boundary conditions of the problem: Rayleigh radiation pressure and Langevin radiation pressure. According to Meyer (1972), Langevin radiation pressure is due to the nonlinear convective term in Euler's equation governing fluid flow dynamics and occurs when there is interaction between the sound beam and the unperturbed medium. Whereas Rayleigh radiation pressure is a result of the nonlinear equation of state of the host medium, as seen in Figure 19, and is usually manifested in conditions where the sound beam is isolated from the unperturbed medium. The nonlinear equation of state for air is also the cause of many finite amplitude acoustic effects, such as: (i) harmonic generation, where the source frequency is ω but the field contains 2ω, 3ω,…; (ii) parametric arrays, which is a special case of harmonic generation, and its when two waves of high frequency sound interact and yield their sum and difference frequencies, ω_1-ω_2, and ω_1+ω_2; and (iii) acoustic streaming, also known as quartz wind, where a time-averaged flow is generated.

The first observation of time-averaged radiation pressure was made by Kundt in 1866 when he observed dust particles collecting at the pressure nodes of standing waves setup in circular ducts (Kundt 1874). The force due to acoustic radiation pressure was first measured by Altberg (1903). King (1934) theoretically addressed both traveling and standing plane waves incident on a rigid sphere and showed that the force due to radiation pressure is proportional to the sound field intensity for traveling waves and proportional to its gradient in standing waves.

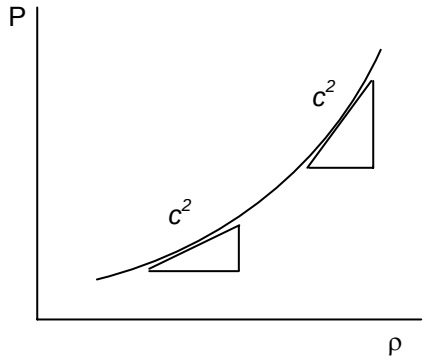

Figure 19 Typical curve of pressure vs. specific volume – adiabatic curve for air

King expressed the primary radiation force as that due to the integrated time-averaged pressure acting on each subsurface element, over the entire particle surface. For this method to yield an analytical solution, which King succeeded in obtaining, it was necessary to express the particle surface in terms of the mathematical coordinate system which is used to express the incident waves (Embelton 1962). King (1934) studied both traveling and standing waves incident onto small rigid particles. Particles were small in relation to the field wavelength. His choice of particle geometry was limited to spherical shapes, and therefore, he expressed the incident waves in terms of Legendre polynomials, spherical Bessel and Neumann functions. In 1951 Rudnick verified King's primary radiation force expression experimentally (Rudnick 1951). Three years later Embelton expanded King and Rudnick's work to include spherical and cylindrical waves and showed good agreement between theory and experiment (Embelton 1962). With all the progress in predicting the primary acoustic radiation force, there was still some confusion as to the exact relation between the force and the time-averaged acoustic energy density. In 1940, Richter clarified the confusion and showed that the time-averaged pressure of standing waves, i.e. radiation pressure, on large

plane surfaces could be expressed in terms of the difference between the time-averaged kinetic and potential energy densities plus a term which depends on the properties of the system under study, and in certain cases, on the equation of state of the host medium (Richter 1940). Embelton notes that in non-planar sound fields attraction forces between particles can be expressed through a mathematical consequence of the fact that the instantaneous pressure is related to the Lagrangian energy density (Embelton 1962). In other words, he showed that irrespective of the incident wave front geometry any gradients in the Lagrangian energy density will result in a force at that point. It is clear that the presence of a scatterer will disturb the field such that it will create gradients in the local energy density and thus contribute to interparticle forces. Around the same time, Gor'kov, with the same line of thinking, came up with a primary radiation force expression that is more general than King's equation (Gorkov 1962). His only assumptions that were shared with King is that the particle is much smaller than the wavelength and that the flow around the particle can be regarded as inviscid (i.e. particle diameter >> δ). One of the main attractions of Gor'kov's equation is that no restriction was made on the wave front geometry, and thus non-plane fields are allowed. Following Richter's claim that the force is related to the Lagrangian energy density, it is not difficult to see that the primary radiation force is conservative in nature and can thus have a force potential. Gor'kov defines this force potential based on the Lagrangian energy density.

In 1939, G. Hertz and H. Mende (1939) clarified the nature of the radiation forces through a famous demonstration experiment. They directed an acoustic beam at a water-carbon tetrachloride interface. These two fluids have relatively close characteristic impedances yet significantly different sound speeds. The characteristic impedance of a fluid is given by the product ρc, where ρ is the fluid density and c the sound speed. The

almost negligible difference in the impedances (i.e. $\rho_1 c_1 = \rho_2 c_2$) enabled the passage of the sound beam with minimal reflections from the interface. As the sound intensity was increased, the interface deformed into the water side (the fluid with higher sound speed), independent of the direction of the beam, i.e. whether it came from the water side or the carbon tetrachloride side. This showed that the force on the interface occurred solely due to the difference in the value of the energy density in both layers which was a result of the different sound speeds. The energy density, $E = I/c$, where I is the sound intensity and c the speed of sound, is different because I remains equal in both fluids due to the minimal reflections at the interface. Therefore, radiation pressure on a surface with area S can be written as $F = S(E_2 - E_1)$.

This allows us to define two processes that may occur when a sound beam emerges from one fluid into another that ultimately leads to a force on the interface. The first process is due to the characteristic impedance mismatch and we will identify as *scattering*. Scattering alters the beam's momentum flow by reflecting and/or refracting the incident beam. The second process is due to the different sound speeds producing different energy densities across the interface. The force on the interface is proportional to the difference in sound speeds (i.e. gradient of sound speed) and is directed towards the medium with the lower energy density. The mechanisms of scattering and wave speed differences have analogues in electromagnetic fields and will be discussed in chapter 6.

3.2.2 Characteristics of sound induced forces

A scattering particle in a sound field will experience a force that is the integral of the radiation pressure across the surface of the particle. As will be shown later, a standing wave field produces orders of magnitude higher forces than those in traveling waves with the same pressure field amplitude. In resonant, i.e. standing wave, fields there are

regions of pressure minima (nodes) and maxima (anti-nodes). Objects that are relatively rigid compared to the host medium (e.g. metal spheres in air) collect at nodal regions, while compressible objects (e.g. air bubbles in water) are attracted to anti-nodal locations (Crum 1969 and Chu 1982). Solid metal objects have been levitated in air using standing waves (Whymark 1975) and (Collas 1989). Moderate sound intensities were used to manipulate and shape droplets in microgravity environments for the purposes of studying the material properties of certain fluids (Barmatz 1982).

An in depth study of radiation pressure exerted on a rigid sphere by a plane traveling or standing wave in an inviscid host fluid was accomplished by King (1934). Experimental verification was then performed by Rudnick (1951). Yosika and Kawasima (1955) extended the theory to include compressible spheres and their predictions matched well with experiments involving air bubbles in water. Experimenting with small air bubbles in water, Eller (1968) has shown that they collect at the pressure anti-nodes. Crum (1971) estimated the minimum acoustic pressure required to trap small liquid droplets in a liquid host thereby filling the gap between the two extremes of rigid (such as glass spheres in air) and highly compressible spheres (such as air bubbles in water).

In all of the earlier work calculating radiation forces assumed inviscid flows. Including viscous effects alters the radiation force due to secondary nonlinear mechanisms such as, acoustic streaming and temperature dependence of the viscosity. Danilov and Mironov (1984) tackled the problem of radiation pressure for viscous media and solve the problem for traveling and standing waves. They show that viscosity alters the phase of the dipole force. The changes may be large enough to cause a significant difference on the order of $(ka)^3$. It is expected that including viscous effects should give rise to the primary forces since there is now an additional entrainment force due to viscosity.

3.3 Some Applications of Acoustic Radiation Forces

Acoustic levitation has been used is several applications. NASA used this principle to study material properties in a microgravity environment where they used the same principles of acoustic levitation to controllably position and deform a droplet in a gaseous fluid host (Barmatz 1982). At NASA Jet Propulsion Lab Barmatz (1984) developed a material transport system where multiple modes were excited simultaneously. As the relative intensities of the modes were varied, the stable location of the particle, which lies in between the potential wells of each mode, was controlled. An interesting application of this force type has found its way in manipulating biological matter. Ultrasonic fields were used to separate particles dispersed in a host fluid medium using radiation pressure (Apfel 1990, Gröschl 1998, Hawkes 2001, Sarabia 2000). Ultrasound was used to exert forces between neighbouring particles in a suspension which led to cells agglomerating into chains (Nyborg 1974; Miller 1976; Nyborg 1978; Weiser 1984).

3.4 Theoretical Study of Primary Forces

3.4.1 Classical Method to obtain Force Expressions

The acoustic radiation force on a rigid sphere placed in an inviscid fluid (i.e. $a>>(\nu/\omega)^{1/2}$) was obtained by King (1934) by solving for the momentum transfer that results from the scattering of a small spherical particle ($ka<<1$) placed in a stationary sound wave. In his derivation, no limit was placed on the relative densities of the particle and its host fluid, however he solved the problem without including the compressibility of the sphere, thus his formula is valid for relatively heavy rigid sphere in a gaseous host medium (Wang 1998). King accomplished this by integrating the total acoustic field, incident and scattered, over the surface of the sphere. Setting the acoustic wavelength-to-particle diameter ratio to 10 or more places the scattering analysis in the Rayleigh scattering

regime. In this regime an analytical expression exists for the scattering cross section of these particles, where only the monopole and dipole terms need be retained (Danilov 1984). We follow Wang's (1998) derivation of the force induced on a small spherical particle in a plane standing wave.

For a 1D standing wave and placing the pressure node at x=0, we can represent the pressure field as follows,

$$p_i = P_o \sin kx \cdot e^{-i\omega t} \tag{9}$$

where P_o is the pressure amplitude, k the wavenumber, and ω the angular frequency of he field. We can collect $P_o sinkx$ into a term p_{io} for simplicity. The spherical particle is placed at an arbitrary x-location X, and a spherical coordinate system (r,θ) is placed such that its origin coincides with the spheres center. The angle $\theta=0$ coincides with the positive x-axis. To represent the field using suitable spherical coordinates such that the problem becomes separable, we use the following identity (Abramowitz 1965),

$$e^{jkr\cos\theta} = \sum_{n=0}^{\infty} (2n+1) i^n j_n(kr) P_n(\cos\theta) \tag{10}$$

along with $x=X + r\cos\theta$ to describe any general point (r,θ). Substituting this and and Equation (2) into Equation (1) now have,

$$p_i = \sum_{n=0}^{\infty} (2n+1) A_n j_n(kr) P_n(\cos\theta) \tag{11}$$

where,

$$A_n = \frac{A}{2i} i^n \left[e^{ikx} - (-1)^n e^{-ikx} \right]. \tag{12}$$

for the field's spatial dependence. In the above, j_n is the spherical Bessel function, and P_n is the Legendre polynomial. To express the scattered wave, we regard it as a wave emanating from the sphere's surface S and is described by, $p_s = p_{so}e^{-i\omega t}$, where p_{so} can be described by

$$p_{so} = \sum_{n=0}^{\infty} B_n h_n^{(1)}(kr) P_n(\cos\theta) \tag{13}$$

where $h_n^{(1)}$ is the spherical Hankel function of the first kind. Adding this scattered field to the incident field we get the total field, i.e. $p_o=p_i+p_s$. The total field can then be described by, $p=p_o e^{-i\omega t}$. Applying the boundary conditions on the surface of the sphere

$$\left(\frac{\partial p_i}{\partial r} \right)_{r=a} = -\left(\frac{\partial p_s}{\partial r} \right)_{r=a} \tag{14}$$

To solve for the coefficient B_n we substitute p_i and p_s into Equation 14 and equate terms with the same n to get,

$$B_n = -\frac{(2n+1) j'_n(ka)}{h_n^{(1)'}(ka)} A_n \tag{15}$$

The last five equations provide enough information to represent the total pressure field at *r=a*,

$$p_o = \Sigma(2n+1)\left[j_n(ka) - \frac{j'_n(ka)h_n^{(1)}(ka)}{h_n^{(1)'}(ka)} \right] A_n P_n(\cos\theta) \quad (16)$$

Applying the small sphere condition *ka<<1*, Equation 16 becomes,

$$p_o = \left[1 - \frac{(ka)^2}{2} \right] A\sin kX + \frac{3}{2}(ka)A\cos kX\, P_1(\cos\theta) - \frac{5}{9}(ka)^2 A\sin kX\, P_2(\cos\theta) \quad (17)$$

Now that we have obtained the pressure field at the surface, the tangential velocity can be easily obtained, the normal velocity component being zero for rigid spheres,

$$u_\theta = \frac{3i}{2}\frac{A}{\rho_o c_o}\cos kX\sin\theta - \frac{5i}{3}\frac{(ka)A}{\rho_o c_o}\sin kX\,\cos\theta\sin\theta \quad (18)$$

The above expressions for pressure and velocity can now be used to evaluate the radiation force by substituting into the following equation described by Langevin as the basis for radiation force on a target due to an unbounded sound wave,

$$P_{Langevin} = \langle PE \rangle - \langle KE \rangle \quad (19)$$

where $\langle PE \rangle = \langle p^2 \rangle / \rho_o c_o$ and $\langle KE \rangle = \rho_o \langle u \cdot u \rangle$ are the time-averaged potential and kinetic energy densities. The Langevin radiation pressure at the surface becomes,

$$\left\langle P_{Langevin} \right\rangle = \frac{A^2}{4\rho_o c_o^2}[\sin^2 kX + \frac{3}{2}(ka)\sin 2kX \cos\theta - \frac{9}{4}\cos^2 kX \sin^2\theta + \frac{5}{2}(ka)\sin 2kX \sin^2\theta\cos\theta] \tag{20}$$

Thus, the Langevin radiation pressure when integrated over the surface of the sphere S will yield the total force,

$$F_x = -\int_s \left\langle P_{Langevin} \right\rangle \cos\theta \, dS \tag{21}$$

Using $dS = 2\pi a^2 \sin\theta \, d\theta$ and solving the integral from 0 to π we arrive at King's force expression (King 1934),

$$F_x = -\frac{5\pi}{6}\frac{A^2 k a^3}{\rho_o c_o^2}\sin 2kX \tag{22}$$

Wang (1998) takes this expression further and obtains a force potential, U from it as follows,

$$U = \frac{5\pi}{12}\frac{A^2 a^3}{\rho_o c_o^2}\cos 2kX \tag{23}$$

where *F=-dU/dX.* Studying the above two equations it is clear that the force can be thought of as the spatial gradient of potential function that includes the time-averaged potential energy density. This will be the basis of the next section where we show how the radiation forces can be obtained by simple means utilized by Gor'kov that are based on energy densities. If the traveling force expression is needed, then the above is repeated but for an incident field given by, $p_i = p_{io}e^{-i\omega t}$, where now $p_{io} = Ae^{ikx}$. When this is done the final result for the force is (King 1934),

$$F_x = \frac{11\pi}{18}\frac{A^2k^4a^6}{\rho_o c_o^2} \tag{24}$$

The main distinction can be clearly seen that the traveling force does not have any spatial harmonic dependence as does the standing wave force, which has a spatial frequency double that of the pressure field. The higher dependency of the traveling wave forces on *ka,* being on the order of $(ka)^3$ times more, is the main reason why standing waves can produce orders of magnitude larger force for the same field intensity. The reason for this difference is based on the different phase relations between the incident and scattered fields in progressive and standing waves, respectively (Gröschl 1998). This force also scales linearly with intensity and cannot be put in a form such that it depends on the gradient of the intensity as does the standing wave force, which will become very important in Chapter 5 where the analogy between acoustic and electromagnetic force fields is documented.

3.4.2 Energy density method of obtaining Forces

While the above derivation is regarded as the classical method of describing the force on a sound scattering particle, we follow Gor'kov's method mainly because it is not limited to one-dimensional fields and for the fact that it is much simpler and more elegant in deriving the primary radiation force as it is based on a scalar force-potential of the field. The conservative nature of the acoustic force in a standing wave field allows for this potential to be defined. The fact that it allows for non-planar wave fields is attractive for our research since we are exciting normal modes of a rectangular acoustic cavity for which all mode shapes have curved wave forms with the exception of axial modes, see Chapter 2 for an illustration of some mode shapes obtainable in a rectangular cavity. The assumptions used in the derivation are that the particle size be much smaller than the wavelength and much larger than the acoustic boundary layer formed on the particle due to the acoustic particle velocity. The force is found by taking the negative gradient of a force-potential, U, such that $F = -\nabla U$. The force-potential is given by (Gorkov 1962),

$$U = V\left[\left\langle PE\right\rangle f_m - \frac{3}{2}\left\langle KE\right\rangle f_d\right] \tag{25}$$

where V is the volume of the particle, and $\langle KE\rangle$ and $\langle PE\rangle$ are the time-averaged kinetic and potential energy densities (Embelton 1962). f_m and f_d are the scattering monopole and dipole contributions, respectively. They depend on the particle's acoustic characteristics, which are given by (Hanock 2003),

$$f_m = 1 - \frac{\rho_o {c_o}^2}{\rho c^2} \quad \text{and} \quad f_d = \frac{2(\rho - \rho_o)}{(2\rho + \rho_o)} \tag{26}$$

By examining the above terms it is evident that the range of the f_m and f_d are as follows: $-\infty < f_m \leq 1$ and $-2 \leq f_d \leq 1$. For our purposes the particles we are interested in are much less compressible than the host fluid, i.e. $f_m > 0$ and much denser than the host fluid, i.e. $f_d > 0$. For heavy rigid spheres the values of f_m and f_d are close to or equal 1.

The Gor'kov force potential derivation given by Haake (2005) is modified to suit our geometrical setup. To express the force potential U in terms of field quantities: pressure p and velocity v, we first define a scalar velocity potential ϕ such that, $v = -\nabla\phi$ and $p = \rho_o \partial\phi/\partial t$. For our rectangular cavity we set the Cartesian coordinate system with its origin at a corner. The walls are made out of ½" acrylic which has an impedance that is much greater than the impedance of the host fluid (air), and can thus be regarded as essentially rigid walls, i.e. normal velocity is zero at the walls. This allows us to describe the velocity potential distribution in the cavity,

$$\phi = -i\frac{v_o}{k}\cos k_x x \cos k_y y \cos k_z z e^{-i\omega t} \tag{27}$$

where $k = 2\pi/\lambda = (k_x + k_y + k_z)^{1/2}$. And for chamber dimensions l_x, l_y, l_z we have the wavenumber components, $k_x = m\pi/l_x$, $k_y = n\pi/l_y$, and $k_z = o\pi/l_z$. This notation allows us to define a normal mode shape by its integers (m,n,o) such that they describe the number of pressure nodes along their respective directions. For example, a (1,0,2) mode means that it has one node along the x-axis, constant in y, and 2 nodes along the z-axis. The pressure can now be described by,

$$p = (\rho_o c_o v_o)\cos k_x x \cos k_y y \cos k_z z e^{-i\omega t}. \tag{28}$$

Likewise, the velocity is solved for and both pressure and velocity substituted back into Gor'kov's force potential given in Equation (25). The resulting potential becomes,

$$\begin{aligned} U = U_o \Bigg(& \frac{f_m}{3} \cos^2 k_x x \cos^2 k_y y \cos^2 k_z z \\ & - \frac{f_d}{2} \Big[(k_x/k)^2 \sin^2 k_x x \cos^2 k_y y \cos^2 k_z z \\ & \quad + (k_y/k)^2 \cos^2 k_x x \sin^2 k_y y \cos^2 k_z z \\ & \quad + (k_z/k)^2 \cos^2 k_x x \cos^2 k_y y \sin^2 k_z z \Big] \Bigg) \end{aligned} \tag{29}$$

where $U_o = \pi a^3 \rho_o v_o^2$ (Haake 2005). The 3-dimensional force field can now be mapped out throughout the entire volume of the sound-filled cavity. We give the force field for modes that vary only in x and y, i.e. tangential modes, by taking the derivative with respect to the direction we want to obtain the force in, and set terms with sin(kz) to zero. This produces the following force field in the x-direction

$$\begin{aligned} F_x = U_o k_x \sin 2k_x x \Big[& \left(f_m/3 + (f_d/2)(k_x/k)^2 \right) \cos^2 k_y y \\ & - (f_d/2)(k_y/k)^2 \sin^2 k_y y \Big] \end{aligned} \tag{30}$$

For the force along y we simply interchange all of the above x and y subscripts. To predict if a particle will reach an equilibrium location within the force field, i.e. all the forces equal zero, an examination of the force potential needs to be performed. For example, if the potential has a location where the gradient is zero, then that amounts to a location where the force equals zero. However, that is not a sufficient condition for equilibrium, since some of these regions could be unstable if there are no restoring

forces all around that point. Therefore, the potential needs to have a minimum for it to be both a zero force location and stable. The formal way to search for such regions is through an examination of the Hessian which is the derivative matrix for the force potential, and it needs to be positive definite for stable equilibrium (Haake 2005).

Another advantage of using a scalar force-potential to obtain the force field is that it accurately describes the two-dimensional velocity field within the cavity. If the MATLAB simulation tool developed in Chapter 2 was used to predict the force field profile in 2-dimensions and then King's equation used to scale the force with then we lose key information on the velocity field. This information may account for the discrepancy seen between experiment and theoretical predictions based on an extension of King's equation alone, i.e. the potential due to the pressure alone. This is illustrated below in Figure 20 and Figure 21. Figure 20 is the potential formed by the pressure field alone, and the resulting forces in x and y, and Figure 21 includes the velocity field for calculating the potential and the resulting x and y force fields are shown. Note that when the velocity field was included in the potential calculation, the center of the cavity is no longer the absolute minimum of the force field. Additionally, in the center there are relatively weak forces that direct the particles towards the walls.

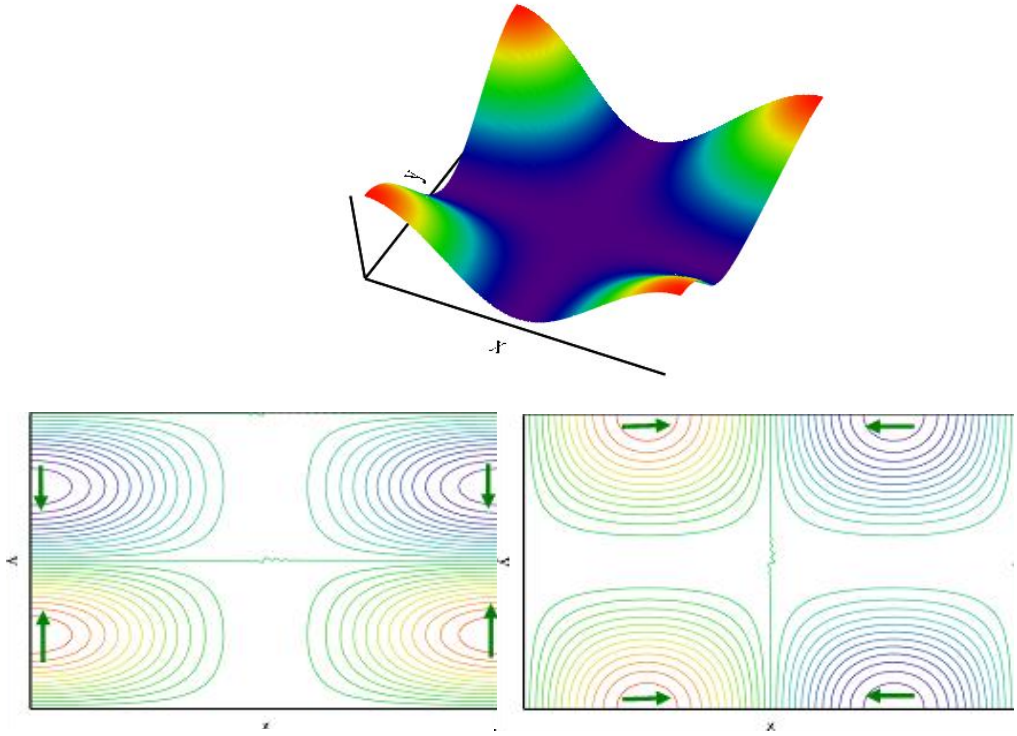

Figure 20 Force potential due to the pressure field alone (top). Resulting force field contours in the y-direction (bottom left), and in the x-direction (bottom right).

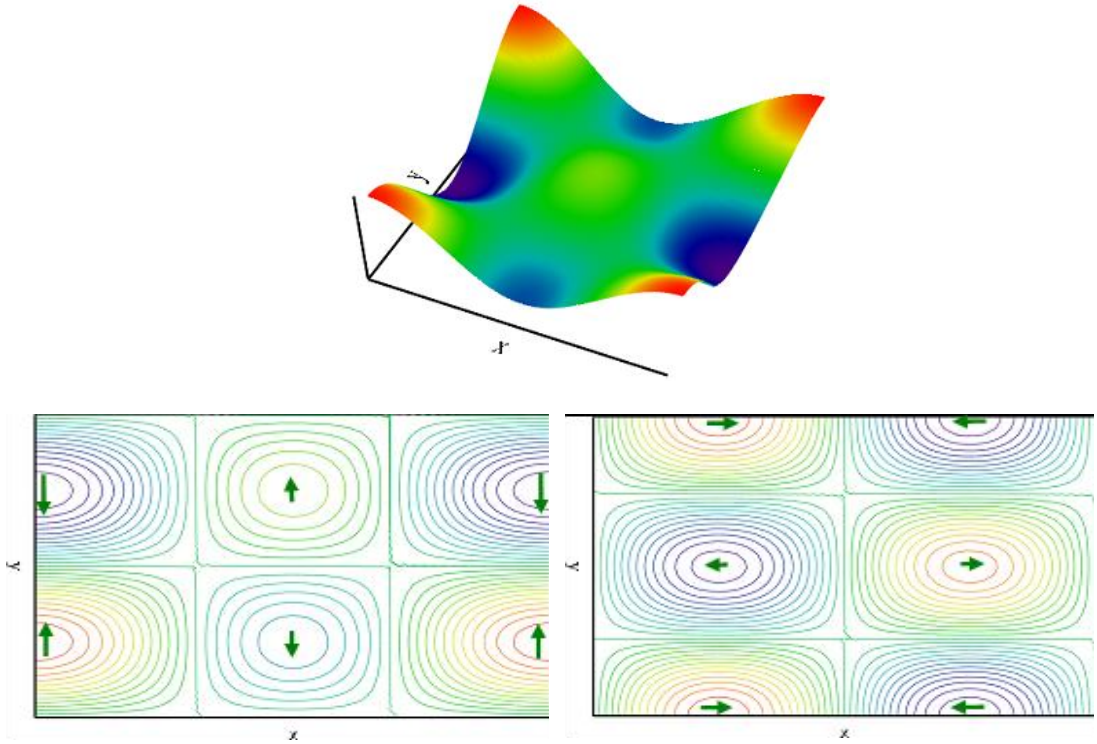

Figure 21 Force potential due to the pressure field and velocity field (top). Resulting force field contours in the y-direction (bottom left), and in the x-direction (bottom right).

3.5 Comparison with Experiment

3.5.1 Force measurement

A simple experiment was devised in order to obtain quantitative estimates on the forces obtainable in our acoustic cavity and compare that with the theory predicting primary forces. A small Styrofoam sphere was suspended from the cavity's top surface into the cavity in a pendulum-like fashion. The test was conducted for mode (1,0,0) and at steady state, the deflection of the pendulum was recorded and the acoustic radiation force induced onto the particle determined. For a 70 μKg sphere an acoustic force of 250 μN was measured at a location along the predicted force profile that corresponds to value of 280 μN. At this location the value of the primary radiation force, which is due to the fundamental field, is expected to be adversely affect by the presence of the 1st harmonic. This will be discussed further in Chapter 4.

3.5.2 Pressure field measurement

A series of experiments captured the pressure field in the cavity. The first set of experiments involved the global surface pressure measurement on one side of the chamber that helped reveal the mode shapes and compare to predictions by the Helmholtz equation. The other set of experiments were conducted using a microphone that was traversed across the cavity in straight lines. This was to capture accurately any harmonic content. Both these experiments are discussed below.

3.5.2.1 Global surface pressure measurements

Pressure-sensitive paint (PSP) is a measurement technique for measuring global surface pressures. The principle behind how it works is as follows. Certain molecules respond to incident optical radiation by absorbing light within a narrow bandwidth and become in an excited state, i.e. higher energy level. These molecules can then return to

their original condition, i.e. ground state, by either emitting light back at a lower frequency than the incident radiation, also known as luminescence, or by interacting with an oxygen molecule. If the pressure on the surface of a test article increases, then the partial pressure of oxygen follows in like-manner. This leads to an increased probability of oxygen molecules "quenching" the excited molecules, and thus the total reflected intensity off of the surface at the lower optical frequency decreases. A sensitive camera then collects the luminescent radiation which is a measure of the oxygen partial pressure. In effect, these molecules are pressure-sensors for the very reason of their characteristic interaction behavior with oxygen and light at the incident and luminescent frequencies. Such molecules are termed *luminophores*. The overall paint consists of a binder, luminophore, and primer. The binder is a paint-like material that serves as a host material for the luminophore molecules. It allows the luminophore molecules to be placed far enough apart from each other so as to allow oxygen molecules to interact with them. Otherwise, if they are too close to one another a self-quenching may occur. The binder has to be porous to oxygen molecules and transparent to both the incident and luminescent light. The primer serves as an adhesive agent of the luminophore-binder mixture to the surface of the test article. It also provides a diffuse reflection mechanism for incident light that has not interacted with any luminophore molecules which increases the chances of luminophore absorption of the incident light and also reflecting some of the luminescent light, that would have otherwise not have been collected, to the cameras (Barlow 1999).

In collaboration with Purdue University a novel experiment was conducted to visualize the actual mode shapes within the resonator (Gregory 2006). Purdue has been developing high frequency and high sensitivity paint for several aerospace applications (Gregory 2006) and wished to test out their paint capabilities using our acoustic resonator.

One of the sides of the chamber was painted on the inside with PSP and illuminated from the opposite end with a pulsed LED system at an optical frequency that is tuned to the resonance frequency of the paint (~ 470nm), see Figure 22 . A high-bit CCD camera captured any gradients in the paint's luminescence as it responded to the pressure field. The camera was fitted with an optical filter (~590nm) to separate the excitation light from the LED and the paint luminescence. A phase-locking mechanism was employed to capture time-resolved pressure history. A signal was taken from a microphone mounted in the chamber's corner to synchronize the LED flashing frequency with the field modulation. Once the data was taken at this time step, a short delay was added for the LED pulsing which enabled a measurement of the complete wave cycle (i.e. phase-locked time history).

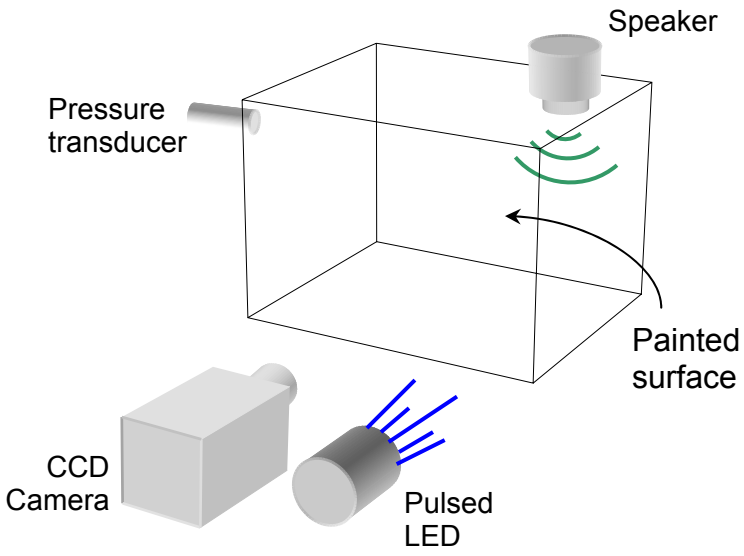

Figure 22 Schematic of setup used to capture global surface pressure using pressure-sensitive-paint.

Three modes were tested: (2,0,0), (1,1,0), and (2,2,0). For the (2,0,0) and the (1,1,0) mode only 12 time steps were taken to capture the entire wave cycle, whereas for the

(2,2,0) 20 time steps were used. Data for each mode is presented below in Figure 23 - Figure 28.

Mode (1,1,0):

A moderate SPL of 145 dB was used in this experiment. The frequency of excitation was 1286 Hz which corresponded to the measured resonance peak for the (1,1,0) mode. For this mode the pressure distribution was calculated as described earlier in Chapter 2 and is shown in Figure 23 below. The peak pressure value used in this calculation was taken from the maximum measured pressure of 480 Pa. It is clear that the pressure contours are smooth and the nodal regions are two orthogonal planes that intersect at the chamber center. Figure 23 shows the measured pressure-sensitive paint data for the (1,1,0) field. This field plot corresponds to one data set at one time-step out of the 12 sets taken which shows the pressure gradient as close as possible to its maximum. The difference between this and predicted theoretical solution is that the isobars are slightly curved. The pressure in the center of the chamber is not the absolute minimum. The maximum pressure values at the corners on the left hand side are slightly greater than the ones on the right. These effects are all due to distortion in the waveform which can be attributed to nonlinear effects.

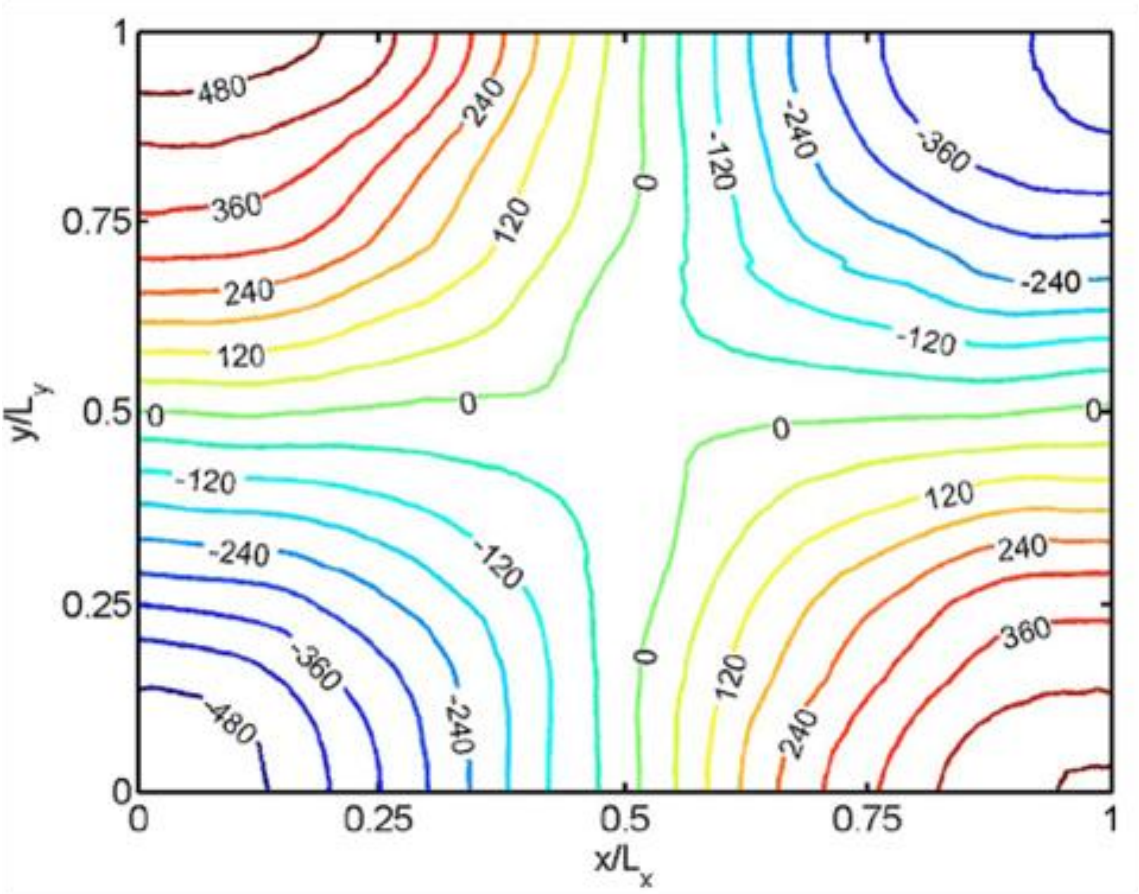

Figure 23 Pressure field for excited mode (1,1,0) captured using PSP

The pressure across the cavity wall along the vertical line ($x/L_x=0$) is shown for all 12 time-steps in Figure 24. The node is shown and the waveform is only slightly distorted in comparison with the perfect cosine wave that linear theory predicts.

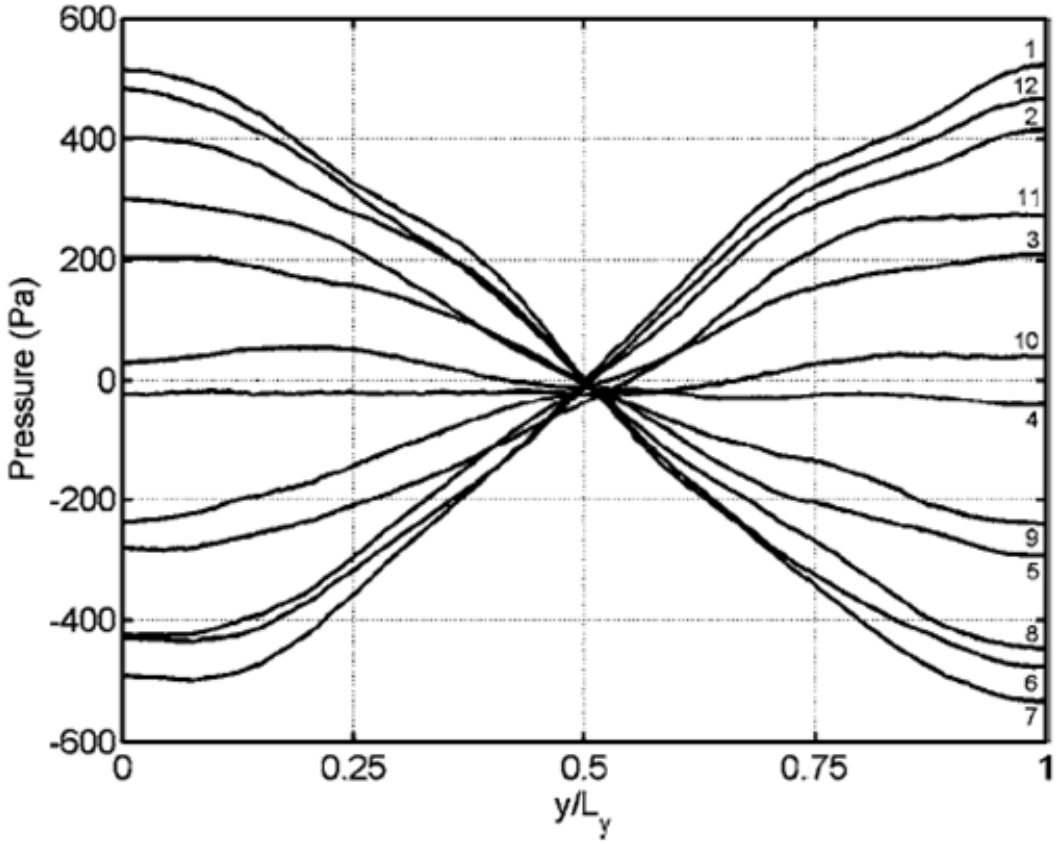

Figure 24 Vertical cross section of the PSP data at x/Lx = 0. The curves represent twelve time steps equally spaced throughout the wave period. Node is clearly seen at y/Ly = 0.5 (Gregory 2006).

Mode (2,0,0):

The difference in this test was that the mode was changed to (2,0,0) and the SPL was raised to 151 dB. At this pressure level nonlinear effects are much more pronounced. Measured pressure contours are shown in Figure 26. The cross section pressure along the horizontal line through the chamber center is shown in Figure 25 and this clearly shows how nonlinearity affects the waveform significantly. Figure 28 shows the data at three time-steps that correspond to the maximum pressure fluctuation and near zero fluctuation.

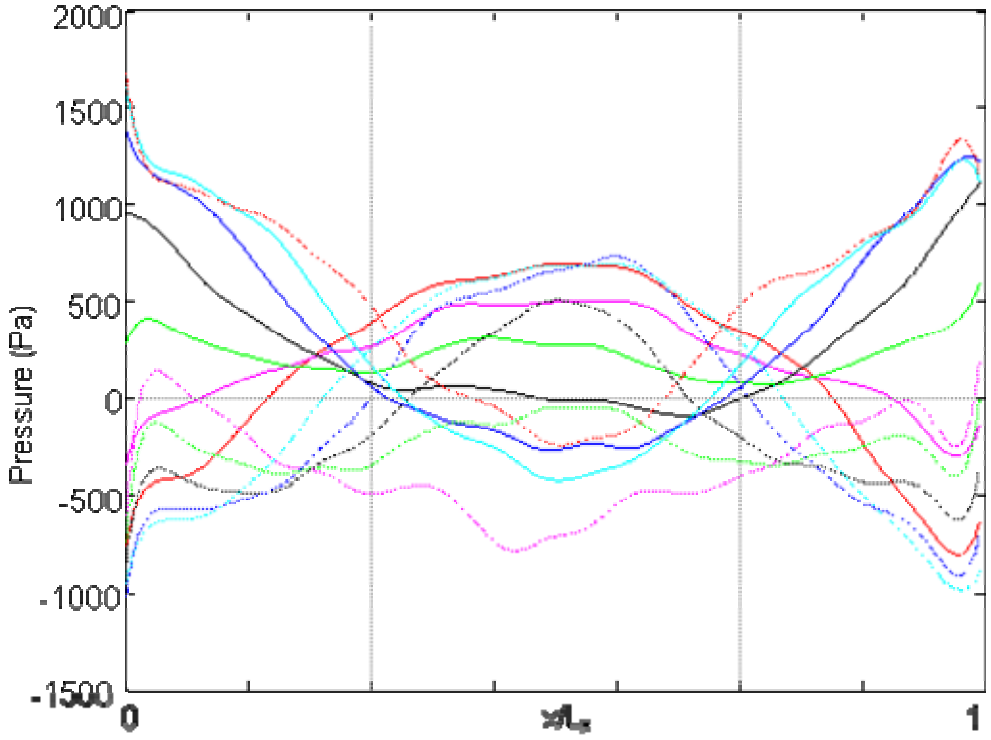

Figure 25 Horizontal cross section of the PSP data at y/Ly = 0.8. The curves represent twelve time steps equally spaced throughout the wave period. High amplitude effects are clearly seen from the distortion at the x/Lx = 0.25 and 0.75 locations.

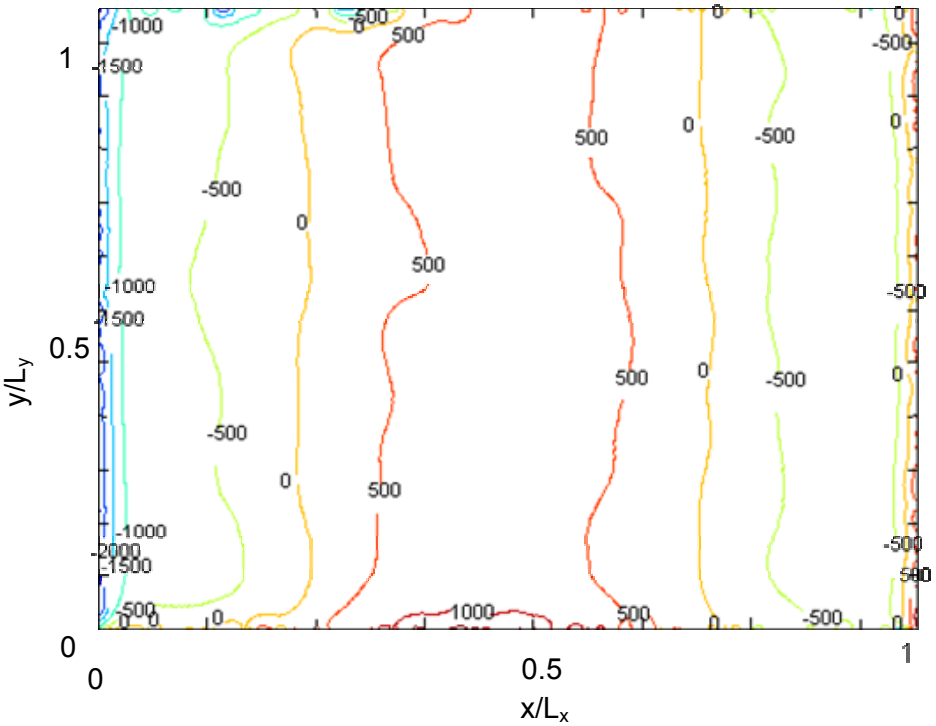

Figure 26 PSP contour data for the (2,0,0) mode excited at 151 dB. Pressure expressed in Pa.

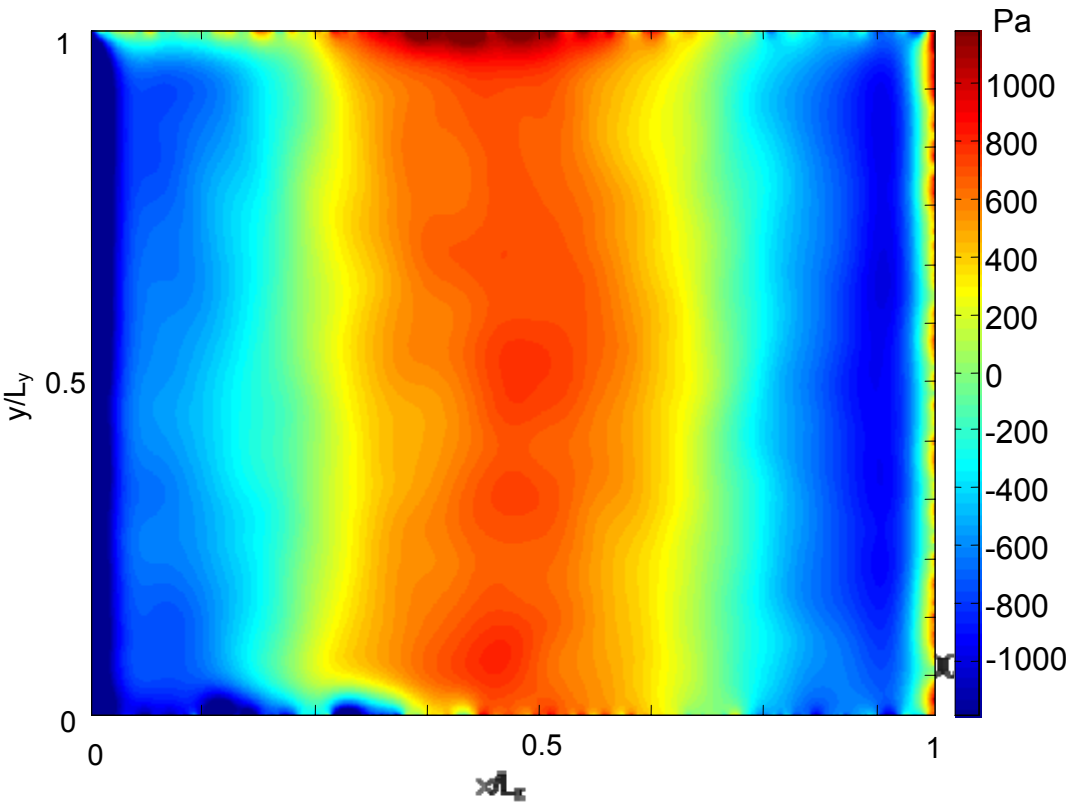

Figure 27 Pressure data for mode (2,0,0) excited at 151 dB.

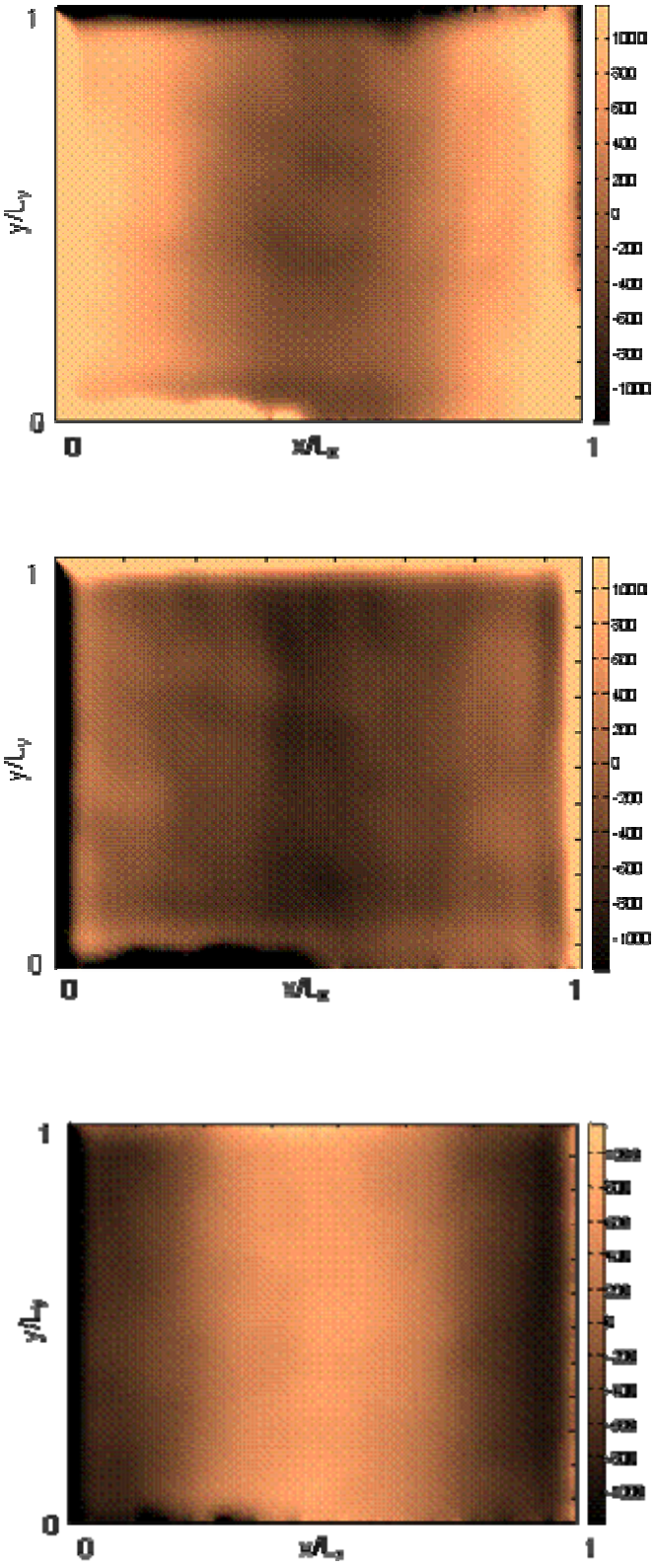

Figure 28 PSP data for (2,0,0) mode shape at 151 dB. Three phase-averaged time steps are represented: (a) 0^o, (b) 90^o, and (c) 180^o.

Mode (2,2,0):

The (2,2,0) mode was run in this test at 157 dB as well. The theoretical and measured pressure fields are shown in Figure 29 below.

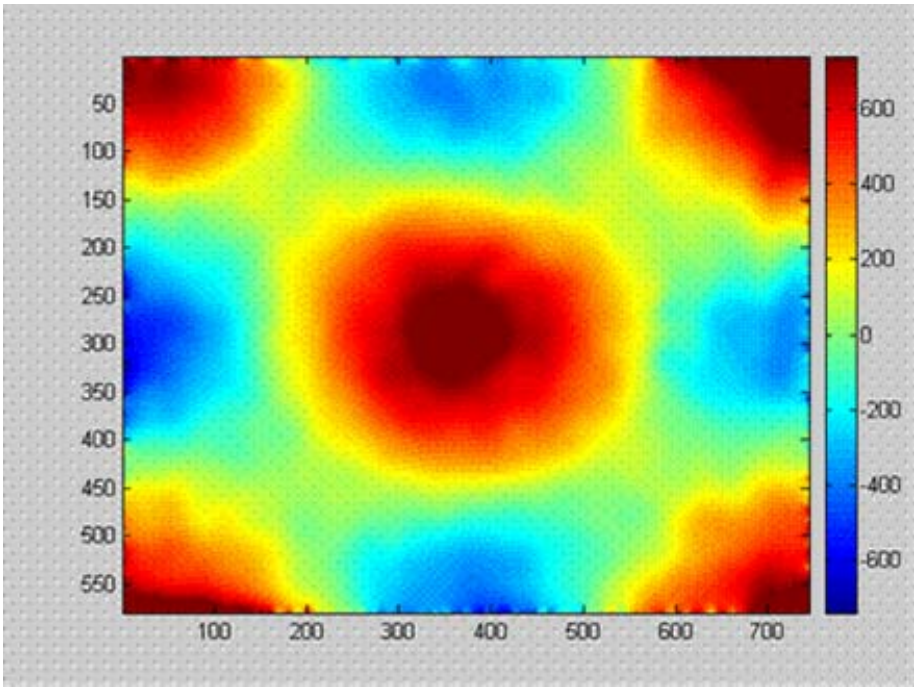

Figure 29 PSP data for mode (2,2,0) excited at 151 dB.

This test established that the pressure field resembles the predicted theoretical solution to a large degree. Differences between the two can be minimized when the 1st harmonic pressure field is superimposed onto the fundamental field in predictions. As anticipated, differences between prediction and actual pressure fields grow with increased SPL's. Clearly, in microgravity, nonlinear effects can be minimized greatly due to the reduced SPL's used. The main reason for using high levels in terrestrial environments is to overcome the force due to gravity.

The results of PSP revealed the presence of harmonic content in the pressure field inside the cavity. By including such harmonics, with an adjustable relative magnitude relative to the fundamental, we were able to achieve a closer solution to that observed

by measurement. To measure the amplitude of the harmonics the next set of experiments were conducted.

3.5.2.2 Microphone pressure field measurement

A ¼" condenser microphone was traversed throughout the cavity to capture the field and resolve the harmonic content. It was found that the 1st harmonic was found to be most dominant at the pressure nodes of the fundamental mode. The first experiment used mode (1,0,0) as the fundamental mode and the pressure amplitude was set to 500 Pa. The 1st harmonic signal was measured to have a pressure amplitude of 150 Pa at the center of the chamber. The 1st harmonic is equivalent to mode (2,0,0) and is thus also resonant in the cavity. At x/Lx = 0.25 and 0.75 the magnitude of the harmonic was negligible, as expected since those points correspond to the nodes of mode (2,0,0). At this high SPL value of 145 dB for the fundamental mode it is expected that harmonics will be present. For the (1,1,0) mode the same test was performed and the following was obtained:

At center of cavity: x/Lx = y/Ly = 0.5:

Dominant frequency = 2540 Hz with pressure amplitude = 94 Pa

Second highest frequency = 5080 Hz with pressure amplitude = 24 Pa

At wall half-way across: x/Lx = 0 and y/Ly = 0.5:

Dominant frequency = 2540 Hz with pressure amplitude = 106 Pa

Second highest frequency = 5080 with pressure amplitude = 27 Pa

This shows that for the (1,1,0) the 1st harmonic was still present but at a lower amplitude than the 1st harmonic when the (1,0,0) mode was run. Including these values of the

harmonics into the simulation tool by superimposing the harmonic mode onto the fundamental mode with a relative strength determined from the data above, we get the following results that show a much closer resemblance to the PSP data.

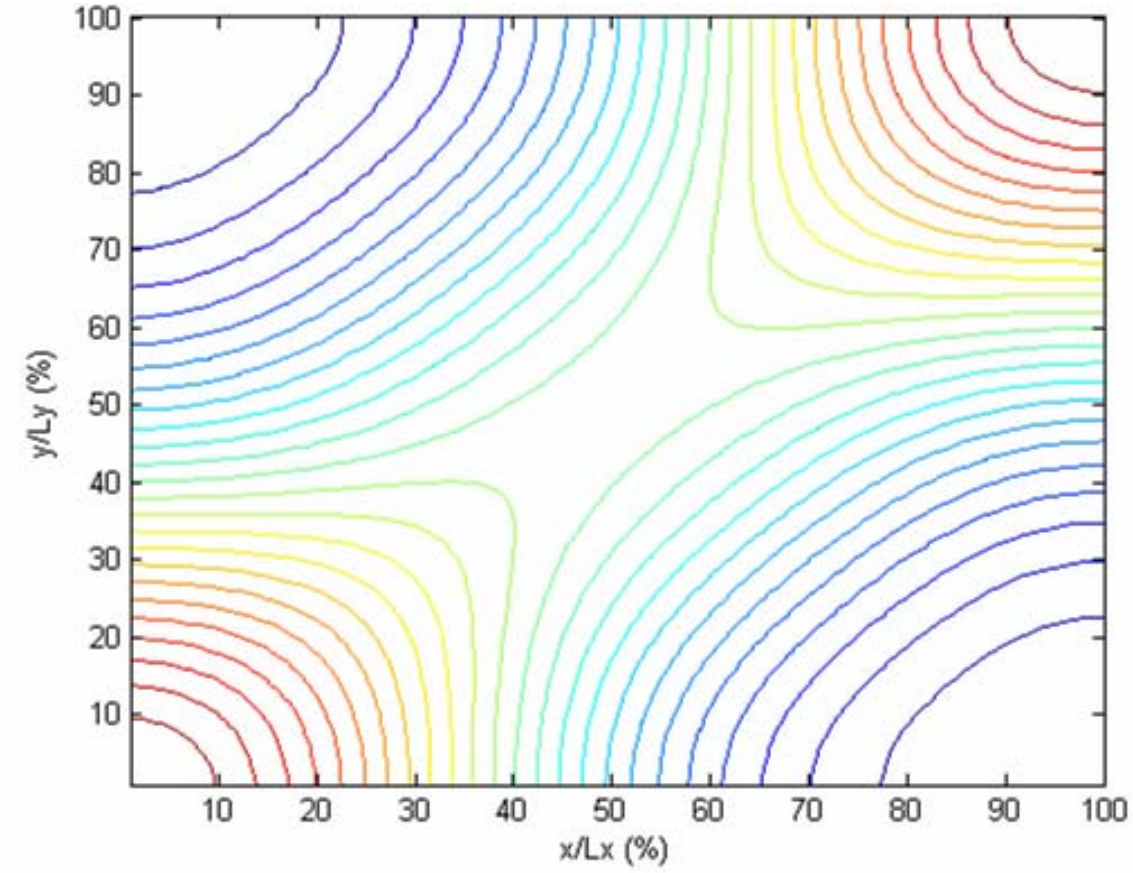

Figure 30 Pressure field for mode (1,1,0) and 1st harmonic (2,2,0) superimposed

The plot for the pressure squared is shown below which compares well with Figure 21**.**

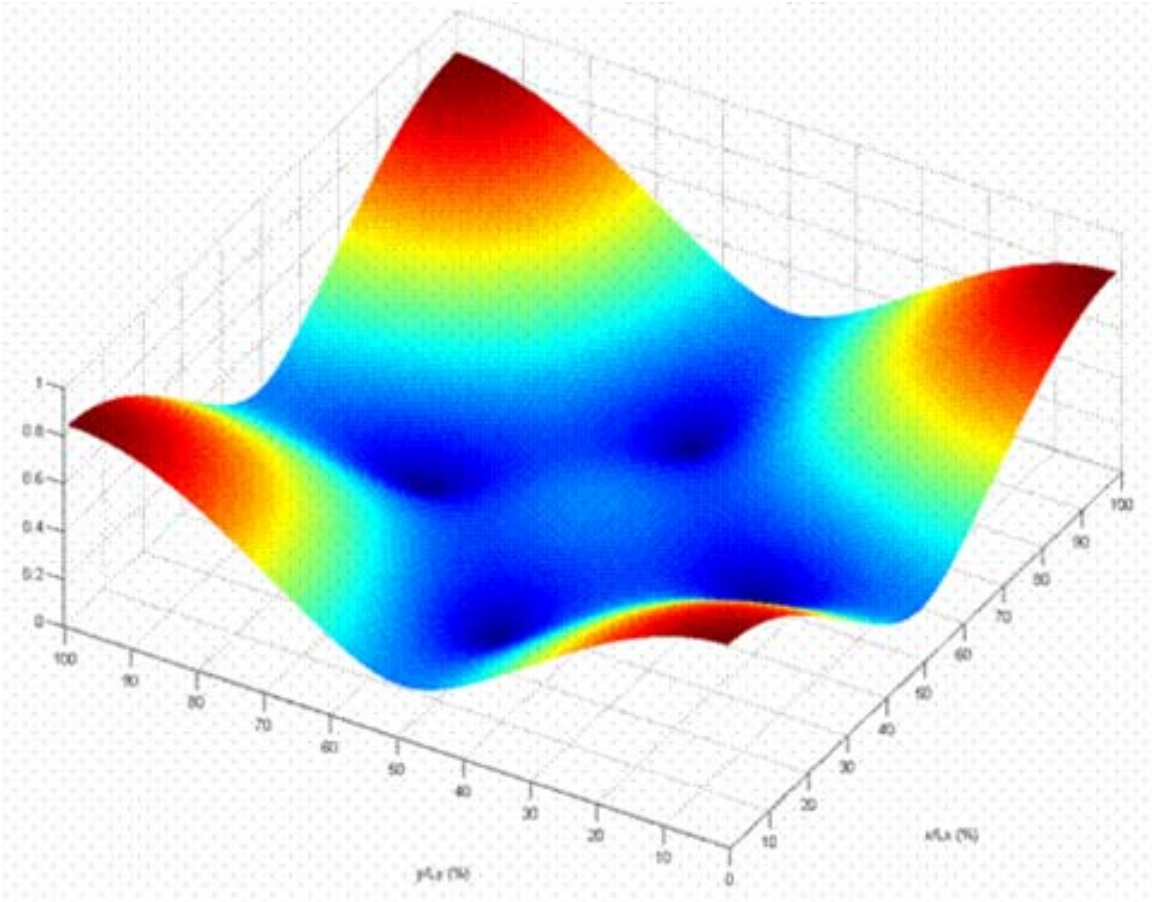

Figure 31 Potential due to pressure field of both (1,1,0) and its 1st harmonic (2,2,0).

This prompted the study of other forces that are present that may contribute to such a behavior. Secondary sound induced forces, besides the primary radiation forces described above, were identified in literature and are listed below. A few experiments were devised to match any of these forces to what we are observing. Numerical and analytical solutions were used to validate the results of these experiments confirming our hypothesized identification of all the forces present in our setup. This is discussed in more detail in Chapter 4.

CHAPTER 4

SECONDARY ACOUSTIC FORCES

4.1 Introduction

The role of primary acoustic forces has been shown. It is to collect particles towards the nodal surfaces of the field. Two questions that remain unanswered are as follows. How do they collect into surfaces that are single-particle thick (as seen in clip # 3 and 4 in Appendix B)? Why are the walls not located at the exact predicted nodal surface of the primary radiation force – but rather shifted to either side? These questions prompted the investigation of other forces that are present in the field. In order to understand the effect of multiple particles in the cavity, secondary forces were studied. The study involved an investigation of an area of nonlinear acoustics termed "acoustic agglomeration." The idea behind this is that tiny particles buoyant in a medium will tend to agglomerate when irradiated with sound waves. Much work has been done in trying to explain the origin of these interparticle forces and there exist several models that attempt to describe many interesting and widely different aspects of particle behavior. It was evident from the number of models and the debate in the literature that determining the particular model to describe the behavior of multiple particles in a sound field is a complicated and sometimes impossible task.

A series of experiments were devised in order to understand and explain the observed behavior. Interparticle forces are regarded as essential to the successful formation of surfaces with no gaps between the particles, i.e. the existence of binding forces between individual particles. In the next few sections a discussion of these forces, experiments, and some numerical work will explain the wall formation process

observed in the proof-of-concept experiments. Any theoretical description of the observed phenomena must account for the following features:

(a) the existence of a “binding force” between the particles,

(b) the single-particle thick surface formation,

(c) the existence of multiple walls for some of the modes tested, and

(d) attraction to cavity walls.

4.2 Background

Secondary radiation occurs when the scattered field of one particle alters the incident field of another. The term Bjerknes force refers to the expression derived by Bjerknes in 1909, who considered the attractive and repulsive forces between two oscillating spheres without the presence of a primary incident sound field. These forces can be regarded as those arising from the contrast in compressibility of the particles relative to the host medium (i.e. interaction between two monopoles). This force type was studied further in later years by Pelekasis (1993). König (1891) was the first to study the interaction between two closely spaced spheres in the presence of a sound wave. Embelton (1962) studied the mutual forces between two spheres in a plane sound wave. His work was aimed at two spheres with their line of centers parallel to the incident plane wave and has shown that these forces may be several orders of magnitude greater than those which would otherwise act on a single sphere in the absence of the other. He attributes this effect to the fact that each sphere lies within the scattered field of the other. Nyborg studied the problem of the mutual force between two rigid spheres oscillating in a fluid due to the influence of an incident sound field at general orientation relative to the incident wave (Nyborg 1978). In standing wave fields, particles will attract or repulse each other depending on their relative orientation to the wave vector (axis of wave oscillation motion). If the displacement vector separating the two particles is

perpendicular to the wave vector then the force is attractive, and the particles come together. If the line separating the particles is parallel to the wave oscillation, then the force is repulsive (Nyborg 1978). It was also discovered (Barmatz 1984) that this force is only effective at relatively close separation distances (on the order of particle diameter). Spengler observed that interaction forces between yeast cells are considerably stronger if the interaction is between a clump of cells and another cell than between two individual cells (Spengler 2001). Spengler concludes that larger clumps of cells act as attractive sinks to other cells in the suspension, and thus continue to become more effective as more and more cells are collected.

4.3 Types of Secondary Forces

The forces that may be involved in our acoustic shaping experiments, excluding the primary radiation force, are:

(i) mutual radiation pressure

(ii) forces due to acoustic wake effect

(iii) Oseen forces

(iv) drag forces

(v) forces due to the temperature dependence of viscosity

4.3.1 Mutual Radiation Pressure

Included in this force type is the Bjerknes force, which is the interparticle force between two monopoles. This compressibility-dependent force goes to zero at the pressure node and is a maximum at the velocity node. In our experiments particles are collecting at the pressure nodes and we will thus ignore the Bjerknes force for our purposes. The density-dependent force between two spheres of the same size was studied by Nyborg (1978) and Embelton (1962). Weiser expressed this interparticle force using the energy

densities of the incident wave fields (Weiser 1984). Groschl formulated this expression such that it includes any relative orientation between the line of centers and the wavevector (Groschl 1998),

$$F_s = 4\pi a^6 \left[\frac{(\rho - \rho_o)^2 \left(3\cos^2\theta - 1\right)}{6\rho_o d^4} v^2 - \frac{\omega^2 \rho_o (\beta - \beta_o)^2}{9d^2} p^2 \right]. \qquad (31)$$

It is clear that the second term is dependent on the relative compressibility and is proportional to the potential energy density. This is basically the Bjerknes force and is thus, for our purposes, small in comparison with the first term which is density-dependant. It is interesting to note that the dipole term is more sensitive to separation distance ($\sim d^{-4}$) than the monopole term ($\sim d^{-2}$) which is intuitive as monopoles are better radiators of sound at low frequencies (Blackstock 2000). The first term is dependant on the orientation of the particles relative to the wave oscillation direction given by the angle, θ. It is a repulsive force when θ is 0° and attractive when θ is 90°. The angle θ is measured from the wave vector to the line-of-centers, as shown in Figure 32 below.

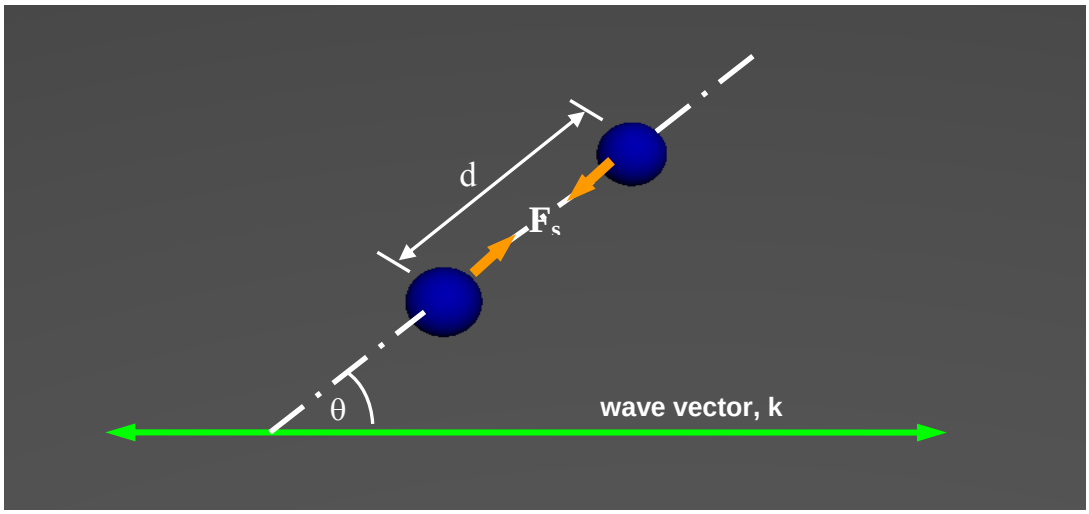

Figure 32 Particles in a standing field with their separation distance vector d at an angle θ with respect to the acoustic axis. Secondary interparticle force, F_s is shown.

Weiser attributed this force to the cluster formation within his pressure nodal planes and he also attributes the fine structure splitting of bands of red blood cells to the repulsive aspect of this force (Weiser 1984). It is believed that this force is the most dominant secondary force in our experimental setup because it provides a force field around each particle that would produce the effects observed namely, the formation of single particle thick walls and the existence of multiple walls. It is interesting to note that our observations are almost identical with those of Weiser using red blood cells in irradiated with ultrasound.

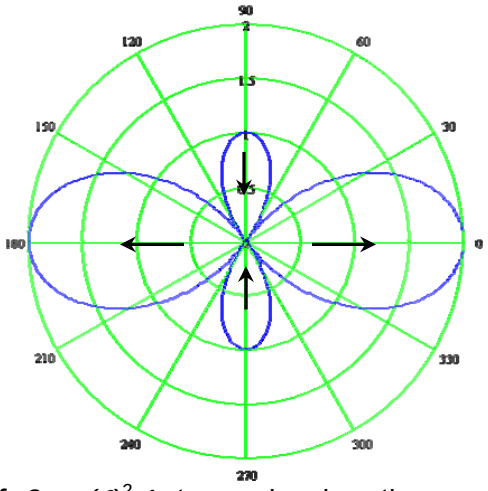

Figure 33 Polar plot of $3\cos(\theta)^2-1$ term showing the angular dependency of the secondary force. Arrows indicate the whether the region is defined as attractive or repulsive for another particle.

4.3.2 Acoustic Wake Effect

Since the propagation of sound waves involves a series of compressions and rarefactions of the fluid that hosts it, particles placed in the field will produce a wake which changes direction twice per wave period. If two particles are positioned such that their line-of-centers is parallel to the acoustic velocity then one particle will be in the wake of the other and the roles will change twice per cycle. If the Reynolds number is sufficiently high to produce a sizeable wake, then the particles will influence one another. Since the wake is a region with reduced pressure it acts as a sink to the particle that is

lagging behind the first one. This causes it to advance a little faster than the leading particle, and the same thing occurs when the roles are reversed (Hoffmann 1996). Overall, the effect is that the particles are attracted to each other. This is clearly the opposite of what the mutual radiation pressure does, with the exception that the acoustic wake effect does not affect particles that are perpendicular to the acoustic velocity axis.

At the sound pressure levels we are using and particle dimensions, it appears that the acoustic wake effect should not be a contributor to the force field. For an SPL of 150 dB the pressure amplitude is 633 Pa. For a plane standing wave the acoustic particle velocity would be only 1.52 m/s. At a frequency of 800 Hz the acoustic displacement amplitude is only 0.3 mm. This is about 1 order of magnitude smaller than the particle diameter. This would mean that the flow is not fully developed over the sphere surfaces before it reverses direction and thus we do not expect this effect to be present.

4.3.3 Oseen Forces

These forces come about as a result of waveform distortion. For finite amplitudes, a sound wave that starts out having a simple harmonic waveform will eventually distort and in the extreme case become a sawtooth wave. This is due to the nonlinearity of the equation of state of the host fluid (i.e. the pressure-density relationship). A particle in the path of a sawtooth wave will experience a higher rate of change of momentum at the leading edge than at the trailing edge of the wave. This will produce different forces at these edges (ter Haar 1978). The derivation of this force expression included a modification of the Reynolds number to include inertial effects in the far field. The Oseen force is given by

$$F_{Oseen} = 6\pi\eta\, a\, \vec{u}(1 + s|u|) \tag{32}$$

where s is a constant signifying the degree of distortion (ter Haar 1978). We have a second harmonic that is about 15 dB lower than the fundamental which means that the relative amplitude of the second harmonic is 18%. Since the Oseen force is basically a modification to the Stokes drag which makes it valid up to a Re of about 10. At the conditions of our experiments, the Re is about 200, and thus the formula for drag is not accurately described by Oseen's formula. It is thus expected that this secondary force is not significant in our experiments. This force type is mentioned in the literature mainly for particles with characteristic length scales on the order of the acoustic displacement.

4.3.4 Effect of viscosity

It was mentioned earlier that the primary radiation force expressions, whether King's or Gor'kov's both assume inviscid flows. Doinikov (1994) demonstrated that viscosity of the host fluid can have a significant effect on the primary radiation force expressions. When viscosity is dominant the effect on the force can be up to order $(ka)^3$. However, for cases where the particle radius is much smaller than the wavelength ($a << \lambda$) and much larger than the acoustic viscous boundary layer ($a >> (2\mu/\omega\rho_o)^{1/2}$) we may neglect viscous dominated effects (Woodside 1997). For our experimental setup we get a viscous boundary layer thickness of about 50 μm, two orders of magnitude smaller than the average particle diameter. We thus neglect viscous effects without sacrificing prediction accuracy.

On the other hand, it has been observed that the surface formation is adversely affected when the sound pressure level is increased beyond a certain threshold that triggers a violent acoustic *streaming flow*. This principle, is best viewed through the spectrum of energy density once again. As described earlier, energy density gradients produce radiation forces, such as the experiment conducted by Hertz and Mende described earlier. In their experiment the force was directed towards the fluid with a

lower energy density. If then, there is a sound wave that encounters a dissipative medium such as air, there will effectively be a reduction in pressure amplitude, i.e. intensity with distance from the source due to absorption. This creates an intensity gradient which corresponds to a gradient in energy density as well (recall $E = I/c$), and thus a force is produced on the fluid and is directed in the direction of decreasing energy density (Hussey 1975). This is the underlying principle behind acoustic streaming. This phenomenon only occurs at extremely high amplitudes and was not a point of interest. At the sound pressure levels used to create surfaces of about 145 dB, streaming was minimal. This was verified by using incense smoke as a particle seeder to any streaming flow inside the cavity. The smoke convection speed was on the order of a few millimeters per second. No coherent structure was being formed due to the sound waves at the SPL's of interest. The onset of streaming was seen to occur at levels near 160 dB.

4.4 Experiments to identify relevant secondary forces

4.4.1 Mutual radiation force experiment

From an examination of the secondary force Fs, given in Equation 31, it is clear that the last term was not a major contributor to the effects seen in our experiments as the particles always moved to the pressure nodes. These particles behave more like dipoles than like monopoles. The density of Styrofoam is about 40 kg/m^3 and they have a longitudinal sound speed of about 500 m/s. This contrast in the product of density and sound speed means that the first term in the secondary force expression (dipole contribution) is two orders of magnitude greater than the second term (monopole contribution), and hence the particles can be taken to be rigid. The experiment which was used to measure the primary radiation force on a single particle, as described in the

previous chapter, was modified to quantify the effect of secondary radiation forces. The fact that the particles tend to the nodes had been qualitatively validated in the very first proof-of-concept experiments. To quantify that observation, two Styrofoam spheres each about 1.5 cm in diameter were suspended from the top of the cavity. Both spheres were placed in the field such that the line of centers ran parallel to the nodal plane, and were placed at the nodal surface itself, see Figure 34. By placing the spheres at the nodal surface we eliminate any movement due to the primary radiation force. Only the lowest two axial modes 1,0,0) and (0,1,0) were run for these tests, corresponding to frequencies of 800 Hz and 1010 Hz. These experiments are shown in Appendix B in clips 5,6, and 7. Clip 5 shows attraction forces, and clips 6 and 7 show repulsion.

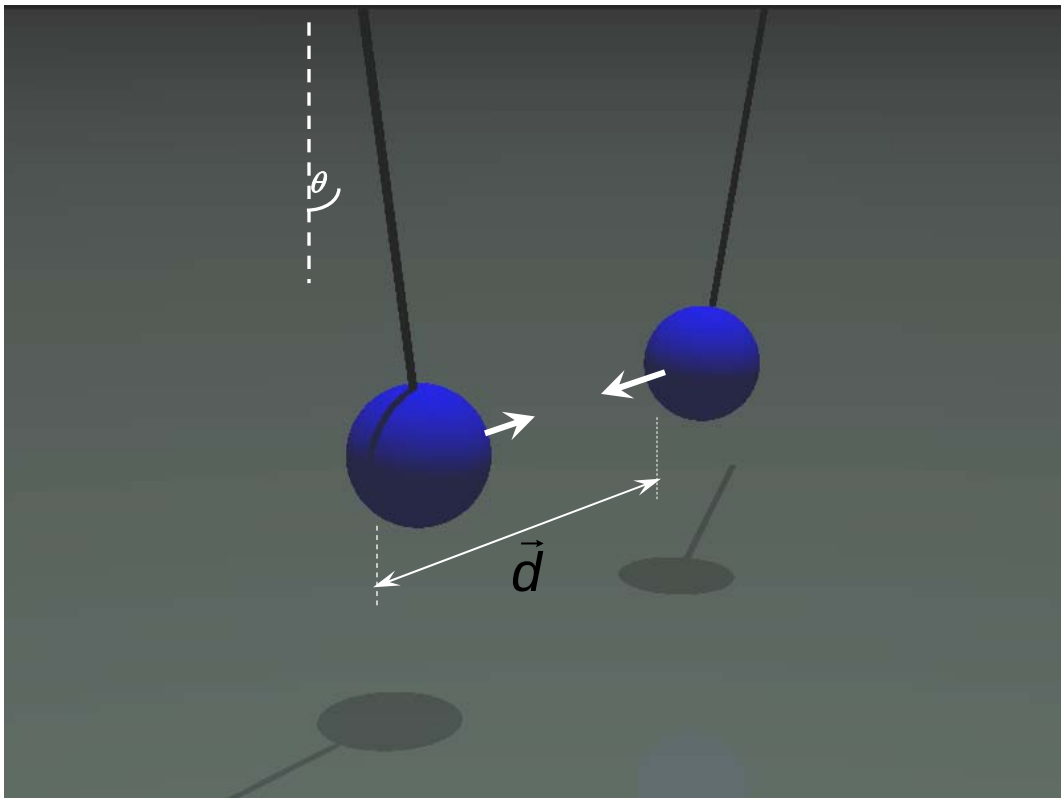

Figure 34 Schematic of experimental setup showing two spheres suspended from ceiling of chamber. In this specific configuration, the particles are in the nodal plane and thus experience attractive forces.

At an SPL of 151 dB, the spheres became displaced in response to secondary forces in the field. At an initial separation of 3 cm, the particles approached each other and made contact with each other. The sharp dependency of the force on the separation distance prevented adjustment of the SPL to a level such that the particles are displaced yet not touching. The relative orientation of the particles to the field was rotated 90^{o} and a repulsion between the particles was observed (see clips 6 and 7 in Appendix B).

4.4.2 Streaming Experiments

The fact that moderately high amplitudes were being used prompted us to question whether streaming was an issue that contributed to any observed behavior in our proof-of-concept tests. It was already determined from the initial tests that beyond a certain pressure amplitude threshold strong air currents were induced that destroyed all surface formation. The SPL value was found to be about 160 dB for a few of the lower frequency modes. Not all modes could be excited as efficiently as the lower modes and thus were never able to reach such a high SPL level for them.

A simple experiment was devised in order to capture any streaming that may be occurring at the moderate SPL levels we use to create structures. A small hole in the corner of the cavity was used to insert a lit incense stick which acted as our smoke generator. The field was switched on a few seconds later after the smoke had had a chance to fill a large portion of the cavity volume. At moderate SPL levels there was no appreciable coherent movement of the smoke. The only movement observed at these low levels was that attributable to thermally induced convection currents. As the sound level was turned much higher into the 160 dB region, the smoke started to become very diffuse as it got sucked into the stream of air now existent in the cavity due to the highly nonlinear sound wave. The streaming was high enough to change the intensity of the lit incense stick and cause it to burn faster. This confirms that streaming is not a

contributing factor to the surface formation process. Note that walls form at a SPL as low as 141 dB. If any, streaming has a negative impact on the formation process, but can be avoided by using lower amplitude sound.

4.5 Numerical field solutions

Once a suitable model for interparticle forces was adopted it was evident that a numerical solution of the field is necessary if multiple particles are to be included. The presence of multiple particles and their effect on the empty cavity field cannot be determined analytically unless a model is used that could replace the particles with elementary sound radiating elements of which the potential fields are well-known, such as monopole and dipole fields. Even if there is strong belief that substituting these particles with elementary sources is adequate, it ought to be verified against a numerical solution which does not make any such approximations. If the dipole model is validated through experiment and numerical solutions, then an analytical approach can be foreseen to be implemented in a future simulation code.

4.5.1 Empty Cavity Field

The 3D geometry of the cavity was defined in FEMLAB in its Acoustics Module. The walls were selected to be perfectly rigid since they are made out of acrylic which has an acoustic impedance that is much higher than the air inside the cavity. The particles were defined as spheres having a diameter of 1 cm. The particle density was set to 100 kg/m^3 and the sound speed in their material to 750 m/s. The boundary condition on the surface of the spheres was selected to be a continuity condition, where FEMLAB solves for the field inside them. Once the geometry of the problem was defined and the physical boundary conditions specified then the code ran an eigenvalue solver by

solving the Helmholtz equation to obtain the pressure field and acoustic particle velocity for a few modes of interest.

The pressure field for the (1,1,0) mode is shown in Figure 35, which matches the MATLAB predictions.

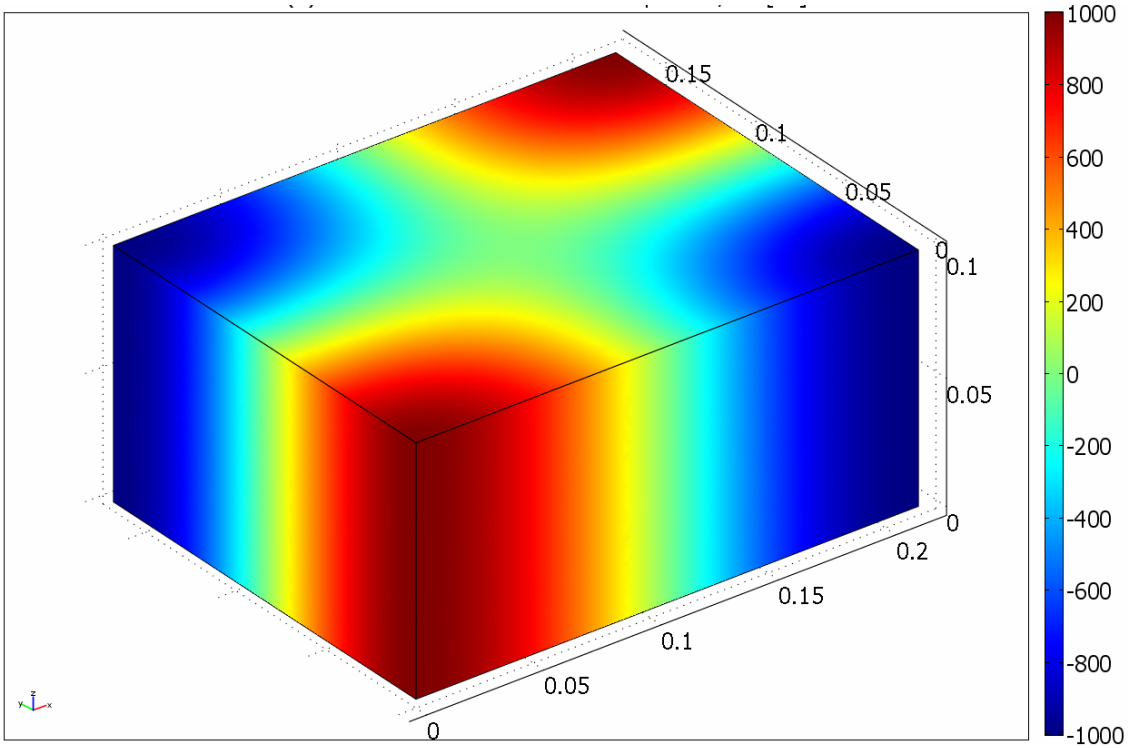

Figure 35 Pressure field for the (1,1,0) mode. Obtained using FEMLAB

4.5.2 Cavity with one particle

The field for the axial mode (1,0,0) was investigated to observe the effect of one particle. The particle was placed at the location where the empty field experiences a pressure node and midway in the other two dimensions. This corresponded to a location that is in the middle of the chamber in all dimensions. The potential was plotted along "probing" lines that were user-selected to run through the cavity. This provided information on the effect the particle has on the local field. A probe-line is shown in Figure 36 below.

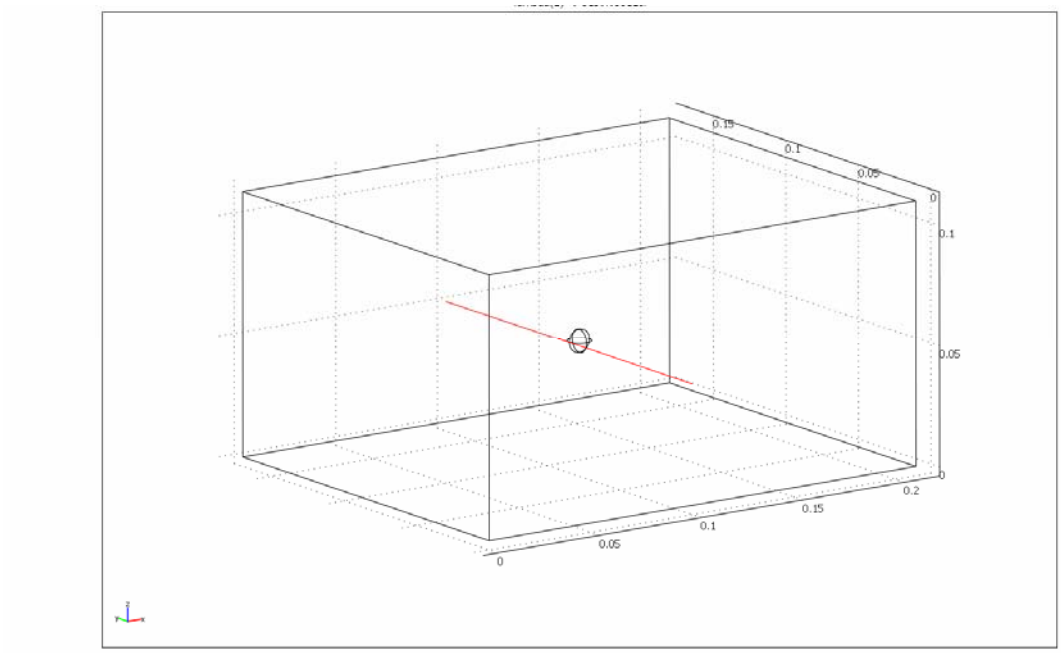

Figure 36 Cavity with sphere in middle. Red line is the line defined by the user to probe the field for any parameter.

When two lines were selected, one immediately near the particle and the other about six diameters away that were parallel to the nodal plane, the following was obtained for the potential in Figure 37. The blue line indicates that other particles will sense the presence of this particle through a repulsion force when approaching it along a line that is close to or equal to y = Ly/2 (or y/2a=8.5), where a is the particle radius. The green line shows that far away the effect of the particle is not felt.

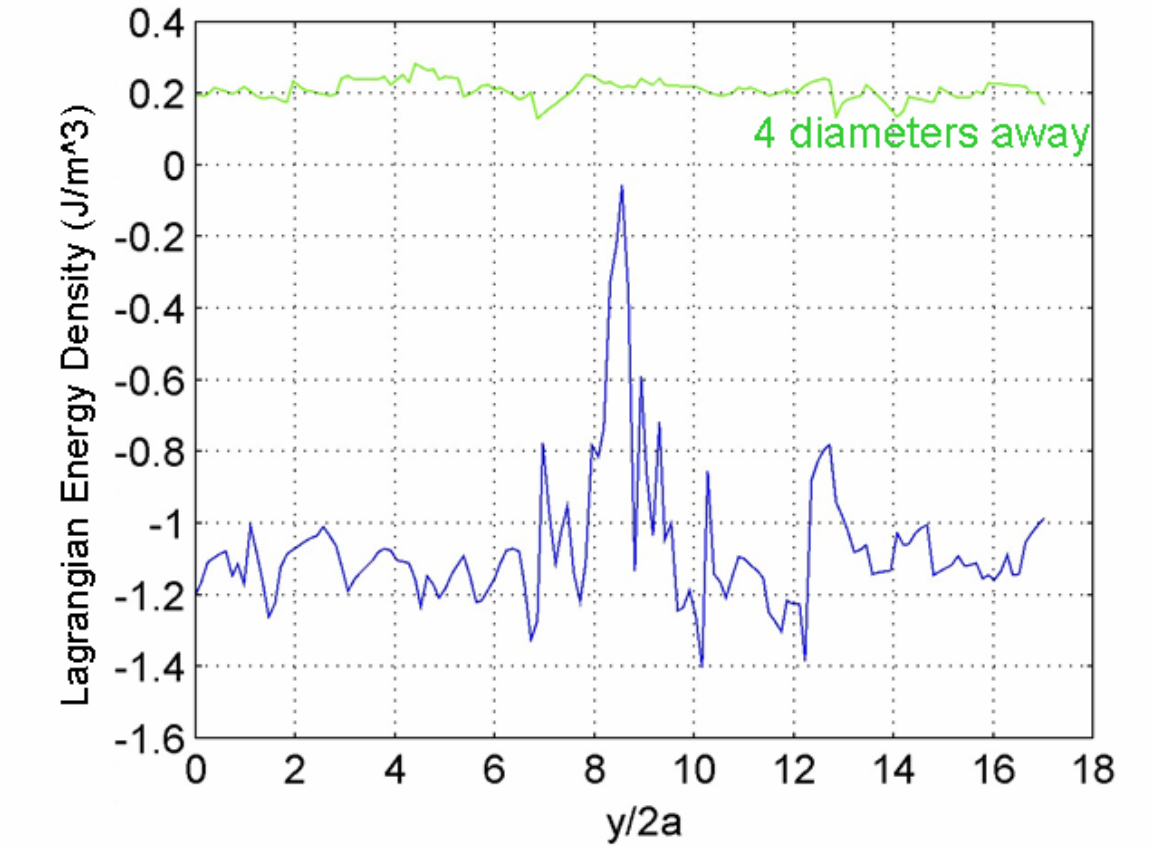

Figure 37 Blue curve is potential field along a line parallel to nodal plane and very close to the particle. Particle is located around y/2a = 8.5, its effect on the external field is that it increases the field around it in a direction perpendicular to the nodal plane. The green line is the potential field along a line that is displaced about 7 diameters away, showing almost uniform field far from the particle.

Next, a probing-line that is perpendicular to the nodal plane was selected in the near vicinity of the particle and compared to another that was further away from the particle (about 6 diameters away), see Figure 38. It is clear that the potential well closer to the particle is slightly deeper (with a larger gradient in potential) than the potential well further away. This indicates that other particles in the area will reside closer to each other because of the deeper potential well set up by neighboring particles.

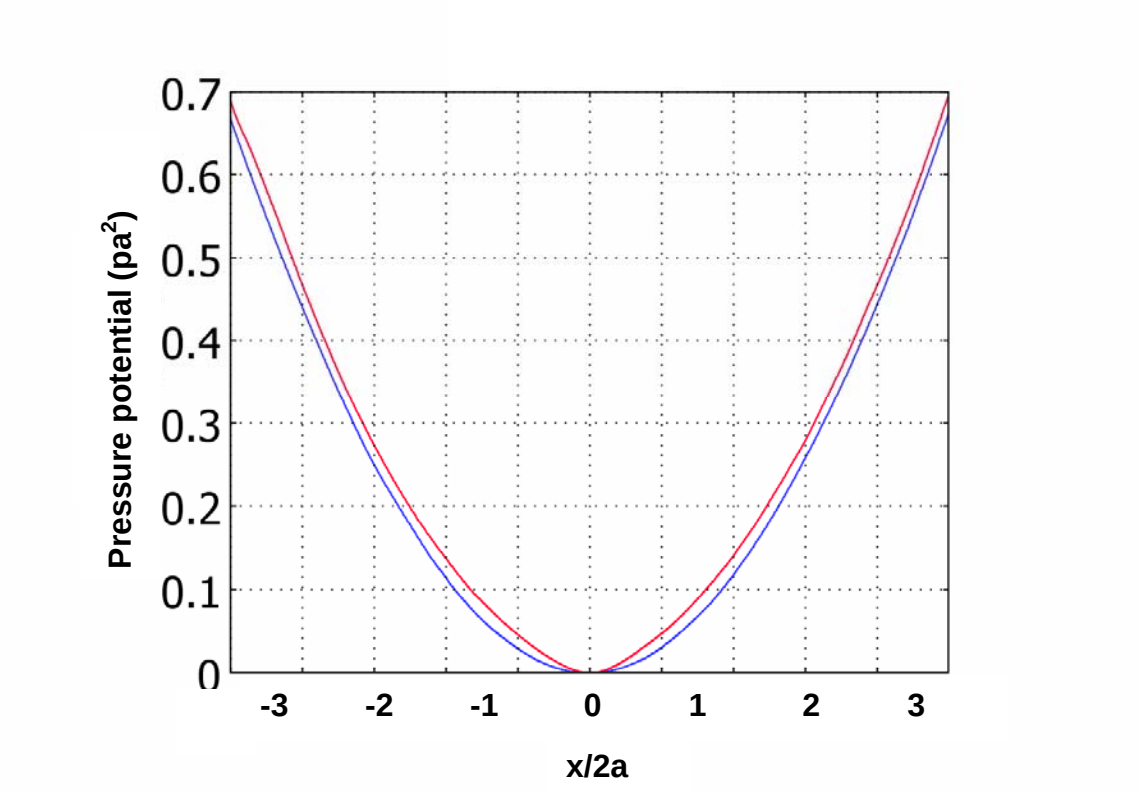

Figure 38 Blue: potential well far away from sphere; and Red: potential well very close to sphere showing an increase in the steepness of the potential well, i.e. favorable position for particles within nodal plane is close to each other.

It is clear from Figure 37 and Figure 38 that the field very close to a particle is that of or very close to that of a dipole field.

4.5.3 Cavity with multiple particles

A few spheres were placed in a line close to the bottom of the box to simulate a situation that is repeatable in the lab. The code was run and the field probed again very close to the line of spheres. The potential shows a consistent increase from the baseline value of about 0.03 every time a new particle is brought in to the line. The blue and red lines are the potential plots which correspond to probe-lines on each side of the line of spheres.

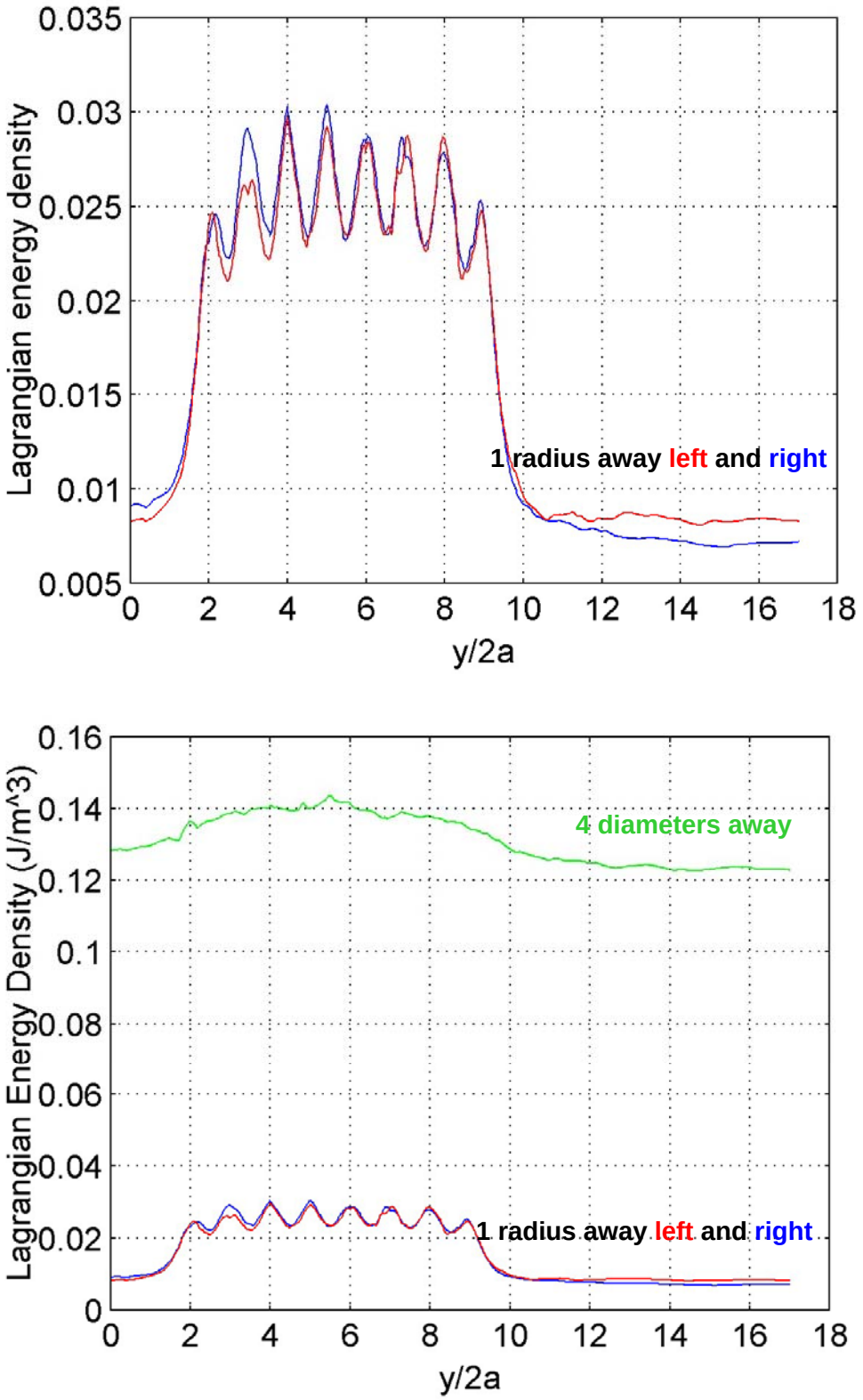

Figure 39 Energy density: ahead of (blue), behind (red), and 4 diameters away from (green) a chain of particles placed at the node.

The dipole nature of the particles in a sound field will be discussed in more general terms in chapter 6 along with analogous particle behavior in electromagnetic fields.

4.6 Results

Experiments and numerical work, show that particles much denser and more incompressible than the host fluid will behave like a dipole if the field wavelength is much larger than its diameter. The Rayleigh scattering regime allows us to neglect all scattering terms that are higher than the dipole term, i.e. only monopole and dipole terms are needed in this regime. The distinction between monopole and dipole depends on the particle characteristics in relation to the host fluid. Here, we are mainly dealing with dipoles.

Experiments revealed that indeed a secondary force field is set up in the vicinity of each particle that allows it to attract other particles along one direction and repel them along the other, orthogonal, direction. This experimental evidence agrees then with the dipole claim for two dipoles pointing in the same direction.

Due to the scale of the particles being much larger than the viscous boundary layer, no viscous effects were essential to account for. This is similar reasoning for ignoring the Oseen drag forces.

CHAPTER 5 ELECTROMAGNETIC FORCE FIELDS

5.1 Introduction

Based on the success in using sound generated force fields analogous force fields using electromagnetic waves were sought. Electromagnetic waves do not require a medium as sound waves do. Thus, electromagnetic resonators offer the promise of use in formation of large structures in space, since the cost of earth-launched objects and materials is extremely high. The concept of using TFF for in-situ space construction is addressed in Chapter 7. This chapter is centered on forces generated from the interaction of electromagnetic fields with matter. A somewhat similar order will be followed to the one used in describing acoustic forces in the previous chapters.

5.2 Literature Review

It is well known that electromagnetic waves carry both momentum and energy. An incoming electromagnetic wave impinging on a perfectly absorbing flat plate will exert a net radiation pressure, $P = QI/c$, where I is the beam intensity, Q is 1 for perfectly absorbing and 2 for perfectly reflecting plates, and c the speed of light. For a perfectly reflective surface the change in momentum is doubled and therefore the pressure is doubled ($Q=2$). The idea that light can exert forces on neutral matter was introduced as far back as Kepler and Newton and was not confirmed until Maxwell's equations for the propagation of electromagnetic waves were introduced. Maxwell calculated the forces to be extremely small for conventional light sources. With the advent of the laser several experiments have demonstrated the capability of manipulating micro-meter sized particles using momentum of laser light (Ashkin 1970). Ashkin and Dziedzic (1973) have shown that a laser beam going into or out of a dielectric liquid (they experimented with water) will exert an outward radiation pressure on the interface separating the water from

air, i.e. away from the water into the air. This is analogous to the acoustic experiment by Hertz and Mende described earlier in Chapter 3.

Ashkin (1970) was the first to report using radiation pressure to trap neutral dielectric particles. He used the radiation pressure of two counter-propagating laser beams. Higher forces were obtained (Ashkin 1986) by focusing a single laser beam and thus creating an intensity gradient. Ashkin distinguishes between gradient and scattering forces (Ashkin 1980, 1983, 1985) and proposes a variety of optical traps for neutral dielectric particles in both the Mie and Rayleigh regimes (1986). The work done by Ashkin laid the foundation for much of the work on optical tweezers. Theoreticians such as Zemanek (1998) have classified trapped objects into two groups: objects having a radius larger than $\lambda/20$ where generalized Lorentz-Mie scattering theory must be applied to express the radiation forces; and objects smaller than $\lambda/20$ (Rayleigh regime) which can be modeled as electric dipoles. In Rayleigh scattering theory, the incident electric field induces an electric dipole in the dielectric particle. The oscillations of the induced dipoles radiate a scattered field that interacts with the incident field and alters the energy density of the latter. Such interaction exchanges momentum between the fields yielding a force on the dielectric particle. This is the so-called *scattering force*. The Lorenz force acting on the induced dipole is termed the *gradient force* (Harada 1996). A detailed account of the axial force produced by a focused Gaussian laser beam on a dielectric sphere in the Mie regime is given by Nemoto (1998).

In section 5.3 a few applications of radiation pressure induced by optic fields are listed. In section 5.4 the underlying physics of the interaction of electromagnetic fields with dielectric materials and the consequent force generation are addressed. This is followed by a description of secondary forces that may be present in the field and can contribute to particle-particle forces in section 5.5. Finally, section 5.6 describes the

application of electromagnetic waves to heat the particles once they form a steady state structure in order to fuse them together.

5.3 Applications of Electromagnetically induced forces

Most of the work on electromagnetic radiation pressure has been limited to the infrared - optical regime in the context of "optical tweezers." Optical tweezers have the ability to manipulate and trap microscopic particles via the interaction between optic fields (i.e. electromagnetic fields) and matter. Starting with Ashkin's demonstrations of using radiation pressure to guide and trap particles, optic tweezers began to gain popularity as this was expanded by the breakthrough that a focused light beam attracts a small particle with index of refraction higher than the host medium, towards its beam focus. The wide range of use of optic tweezers is evident from its use in trapping and cooling neutral atoms (Chu 1986) to manipulating single living cells (Ashkin 1987). A few years later they were used to measure elastic properties of cells and molecules (Svoboda 1992). Constable (1993) has shown that a pair of pig-tailed optic fibers can be used to utilize both scattering and gradient forces to trap particles in the gap between the fiber ends. This was later used by Guck (2000) to stretch soft biological samples. The sample was being stretched due to it having a higher index of refraction than the surrounding medium. Most recently, McGloin (2004a) used laser tweezers composed of a pair of pig-tailed fiber optics to controllably push-and-pull trapped particles of various sizes. An excellent summary of the current state-of-the-art on manufacturing with light is given by Dholakia and McGloin (2004b). Tailoring of the light field is mentioned as a means of enhancing the capability of optical tweezers in molecular level manufacturing.

5.4 Theoretical Description of Electromagnetic Forces

The interaction of a neutral particle with an electromagnetic field can be characterized by the resulting momentum transfer that occurs as a result of reflection, refraction, or absorption of the wave when it meets the particle (scattering force). This occurs as a result of the difference in impedance between the particle and the background host medium. There is another force on the particle is due to the attraction of electric dipoles to regions of high electromagnetic field intensity (dipole force). These forces can be described using the Maxwell stress tensor (Mulser 1985).

In much of the literature, the scattering and gradient forces are derived independently, yet it is clear that they both originate from the same source. A neutral dielectric particle placed in an alternating electric field will polarize in response to the field. The amount of polarization is determined by the ratio of the dielectric constant of the particle to the host medium. If the physical dimensions of the particle are smaller than the wavelength (by about one order of magnitude) then the field radiated by the polarized particle will resemble that of an electric dipole. It is this field that, when combined with the external field, results in the above two forces. It is then more elegant to pursue a derivation of these two forces (scattering and gradient) from basic electromagnetic equations. Rohrbach (2001) gives a theoretical derivation of the optical forces onto dielectric matter which traces the origin of both forces to one force expression. The two forces are obtained as components of one electromagnetic force.

Starting with the well-known total electromagnetic force on a charged particle, also known as the Lorentz force,

$$\boldsymbol{f} = \boldsymbol{q}\left(\boldsymbol{E} + \boldsymbol{v} \times \boldsymbol{B}\right) \tag{33}$$

the electromagnetic force density *f* acting on a small dielectric particle or volume element with dipole moment density P is given by (Rohrbach 2001)

$$\boldsymbol{f} = \boldsymbol{P}\nabla\boldsymbol{E} + \frac{\partial \boldsymbol{P}}{\partial \boldsymbol{t}} \times \boldsymbol{B}. \tag{34}$$

Representing the external electric field

$$\vec{E}_i = \vec{E}_o e^{i(kx-\omega t)} \tag{35}$$

For small spheres, the field is uniform throughout the volume, such that,

$$\vec{\mathrm{E}}_{\mathrm{i}} \approx \vec{\mathrm{E}}_{\mathrm{o}} \qquad \mathrm{r} \le \mathrm{a} \tag{36}$$

The external electric field across the sphere causes it to polarize such that charge densities ρ_s and current densities J_s are induced on the surface. A schematic of the spatial distribution such surface charges take is shown in Figure 40.

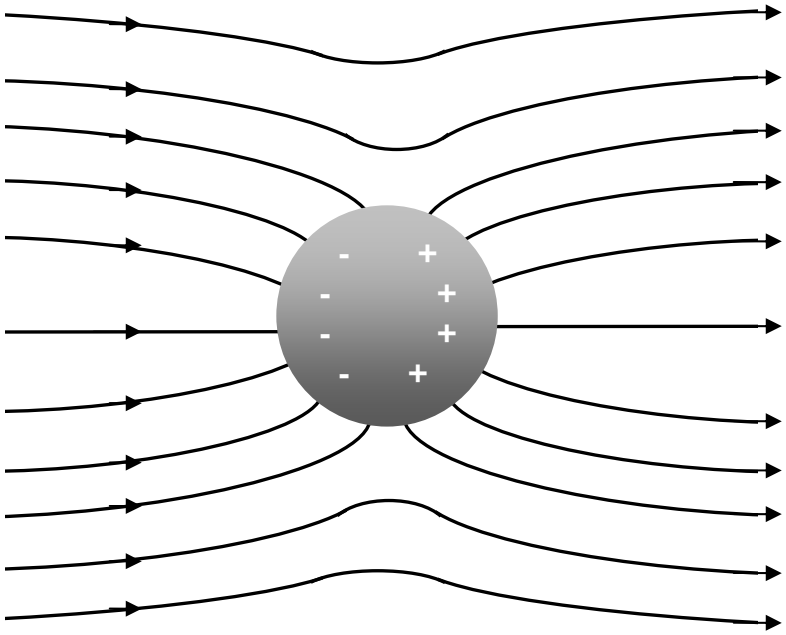

Figure 40 Dielectric sphere becoming polarized when placed in a uniform electric field pointing from left to right.

It is possible to replace the physical sphere with an equivalent charge distribution to match that shown above in Figure 40 to determine the scattered field, E_s. Since the total field, E_{tot} has to equal zero within the metallic sphere volume,

$$\begin{aligned} \vec{E}_{tot} &= \vec{E}_i + \vec{E}_s = 0 \qquad && r \le a \\ \therefore \vec{E}_s &= -\vec{E}_i \qquad && r \le a \end{aligned} \tag{37}$$

At large distances from the sphere, i.e. r>>a, the charge and current surface densities approximate that of an electric dipole. In this case, it makes the calculations much easier if the sphere is replaced with an equivalent dipole, since we know the field due to a dipole in closed form. The field due to an electric dipole is shown in Figure 41.

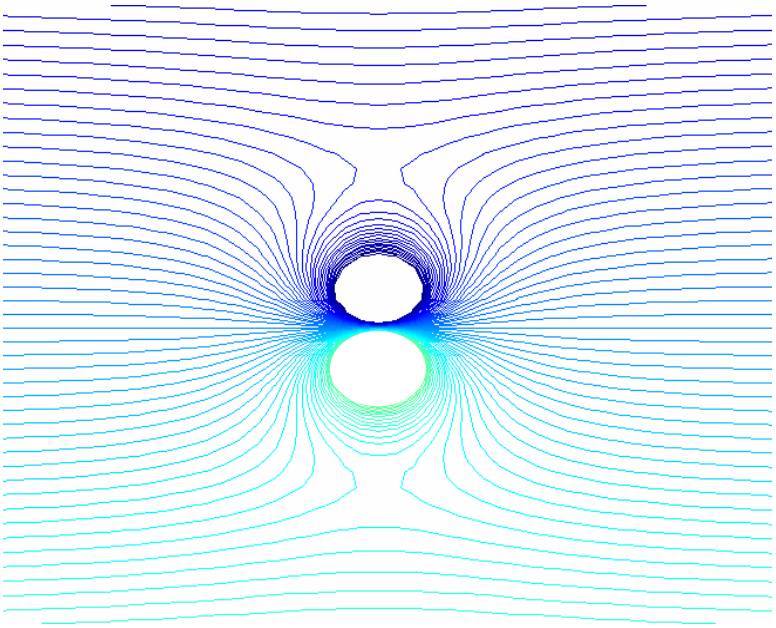

Figure 41 Field radiated from a dipole. Plot produced in MATLAB.

The vector p is the polarization vector and for dipoles always points from the –ve to the +ve charge according to convention. The polarization vector is given by

$$\vec{\boldsymbol{p}} = \alpha_{\boldsymbol{e}} \varepsilon_{\boldsymbol{o}} \vec{\boldsymbol{E}}_{\boldsymbol{i}} \tag{38}$$

The problem now reduces to a solution of the polarizability α_e. Since the field is uniform throughout the sphere volume, and the field varies negligibly during the time taken for the wave to cross the particle ($2a/c << 1/f$). Therefore the dynamic response to an alternating field is approximately that to a static field. This is the long wavelength or electrostatic limit. This approximation and the dipole equivalency simplify the problem. We can now approximate the real problem of the field scattered by the sphere by solving the field due to a dipole in an electrostatic field. The strength of the dipole is determined by the boundary conditions such that the field right outside the sphere matches the

dipole field at that location. The boundary conditions for a metallic surface are basically constraints on the electric field such that the tangential electric field is zero, i.e.

$$n \times E_{tot} = n \times E_i + E_s = 0 \qquad r = a$$

or

$$n \times E_s = -n \times E_i \qquad r = a \tag{39}$$

The electric field of a dipole is given by (Smith 1997)

$$E_{dipole} = \frac{k_o^3 p}{4\pi\varepsilon_o}\left[2\cos\theta\left(\frac{1}{(k_o r)^3} + \frac{j}{(k_o r)^2} \right)\hat{e}_r + \sin\theta\left(\frac{1}{(k_o r)^3} + \frac{j}{(k_o r)^2} - \frac{1}{k_o r} \right)\hat{e}_\theta \right] \tag{40}$$

Applying the electrostatic condition, i.e. $k_o \rightarrow 0$, and substituting into the boundary condition given by Equation 39,

$$\frac{-1}{\pi\varepsilon_o a^3}\hat{e}_r \times \vec{p} = -\hat{e}_r \times \vec{E}_i \tag{41}$$

The polarization vector p is always parallel to the electric field vector, E_i since its an induced dipole moment, and $\hat{e}_r$ can point in any direction. This produces a simple expression for the polarization vector,

$$\vec{p} = 4\pi a^3 \varepsilon_o \vec{E}_i \tag{42}$$

from which we can deduce the polarizability for a conductor,

$$\alpha_e = 4\pi a^3 \tag{43}$$

Substituting the above results into Equation 34 and the vector identity (**E**∇)**E** = ∇(**E**^{2}/2) – **E** x (∇ x **E**) and the Maxwell relation ∇ x **E** = -∂**B**/∂t, we get the force on a particle to be,

$$F = \alpha_e \varepsilon_o \left(\nabla \left|E^2\right| / 2\right) + \alpha_e \varepsilon_o \frac{\partial}{\partial t}\left[E \times B\right] \tag{44}$$

It can be clearly seen now that the total force F can be split up into its components, the first term F_{grad} which is characterized by the gradient of intensity ~ E^2, and the second F_{sctr} which is proportional to the time rate of change of momentum due to scattering. Now that a description of the behavior of a small neutral dielectric particle placed in an alternating external electric field is given and the origin of the forces onto it, we can go on to show the origin of the components of this force, i.e. the scattering and gradient forces.

5.4.1 Scattering Forces

Recalling the force exerted by a beam of light onto an infinite plane goes as *F=QI/c* with *Q=1* for perfectly absorbing and *Q=2* for perfectly reflecting implies the presence of a force everywhere the beam of light illuminates the surface. In other words, the cross section of the beam is the area on the surface that experiences a radiation pressure. This is also called the scattering cross section. In the case of finite objects the scattering cross section has to be determined. For objects in the Rayleigh regime, there exist analytical solutions. When the size of the particle becomes comparable to that of the

wavelength (Mie particles), numerical techniques have to be employed. To obtain the scattering cross section, we substitute the polarization vector in Equation 42 back into the radiated part of the dipole field in Equation 40, i.e. the 1/r terms, and the Poynting vector is solved for. When the scattering is isotropic, i.e. in the Rayleigh regime, the scattering cross section equals the cross section for the radiation pressure (Kerker 1969) and can now be expressed as,

$$C_{sctr} = C_{pr} = \frac{10}{3}\pi a^2 \left(k_o a\right)^4 \tag{45}$$

This is a classic result of the Rayleigh scattering from small perfectly conducting objects. To generalize this result to a dielectric sphere having dielectric constant ε and host medium ε_o the *Clausius-Mossotti* term gets multiplied by the polarization vector,

$$\varepsilon_o \left(\frac{\varepsilon - \varepsilon_o}{\varepsilon + 2\varepsilon_o} \right) \tag{46}$$

This term comes about as a result of the difference between the fields inside and outside the sphere, and was obtained by solving for the potential inside and outside the sphere. Appendix A gives the derivation. For the perfect conductor, the field inside is exactly equal to the external field so as to achieve the zero boundary condition at the surface. This is why for the conductor case that term did not appear because it was equal to one. The modified radiation pressure cross section becomes

$$C_{pr} = \frac{10}{3}\pi a^2 (k_o a)^4 \left(\frac{\varepsilon - \varepsilon_o}{\varepsilon + 2\varepsilon_o} \right)^2 \tag{47}$$

Intensity I, and electric field intensity E, are related by the following relation, $I = \frac{1}{2}\varepsilon_o c E^2$ (Griffiths 1989). For a harmonic electric field spatial distribution, $E = E_o \sin(k_o x)$, the force can be expressed as,

$$F_{sctr} = \frac{C_{pr}}{c} I = \varepsilon_o C_{pr} |E_o|^2 \tag{48}$$

For completeness the entire force expression is written out below, and will be used for comparisons in the next chapter, where the analogy with acoustics is discussed.

$$F_{sctr}^{emag} = \frac{5}{3}\pi\varepsilon_o a^2 (k_o a)^4 \left(\frac{\varepsilon - \varepsilon_o}{\varepsilon + 2\varepsilon_o} \right)^2 E_o{}^2 \sin^2(k_o x) \tag{49}$$

5.4.2 Gradient Forces

Going back to the Lorentz Equation 34, we study the first term in more detail. Again, for small particles, such that we can consider the external electric field to be constant over its dimensions, we can treat the problem as equivalent to an induced, simple point dipole. In this regime, the instantaneous Lorentz force acting on the dipole can be found using the electrostatics polarization found earlier in Equation 42 modified to the general dielectric case (Harada 1996) ,

$$\mathrm{F}(\mathrm{t}) = [\mathrm{p}(\mathrm{t}) \cdot \nabla]\mathrm{E}(\mathrm{t}) = 4\pi\varepsilon_o \mathrm{a}^3 \left(\frac{\varepsilon - \varepsilon_o}{\varepsilon + 2\varepsilon_o} \right) \frac{1}{2} \nabla \mathrm{E}^2(\mathrm{t}) \tag{50}$$

The vector identity, $\nabla E^2 = 2(E \cdot \nabla)E + 2E \times (\nabla \times E)$ was used with $\nabla \times E = 0$ as a result of Maxwell's equations in the electrostatic limit. To find the gradient force, the time-dependent force in Equation 50 is time-averaged. For a time harmonic electric field, the time average is taken over one period which results in the amplitude squared and a factor of ½ is introduced,

$$F_{grad}^{emag} = \langle F(t) \rangle = \pi\varepsilon_o a^3 \left(\frac{\varepsilon - \varepsilon_o}{\varepsilon + 2\varepsilon_o} \right) \nabla |E|^2 \tag{51}$$

It must be noted that in all of the above analysis, after time-averaging the form of the electric field $E = E_o \sin(k_o x)\sin(k_o y)\sin(k_o z)$. Therefore, to calculate the gradient force in the x,y,z directions, the gradient is taken in each corresponding dimension. Compare this to the scattering force which always points in the direction of the wave, i.e. along the Poynting vector direction.

5.5 Secondary Forces

It is clear from the above discussion that the main characteristic a dielectric particle takes when placed in an electric field is that of an induced dipole. Both the gradient and scattering forces were determined from the dipole approximation. In an effort to better understand what would happen when a collection of particles are introduced into the field is the subject of this section. In principle, the influence one particle has on another is expected to follow a dipole-dipole interaction.

5.5.1 Background

Based on the success of optical tweezers in manipulating single particles there has been considerable interest in organizing multiple particles to form 3D structures with features that vary from a few nanometers to a few millimeters. The challenge here is in creating an optical force field that permits a 3D structure to form with adequate interparticle attractive forces as well as a method to permanently fuse the individual particles. In 1992, Misawa et al were able to use optical tweezers to manipulate, in three dimensions, polymer latex particles suspended in solution where they created arbitrary 3D structures. They used a second, higher frequency, laser to induce photopolymerization whereby permanent fixation of the particles in three-dimensional structures was achieved (Misawa 1993). (Galajda 2001) was able to both nanofabricate a turbine and drive it by light. Terray et al (2002) used laser-initiated photopolymerization to fuse micron-sized silica spheres together. They were able to create a micro-valve which was actuated by the same optic tweezer used for fabrication. An excellent review article which identifies future prospects of this technology is given by (Grier 2003).

Following the study of interparticle forces sintering methods available using electromagnetic fields were also studied. The terms used in the literature are optical binding or photocoagulation for the attractive forces between optically trapped particles. Silver colloids were observed to coagulate when irradiated at visible wavelengths and coalesce when irradiated with UV (Satoh 1994). Hallock calculates the optical forces between two closely spaced metallic particles by regarding their radiated fields as those due to electric dipoles (Hallock 2005). They show that the interparticle force is attractive when the dipole moments are parallel and collinear (i.e. head to tail configuration) but repulsive when they are not collinear. Thus, for linearly polarized light, particles should form lines along the polarization direction. In electrostatic fields particles were shown to form lines (Park 1998). Microwave fields were responsible for the formation of “pearl

chains" of oil droplets in water as was observed by Herrick (1958). The dipole-dipole interaction force scales linearly with electric field intensity E^2 and falls off as r^{-4} (Hallock 2005). Karpov et al gives the energy of a dipole-dipole interaction as

$$U(r) = -2\alpha^2(\omega)|E|^2 r^{-3} \tag{52}$$

where $\alpha(\omega)$ is the optical polarizability of the particles, E is the electric field strength, and r is the distance separating the two particles (Karpov 2002). It is clear that the force goes as r^{-4} since it is obtained by taking the gradient of the interaction energy, U. Surface plasmon resonance can greatly amplify the dipole-dipole force due to resonant increase in the polarizabilities of metal colloids. Iida et al calculated that 10 nm particles of zinc oxide of copper chloride should experience 10,000 to 100,000 times more force from lasers tuned to their surface plasmon resonance frequency than from lasers that are not (Iida 2003).

5.5.2 Dipole-Dipole Force

Searching for the origin of the dipole-dipole interaction energy, we recall that in general, the energy of a single dipole p in an electric field E

$$U = -p \cdot E \tag{53}$$

The electric field produced by the first dipole p_1 is

$$E_1 = \frac{1}{4\pi\varepsilon_o r^3}\left[3(p_1 \cdot \hat{r})\hat{r} - p_1\right] \tag{54}$$

So now, a second dipole p_2 brought close to p_1 and separated by a distance r should have an interaction energy given by

$$U = -p_2 \cdot E_1 = \frac{1}{4\pi\varepsilon_o r^3}\left[p_1 \cdot p_2 - 3(p_1 \cdot \hat{r})(p_2 \cdot \hat{r})\right] \tag{55}$$

This interaction potential energy is plotted below in a 3D polar plot using MATLAB.

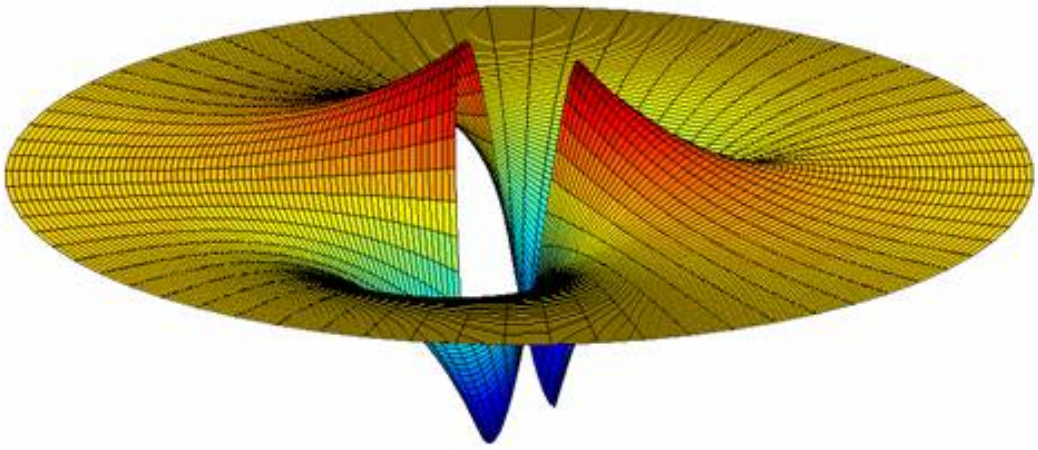

Figure 42 Polar plot in 3D of the potential interaction energy between two interacting dipoles with dipole moments p_1 and p_2 pointing in the same direction. Clearly, the field is such that there is attractive forces along one axis (almost perpendicular to page) and repulsive forces along a perpendicular axis (almost horizontal across page). Plot produced in MATLAB.

From this energy, the force can be computed by taking the negative of the gradient,

$$F_s = \frac{p_1 \cdot p_2}{r^4}\left[1 - 3\cos^2(\theta)\right] \tag{56}$$

The polarizations p_1 and p_2 contain both electric field E and particle radius cubed a^3 and thus this makes the force proportional to E^2 and a^6. A schematic polar plot of the behavior of this force is shown below,

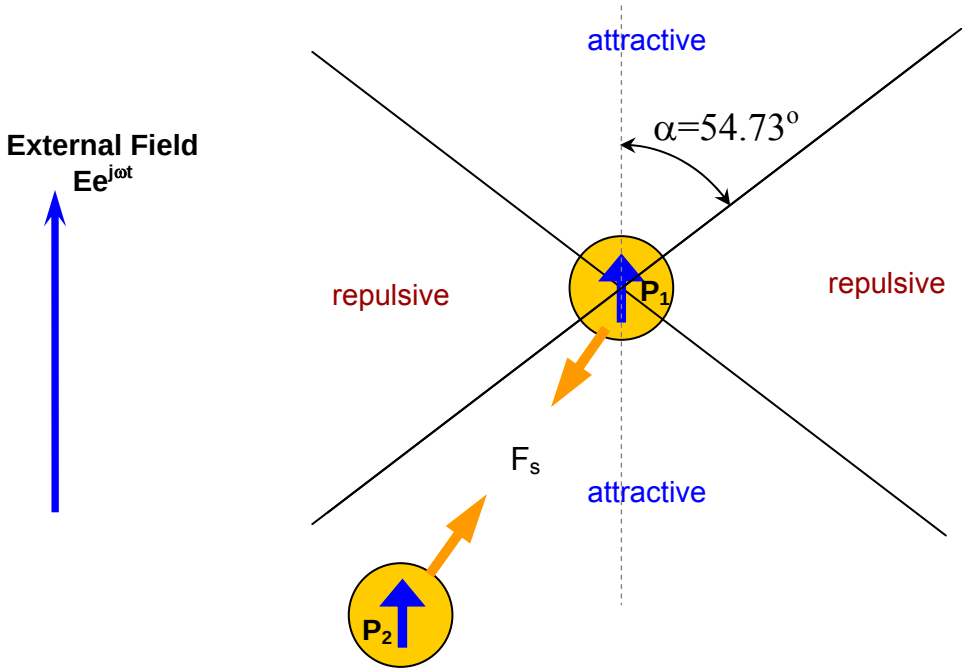

Figure 43 Schematic showing the regions of attraction and repulsion between two induced dipoles P_1 and P_2 in 2D.

It is clear that the presence of multiple dielectric particles in an electromagnetic field influence each other through their coherent radiated fields. This interaction can be described analytically using the dipole-dipole interaction force. These analytical expressions describe the behavior of two dipoles in 2D. For the 3rd dimension it is clear, albeit qualitatively, that to extend this theory we rotate the above attraction/repulsion zone about the dotted axis shown. This yields a space around each induced dipole that experiences attraction along one axis and repulsion along the other two. Thus, the resulting structures in electromagnetic resonant fields are chains that can vary in 3D space. A comparison is made with the structures formed in acoustics in the next chapter.

5.5.3 Numerical calculations

In an effort to build up a prediction capability of the behavior of particles in an electromagnetic force field a numerical calculation of the field was achieved in FEMLAB (now named COMSOL Multiphysics). The field around a spherical particle placed in a resonant cavity is of particular interest to determine if our theoretical claims above are valid. FEMLAB has an Electromagnetics Module for modeling electromagnetic fields and waves. The range of problems that this module can solve is: electrostatics, magnetostatics, low-frequency electromagnetics, in-plane wave propagation, axisymmetric wave propagation, full 3D vector wave propagation, and full vector mode analysis in 2D and 3D (COMSOL 2006).

5.5.3.1 Geometry definition

A rectangular cavity with dimensions identical to the acoustic cavity defined previously was defined using COMSOL's drawing tool. The reason for choosing equivalent cavities is to allow for a one-to-one comparison, which will be done in the proceeding chapter. Two spheres were then added to the geometry such that they were both located inside

the cavity such that their line-of-centers lied in a plane that was located half way along the cavities longest dimension (i.e. an yz plane at x=Lx/2). The composite geometry is shown in Figure 44.

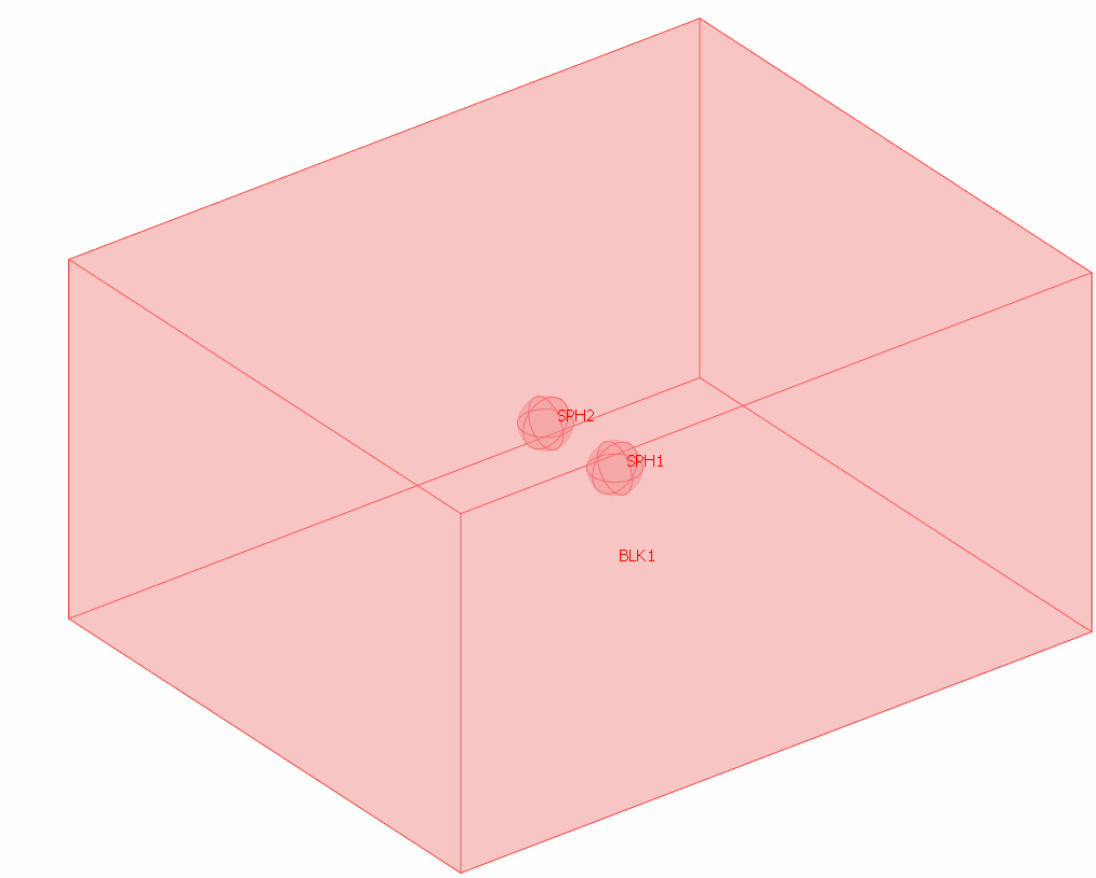

Figure 44 Rectangular cavity and two spheres located within its volume define the geometry to be solved for.

5.5.3.2 Physical properties and equations definition

The 3D Electromagnetic Waves application mode was selected from the Electromagnetics Module within COMSOL 3.2a to solve the problem defined above. The application mode properties were as follows with underline denoting selection:

Default element type:	Vector - Linear, Vector - Quadratic, Vector - Cubic
Analysis type:	Harmonic propagation, Eigenfrequency, Transient propagation
Solve for:	Electric Field, Magnetic Field

The governing Helmholtz equation can be written in the following form

$$\nabla \times \left(\nabla \times \mathrm{E} \right) - \mathrm{k}_\mathrm{o}^2 \varepsilon_\mathrm{r} \mathrm{E} = 0 \tag{57}$$

where the free space wavenumber k_o is given by

$$\mathrm{k}_\mathrm{o} = \omega \sqrt{\varepsilon_\mathrm{o} \mu_\mathrm{o}} = \omega / \mathrm{c}_\mathrm{o} \tag{58}$$

where c_o is the vacuum light speed. Taking the divergence of Equation 25 the electric form of Gauss' law is obtained

$$\nabla \cdot D = 0 \tag{59}$$

This is satisfied implicitly from the Helmholtz equation, unless a periodic boundary condition is used in which case this has to be explicitly solved for. When using vector elements, the eigenfrequency solver may find a large number of false eigenfrequencies that are almost zero. The above condition helps avoid these false modes when explicitly imposed.

5.5.3.3 Boundary and initial condition specification

The problem is defined such that the cavity interior walls perfectly reflect all the incident waves upon them, i.e. perfect conductors, for which the boundary condition is defined as

$$\mathbf{n} \times \mathbf{E} = 0 \tag{60}$$

At the interface between the surface of the two spheres and the host medium, which is vacuum in this case, we use the natural boundary condition which ensures continuity of the tangential component of the electric field

$$\mathbf{n} \times \left(\mathbf{E}_1 - \mathbf{E}_2\right) = 0 \tag{61}$$

This is known as the continuity boundary condition within the Electromagnetics Module.

5.5.3.4 Grid generation

The built-in grid generator automatically generates finer mesh where there are fine geometrical details. There is an option to refine the mesh more than once. Standard practice states that a minimum of 10 linear elements per wavelength is needed to adequately resolve a wave. The image in Figure 45 is an image depicting the final mesh used in the calculations that follow.

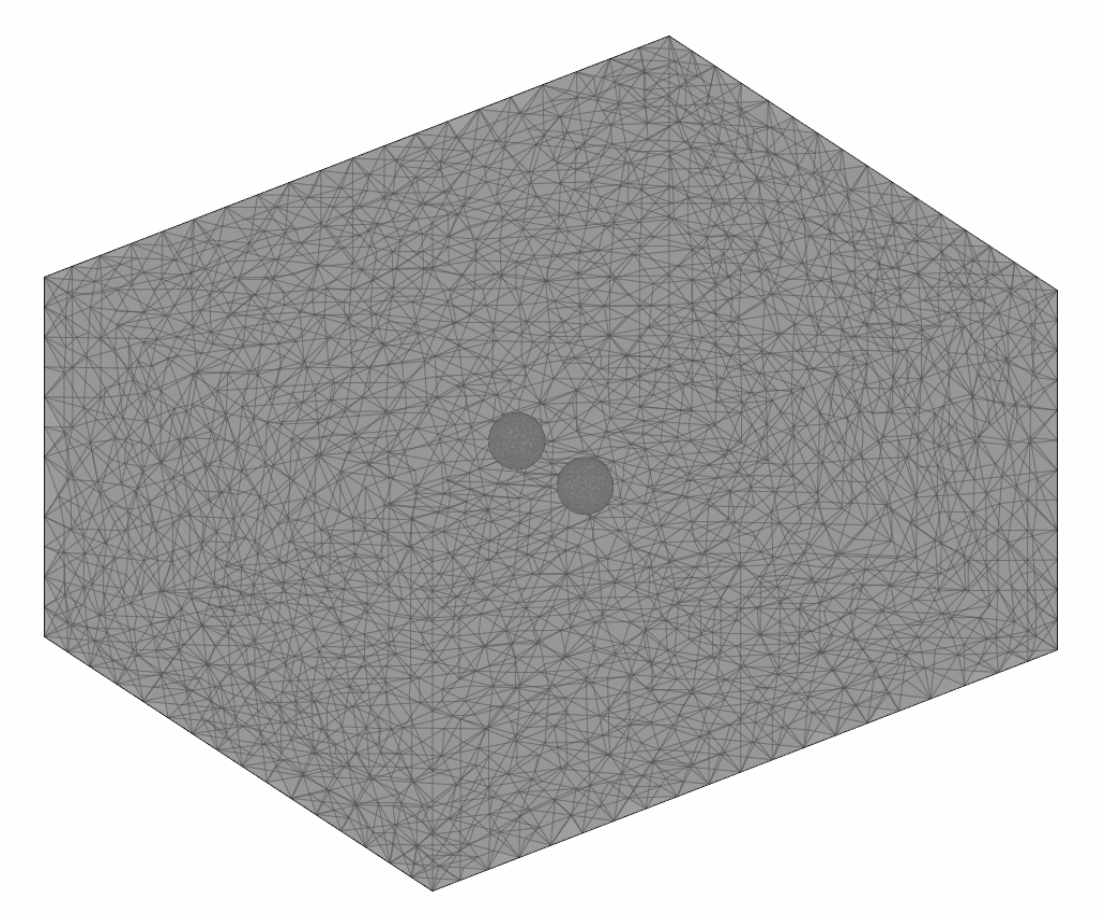

Figure 45 Final meshed geometry using FEMLAB's built-in grid generator.

The final mesh statistics were: number of degrees of freedom 218,529; number of elements 156,700; number of boundary elements 6,412; and number of edge elements 352.

5.5.3.5 Analysis specification and execution

FEMLAB's default solver is optimized for the typical case for each application mode and analysis type within the Electromagnetics Module. For 3D problems a large amount of the machine's memory is used, and thus tuning the solver is a time saver. This is done in the solver settings. One way to save memory is to impose only symmetric matrices. In our problem this is the case since we are solving for the eigenfrequencies of a cavity.

Problems where that is not the case usually involve time-harmonic analyses or periodic boundary conditions.

5.5.3.6 Postprocessing and visualization of results

The second eigenfrequency (1.53 GHz) solution was chosen since it had a dominant electric field in the y-direction. With the two spheres positioned such that their line-of-centers is parallel to the y-axis as well, this mode enables us to examine our earlier hypothesis of interparticle attraction forces in this configuration. The electric field was plotted along the plane that cuts through the center of the cavity as well as through both spheres with a normal directed along the x-direction, as seen in Figure 46. The white areas in the plot are due to values of the electric field at that point lying outside the range. This was done to allow a better visualization of the field due to the normal mode of the cavity, otherwise the range becomes so large that the details of the field are masked by the high values near that spheres.

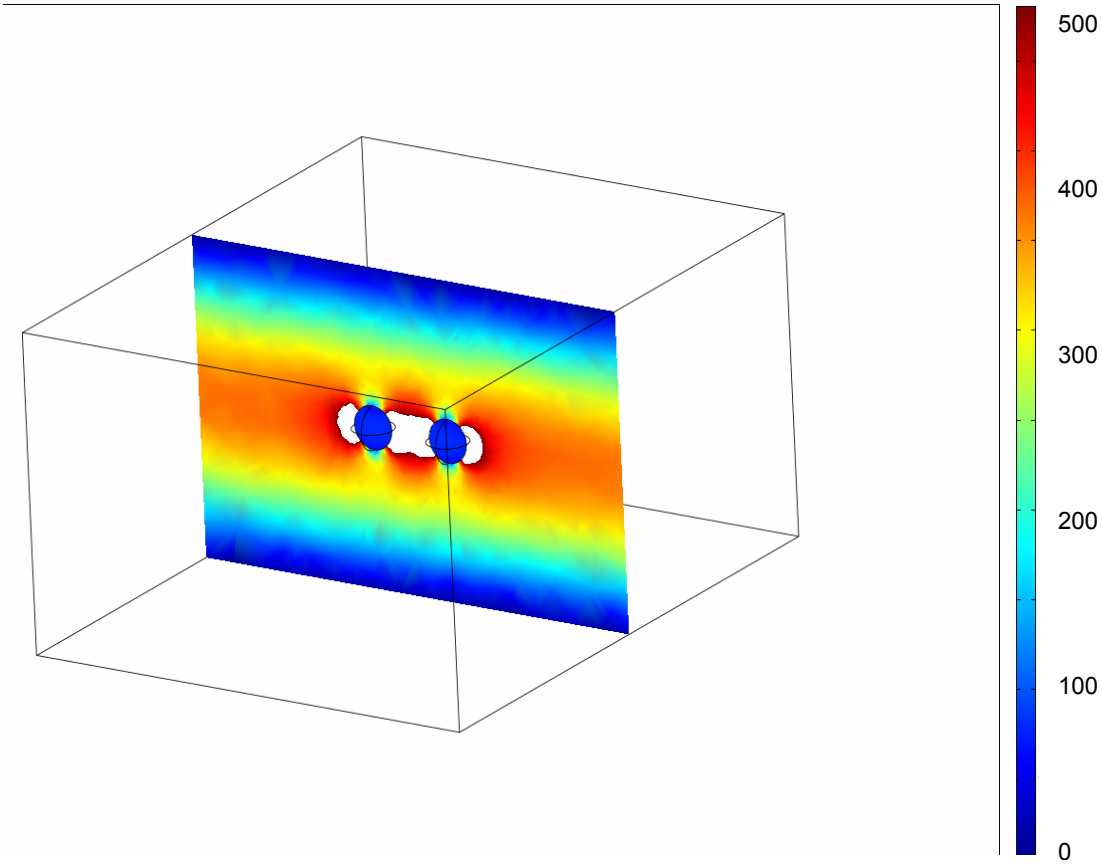

Figure 46 Electric field along yz plane located midway at x=Lx/2.

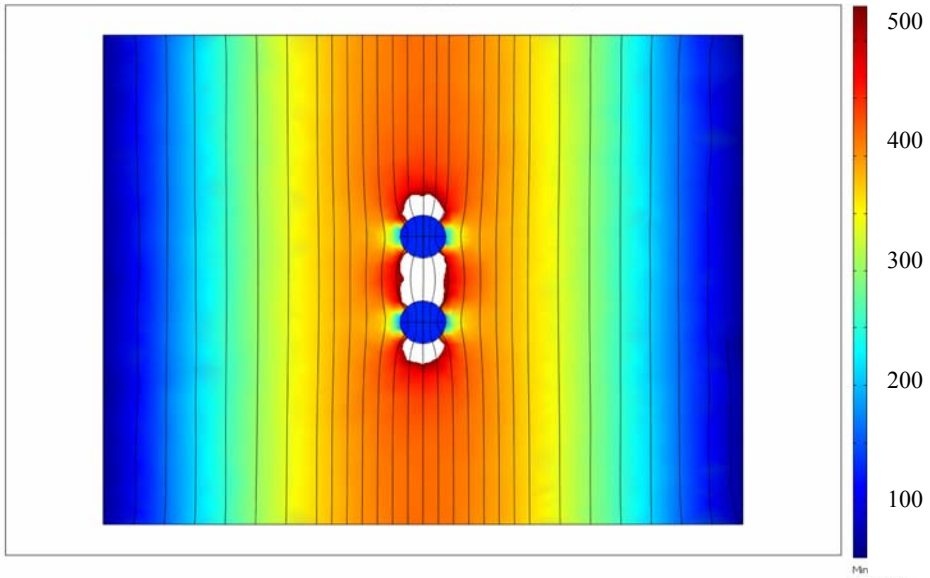

Figure 47 Electric field plotted along xy plane located halfway up the height of the box at z=Lz/2. Streamlines are also added to illustrate dipole behavior.

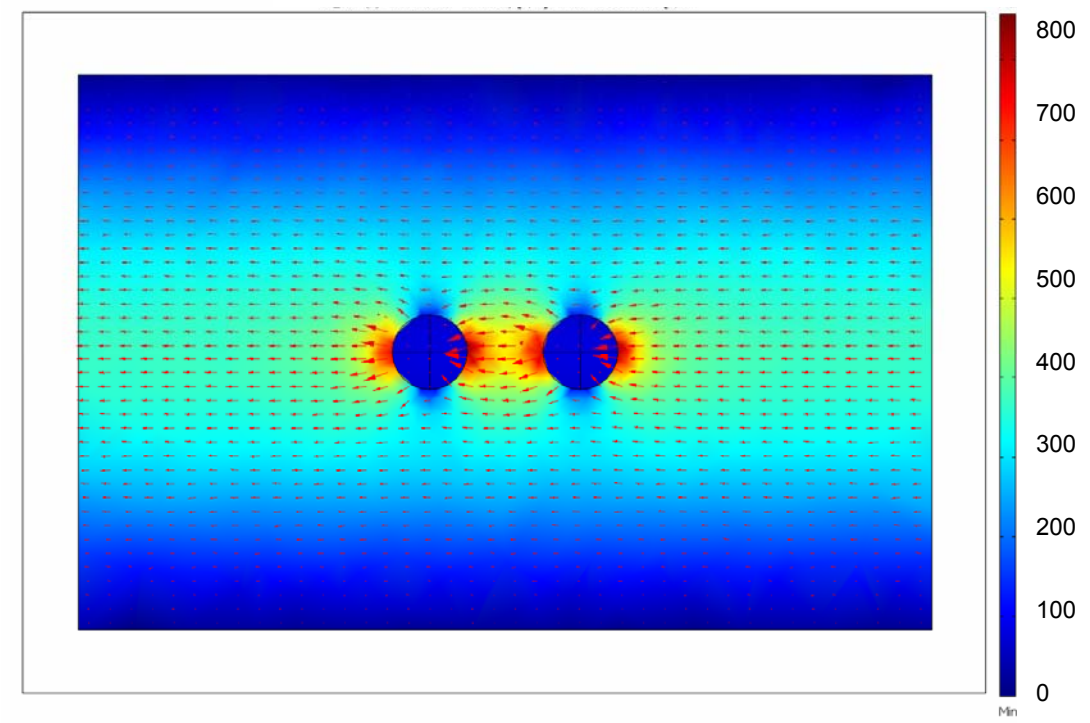

Figure 48 Electric field plotted on same plane defined in Figure 46 with a larger range for the electric field magnitude. Dipole fields are clearly seen to exist around each sphere. Arrows are electric field vector field.

To investigate the attractive-repulsive force field generated around a dipole as described in Figure 42 and Figure 43 we place a line through the cavity to probe the field with at the location the line is placed at, as was done in the previous chapter. First we place a line that runs parallel to the x-axis and somewhere far from the spheres (about 4 diameters away). The electric field along that line is shown in Figure 49 as the blue curve. Next, this line is then moved closer to one of the spheres yet without intersecting it. The field along that line is shown as the red curve. The abscissa is normalized by the particle diameter 2a.

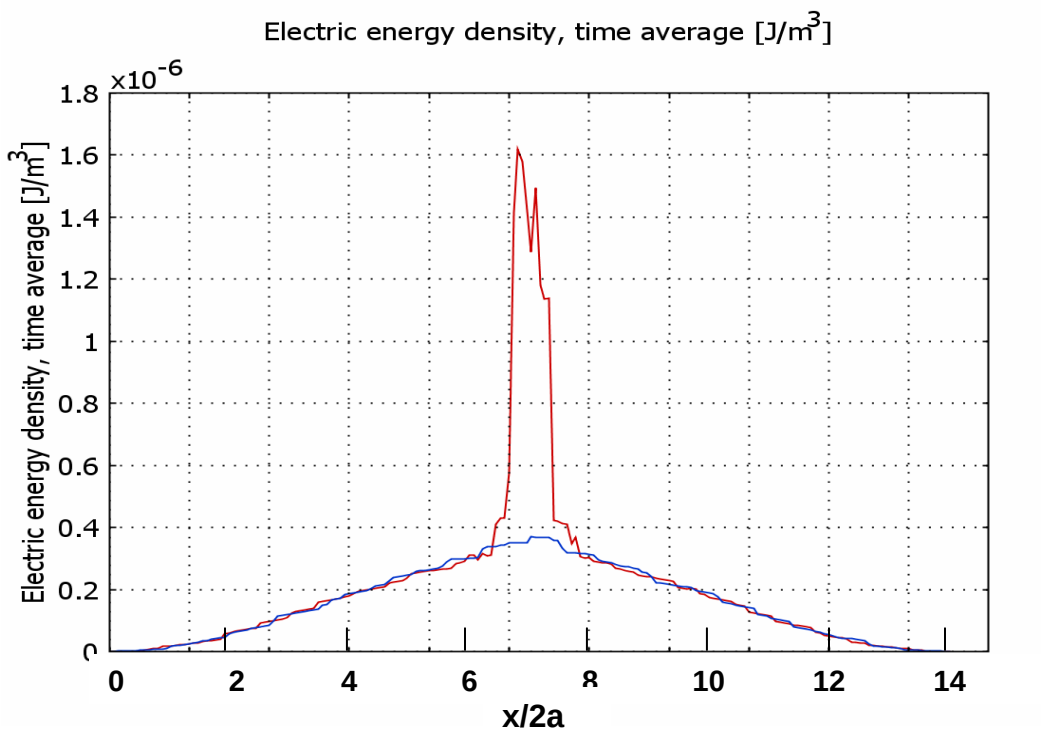

Figure 49 Plot of energy density along two lines that lie parallel to the x-axis. (Blue) line is far away from spheres, (red) line is very close to one of the spheres.

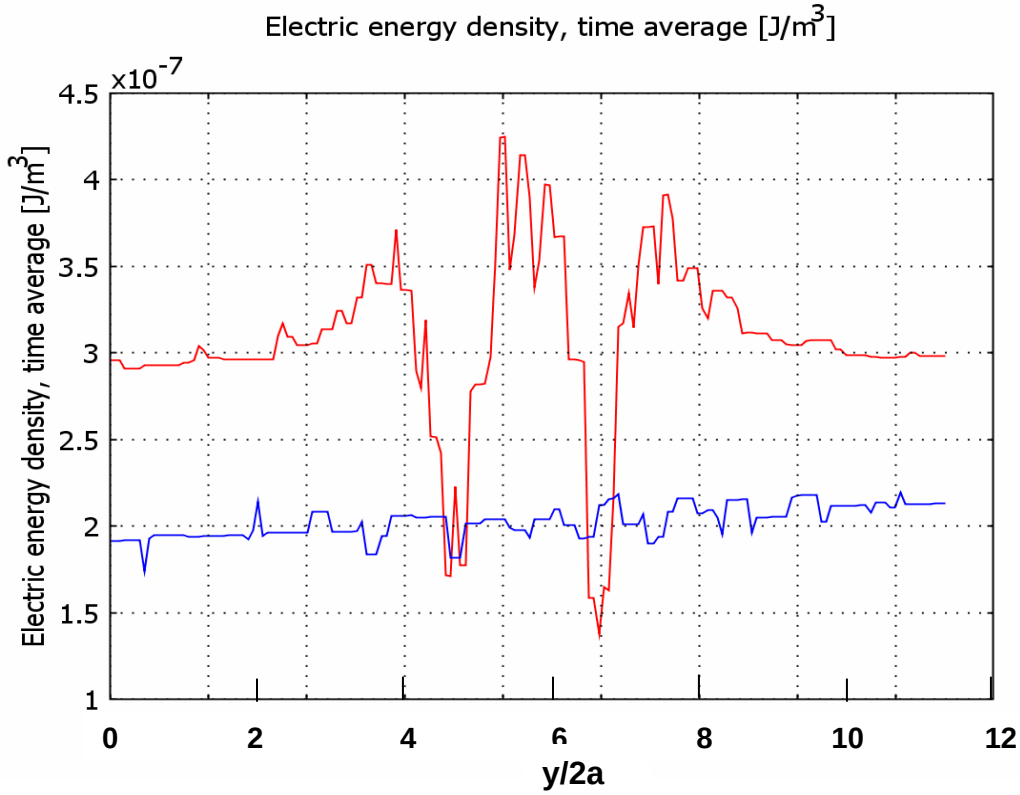

Figure 50 Energy density along two lines parallel to the x-axis. (Blue) line is far from spheres, (red) is close to both.

From the two figures above it is clear that the field around each sphere is such that it could be modeled by an electric dipole. The large increase in energy density in Figure 49 in the vicinity of the sphere shows that this region will attract other dipoles since its another local intensity maximum. Along the y-dimension, we see in Figure 50, that the region right next to the spheres experiences a local energy density minimum which would repel other dipoles close by. The red curve shows that between the twp spheres there is a slightly higher energy density which is what will cause the two particles to coagulate. In other words, the analytical plot in Figure 42, was qualitatively reproduced using a numerical solution. Thus a chain of particles can form along the y-axis for this specific mode. The formation of a complete wall would mean that there has to be another attractive force mechanism between individual chains. This is explained briefly in the next chapter.

Along with the work found in the literature, it is appropriate to hypothesize that dielectric spheres in an electric field will behave as dipoles and thus will influence each other through their mutual scattering and thus their interaction is determined through the dipole-dipole interaction.

5.5.3.7 Simpler 2D geometry to obtain qualitative results

For the interaction between two small particles a two-dimensional electrostatic equivalent problem was solved. An in-plane electric currents application mode within the Electromagnetic Module was used as the environment in which to solve this approximately equivalent 2D problem. A trapezoid domain was defined to obtain a linear gradient in the electric field. The smaller side had a defined electric potential V=100 volts and the larger side was grounded (V=0 volts) whereas the two “angled” sides were insulated $n \cdot J=0$. A circular subdomain was defined within that domain and had a relative permittivity of 5 compared to the main trapezoid domain which was set to 1. All

geometries defined had a thickness of 1 m. The boundary condition between the circular and trapezoidal domains was a continuity condition $n\cdot(J_1-J_2)=0$.

The entire domain was meshed using the grid generator built in FEMLAB. For quasi-static problems we can neglect the coupling between the electric and magnetic fields. This is justified in our case since we are interested in the field behavior in the neighborhood of a single particle which is much smaller than the wavelength so that the changes occurring across the particle can be regarded as uniform and changing slowly relative to the time it takes for the wave to propagate through the entire particle volume. In other words, induced currents are neglected. As described in previous sections, this implies that the following is true, $\nabla\times E=0$. Since the electric field is irrotational, it can be described in terms of an electric potential V such that $E=-\nabla V$. Combining the time-harmonic equation of continuity of charge,

$$\nabla \cdot J = \nabla \cdot \left(\sigma E + J^e\right) = -\omega\rho \tag{62}$$

with the equation,

$$\nabla \cdot D = \rho \tag{63}$$

results in the following

$$-\nabla \cdot \left(\left(\sigma + j\omega\varepsilon_o\right)\nabla V - \left(J^e + j\omega P\right)\right) = 0 \tag{64}$$

In effect, since we did not specify any conductivity and both J^e and P = 0, the equation solved was Laplace's equation.

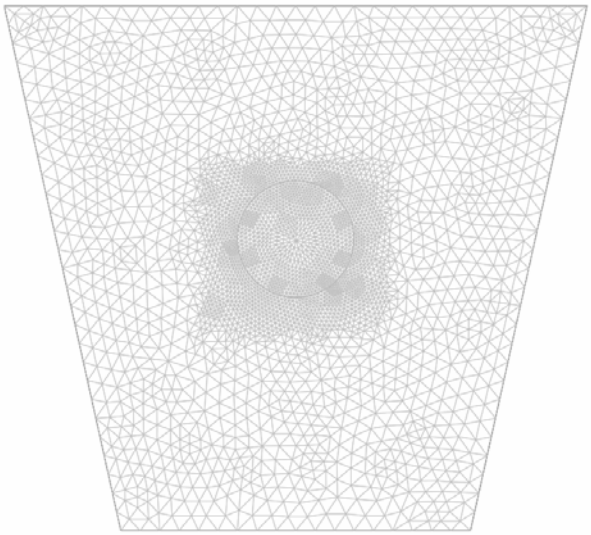

Figure 51 Meshed 2D geometry produced in FEMLAB.

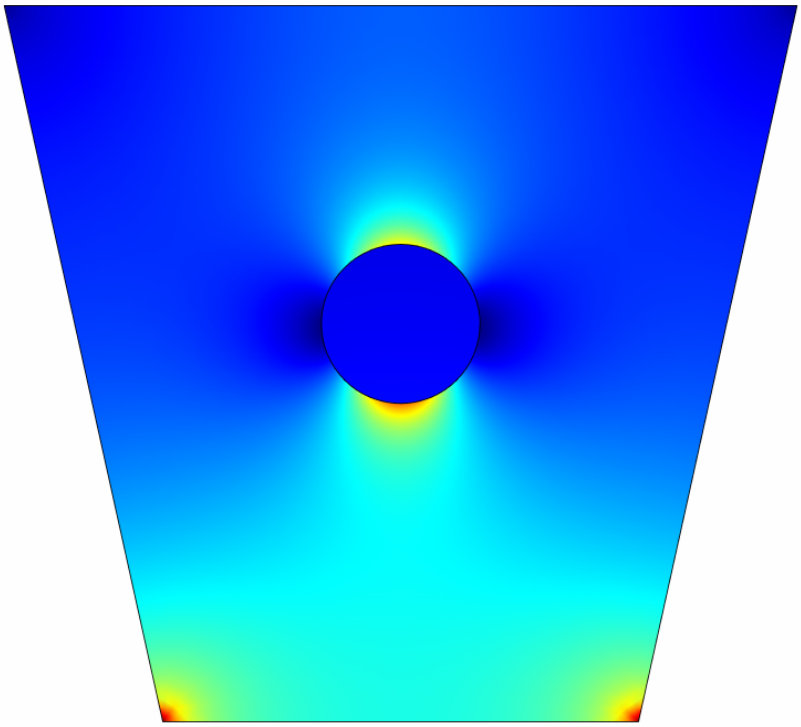

Figure 52 Time-averaged energy density showing a peak along vertical and trough along horizontal lines running through the dielectric particle.

Note the “more positive” energy density value right under the particle in Figure 52 signifying a higher attractive force pulling it downwards towards the region of higher intensity, as expected.

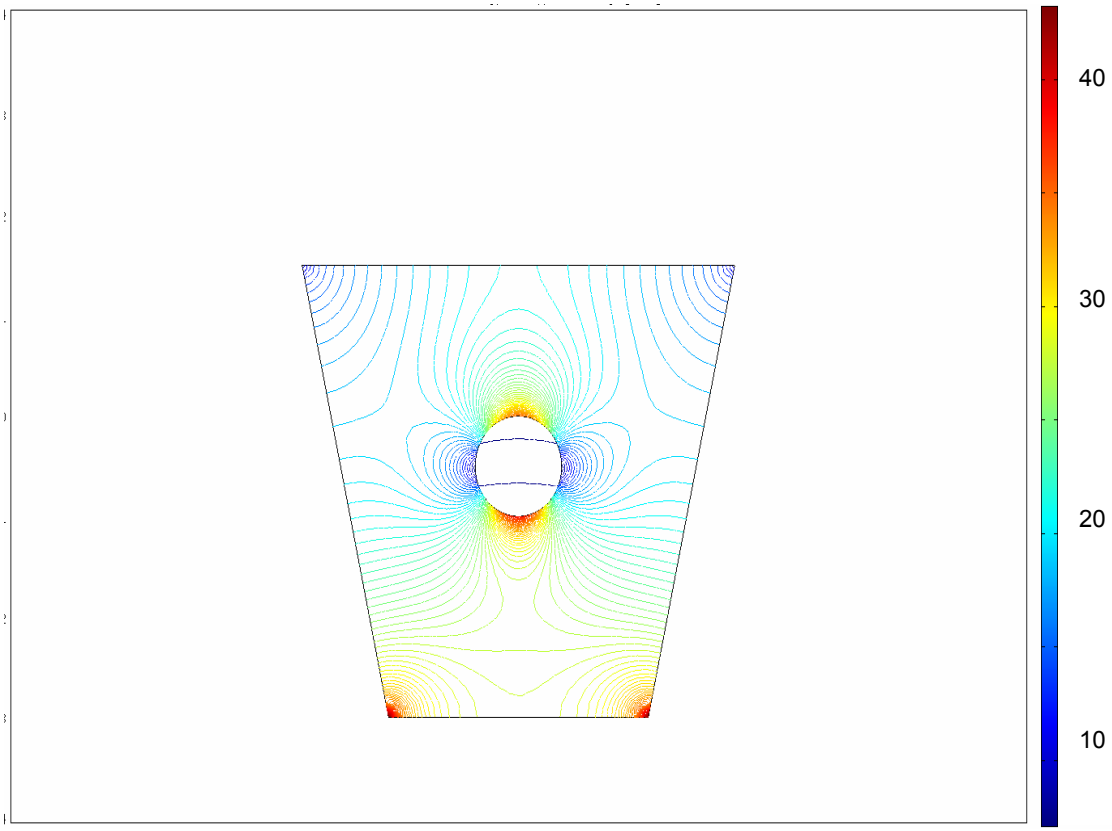

Figure 53 Contour plot of energy density around particle (J/m^3)

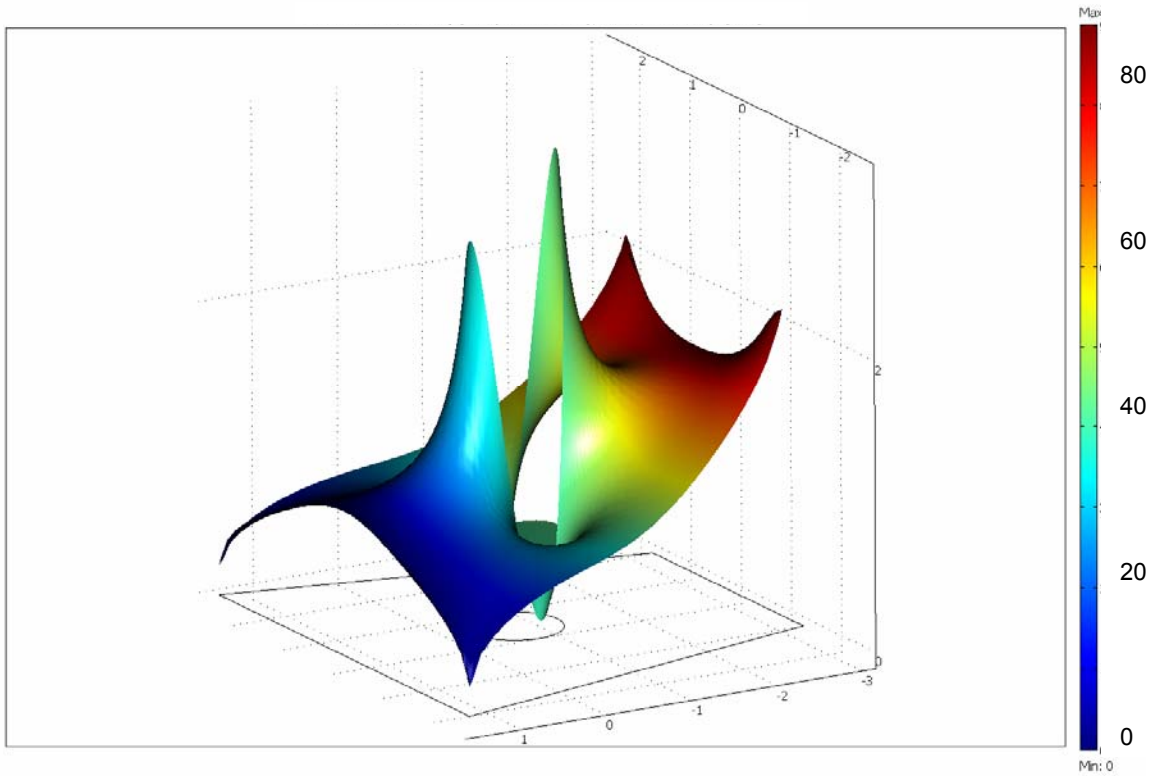

Figure 54 Surface plot of energy density around particle (J/m^3). This confirms the dipole-dipole attraction/repulsion zones discussed earlier.

If Figure 42 is compared to Figure 54 a strong similarity is observed. Clearly, they both show that along one axis the gradient is favorable, while unfavorable along the perpendicular axis.

5.6 Heating with Electromagnetic Fields

This section describes the potential of using electromagnetic fields to cure surfaces formed using force fields derived from standing electromagnetic waves. It is envisioned that once the construction particles are in their intended location, i.e. steady state is reached in terms of the shaping process, then a hardening technique could be employed to hold the particles together keeping the structure intact once the force field is switched off. Heat generation from electromagnetic waves was studied as a means of surface curing by way of sintering. The physics of heating by electromagnetic waves is heavily

dependent on the dispersive nature of the dielectric constant. An example of this phenomenon is the fact that white light passing through a prism becomes separated into a rainbow of colors with blue being refracted the most and red the least. This is a manifestation of the dispersive light speed in materials. Recall that the speed of light can be determined from, $c=(\varepsilon\mu)^{-1/2}$. Thus, if $c = c(\omega)$ then either the permeability μ or the permittivity ε or both are functions of ω. In practice, most materials have a permeability μ that varies very little with frequency (Griffiths 1989). It is the permittivity ε that can vary significantly. Equivalent elementary circuits can be used to describe this behavior as will be shown below (Williams 1998).

5.6.1 Physical principles of heating

Electromagnetic heating is the conversion of electromagnetic energy into heat within a dielectric material. This heating technique is distinct from conventional heating, which require thermal heat-flux through heat conduction and convection, in that it is a volumetric heating technique. As a dielectric material is placed in an alternating electric field the constituents making up the material respond according to their respective charges. As described earlier, in the simple example of electrostatics, the positive charges (protons) are shifted slightly in the direction of the electric field, while the negative charges (electrons) respond by shifting slightly in the opposite direction, in other words, a collection of dipoles is induced within the materials volume. In this configuration, the particle is said to be polarized. This situation becomes complicated quickly as the external electric field becomes unsteady, i.e. starts to alternate its direction back and forth. The induced dipoles in turn respond to such field oscillations by switching their dipole moment p direction back and forth. For a hypothetical massless ideal dipole with only two opposite charges, it is clear that this dipole would manage to maintain perfect alignment of its dipole moment p with the electric field E at infinite

frequency. Now, turning to real materials, we consider the response of a single molecule located at a general point within the particle. The oscillation of its charges back and forth, or the response of the induced dipole formed within the molecule, will be in response to the local field produced at that point. The local field is affected by the neighboring molecules and their induced dipoles. It now becomes evident that the material's molecular and atomic structures plays a major role in determining the polarization behavior. It is possible that at certain frequency bandwidths the response of the material can change dramatically. The behavior of the material's constituents (i.e. charges) depends on the binding forces that hold the electrons in place. It is assumed that since the electron mass is much less than the proton mass, and that the electrons move relative to the relatively fixed nucleus). This is only adequately addressed using quantum mechanics. However, classical approaches have been used to approximate such behavior by studying the response of a mass-spring-damper system with excitation frequency (Hunter 2001). In the years before quantum theory was accepted (Debye 1909) and (Mie 1908) addressed the problem of electromagnetic interaction with a particle consisting of many thousands of atoms. Rayleigh in 1871 developed an approximate analysis which is valid for very small particles (Hunter 2001). The polarization using the Clausius-Mossotti relation shown earlier, and developed in Appendix A, is a result of the continuum theory of dielectrics.

For the purposes of this thesis, it is enough to state that the dielectric constant is a function of frequency and can be re-written as, $\varepsilon(\omega) = \varepsilon'(\omega) + i\varepsilon''(\omega)$. The real component describes the ability of a material to polarize in response to an external electric field, whereas the imaginary component is a measure of the loss in the material. This "loss" is the mechanism by which energy in the external electric field is transferred to the material and dissipated into heat. Clearly, the part of the wave's energy density that goes into polarizing the material through ε', is stored within the particle volume U = -

p·E. Ideally, the polarization process is reversible. On the other hand, the energy density that goes into the material through ε" becomes absorbed. This contributes to translational, rotational, and vibrational motion of the charges, raising the material's temperature. This energy gets dissipated throughout the volume of the particle. This is an irreversible process.

In linear systems, the response is proportional to the stimulus in equilibrium. At very low frequencies any dipoles in a medium will have enough time to match the variations of the external electric field. At this point the dielectric constant is at its maximum value since the bound charge density reaches its maximum value and energy from the external field is stored within the dielectric material. As we increase the frequency, the dipoles are no longer able to restore their original positions during field reversals and as a consequence the polarization lags the applied external field. When the polarization lags behind the applied field there exists a component along the direction of E in phasor space as shown in Figure 55). This real component gives rise to absorption of electromagnetic energy in dielectric material.

Relaxation describes the phenomena responsible for the delayed response of the system to a changing stimulus. In resistance-capacitance (RC) circuits we know that the relaxation time is simply the product *RC* (resistance times capacitance). It can be shown that $RC = \varepsilon/\sigma$. The value of ε/σ is the relaxation time where the charge deposited inside a lossy dielectric will decrease by a factor of 1/e. This is one example where the microscopic picture corresponds accurately with the more familiar macroscopic one.

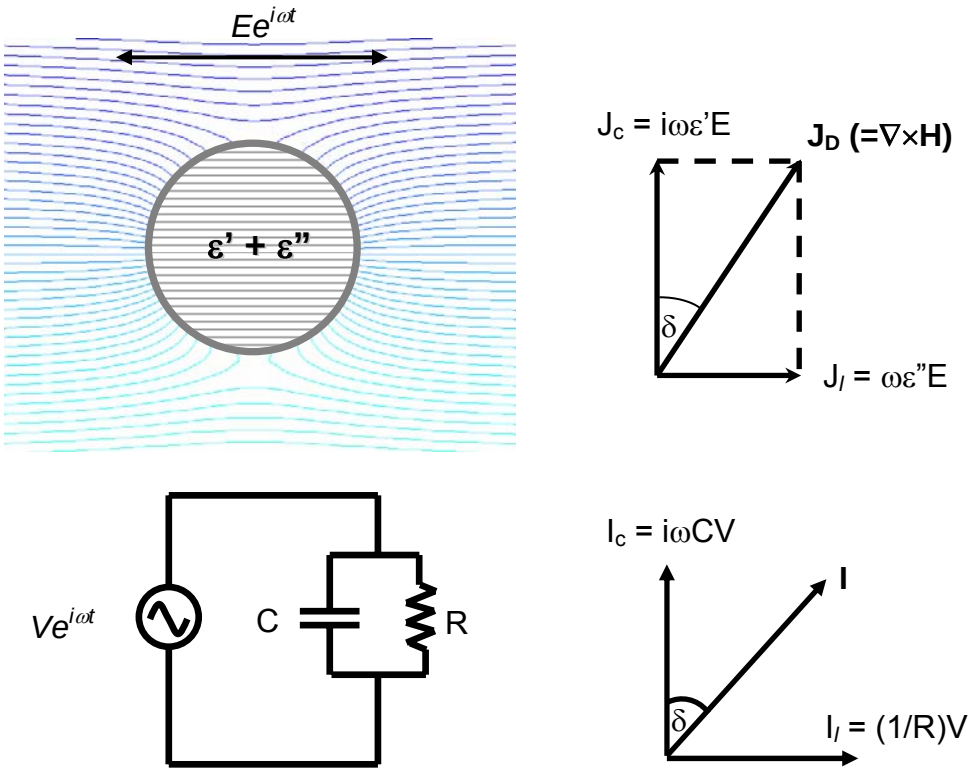

Figure 55 (Top) Dielectric sphere in alternating electric field and its corresponding phasor diagram where Jc is the polarization or charging displacement (i.e. electrical flux density) and Jl is the loss charge. (Bottom) Equivalent electrical RC circuit and corresponding phasor diagram where Ic is the charging displacement current going through the capacitor C and Il is the loss current going through the resistor R.

The reduction of the effective polarization manifests itself as a fall in the dielectric constant and a rise in the loss factor as shown schematically in Figure 56. Now, energy is drawn from the field and dissipated within the dielectric as opposed to being conservatively stored in it. This dissipation of energy is the heat source that we use to raise the temperature of the particles.

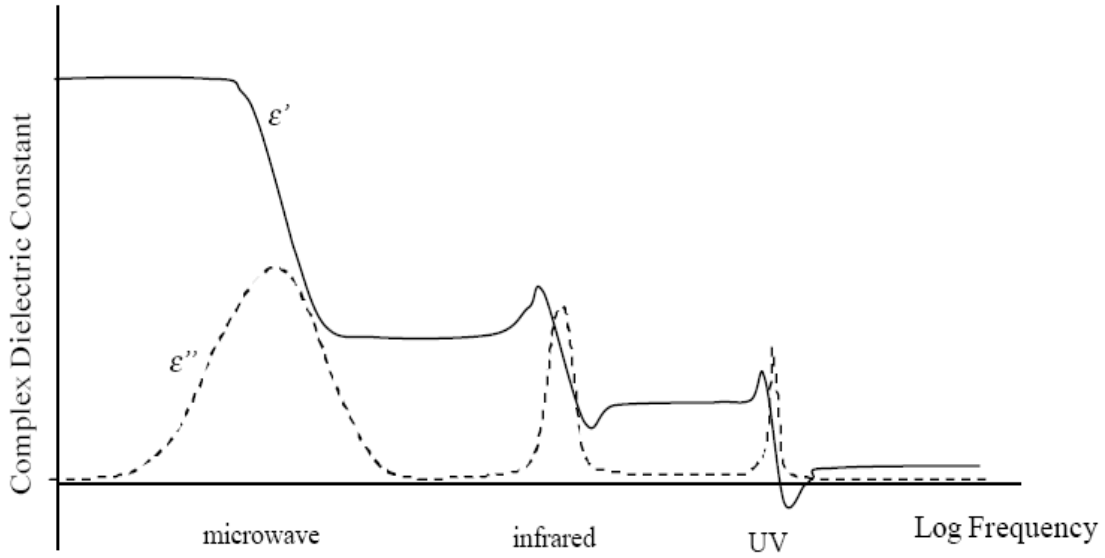

Figure 56 Dispersive nature of dielectric constant and loss of an ideal nonconductor.

The dielectric constant is a complex number, meaning that the polarization does not follow the electric field but is shifted in phase. The frequency dependence of ε' and ε" is shown in Figure 56 for an ideal non-conducting material. At low frequencies, ε' is composed of contributions by all three polarization mechanisms discussed later. The dominant mechanism is the dipole orientation process. As the frequency increases the dipoles start exhibiting relaxation and are unable to respond fast enough to keep up with the imposed external alternating electric field. At this stage atomic polarization becomes the most effective polarization process induced by vibrational motions of the individual atoms in a molecule. At even higher frequencies, inter-atomic vibrations cannot respond fast enough and give way to electronic oscillations, which now become excited. This typically occurs around the UV region of the spectrum. Finally, as the frequency continues to increase, we reach a point where all electronic modes are exhausted and ε' approaches unity. It is clear from Figure 56 that wherever ε' changes most dramatically there is an associated peak in ε", which characterizes the absorption of radiation by the

dielectric. This absorption arises from the resonances associated with vibrations of atoms and molecules composing the material. In solids, the molecules are close enough that significant interactions occur between them. The internal modes of oscillation are therefore modified and the natural frequencies of the atomic oscillations are spread out by the interactions producing a broadening of the absorption lines. This is also referred to as dispersion. This means that instead of well defined characteristic energy levels associated with molecular vibrational and rotational states there will now be a more continuum band of energy levels.

Since energy bands in solids are sums of the energy levels of individual molecules, the spectral positions of the more continuous absorption bands overlap the absorption spectrum of individual molecules. This is important when considering scattering from an object. For example, the electrons in a given material have an overlapping continuous distribution of energy levels. If one of the overlapping bands is partially empty and an electric field is applied, then it will be able to excite electrons into adjacent unoccupied states. This is how an electric current is produced in a conducting material under the application of an alternating electric field.

5.6.2 Polarization Mechanisms

Induced dipoles in a material are physically due to the response of the constituents of matter (atoms and molecules) to the field. Thus they arise through a variety of mechanisms, any or a combination of which contribute to the value of α. The total polarizability is expressed as a superposition of individual polarizabilities each arising from one particular mechanism, i.e. $\alpha = \alpha_e + \alpha_a + \alpha_d + \alpha_i$.

5.6.2.1 Electronic Polarization (α_e)

When a field is applied the electron clouds are displaced with respect to the nucleus. This induced dipole moment being caused by an elastic motion of the electrons has resonances around the visible light frequencies.

5.6.2.2 Molecular Polarization (α_a and α_d)

This mechanism is found in multi-element molecules. The imposed electric field causes a redistribution of the anions and cations relative to each other. Large molecules experience a magnified effect. This gives rise to a configuration where the positive charge is separated from the negative charge by a small distance, thus forming a dipole. When an alternating field is applied one of two things may occur: (i) the individual charges may displace relative to each other, i.e. varying the small distance separating the opposite charges and thus altering the dipole moment of the molecule - this is called *atomic polarizability* α_a; or (ii) the molecule as a whole may rotate about its axis of symmetry in an effort to align with the field if it has an inherent permanent dipole. This is called *orientational polarizability* α_d. The most well known material to exhibit this phenomenon at microwave frequencies is water in liquid form. H_2O molecules being naturally dipolar rotate at microwave frequencies and this is the means by which energy in the external field is converted into heat.

5.6.2.3 Interfacial Polarization (α_i)

Surfaces may contain charges that would contribute to the particle's dipole moment in the presence of an external electric field. This occurs in crystals and is due to defects or impurities that avail of free charges.

5.6.3 Dielectric Classification

The three atomic polarizabilities α_e, α_a, and α_d, lead to the following categorization of dielectrics:

i. Non-polar materials which exhibit variations of permittivity at optical range frequencies

ii. Polar materials showing variation of permittivity in infra-red and optical frequencies

iii. Dipolar materials which, in addition, exhibit orientational polarization

Materials in category (i) produce elastic displacements of electrons only. Dielectrics composed of a single atomic species fall in this group. In (ii) polar materials exist that show elastic displacements. This group includes substances whose molecules have net dipole moment of zero even though they contain dipolar groups of atoms such as CO_2. The most important materials in this group are the ionic salts, such as rock-salt, TiO_2 etc. These all allow very large infra-red polarizabilities. However, if several possible equilibrium positions are available the material belongs to group (iii). In group (iii) are materials consisting of dipolar molecules (Anderson 1964).

The difficulties in calculating permittivity and its frequency dependence give rise to approximate models, such as the equivalent circuit elements approach. Calculating the electric dipole moment that results in a material due to an external electric field, will require a deeper study of these models. These models will connect the microscopic and macroscopic behavior, the former governed by the dielectric's atomic and molecular structure, and the latter by its permittivity (Anderson 1964). For example, in the case of atomic polarizability, the precise configuration of the +ve ionic core and its electron cloud

must be known. This is usually only known for very few simple cases and requires a study of quantum mechanics.

5.6.4 Temperature change

Starting from conservation of energy and following Metaxas' (1996) derivation, we get the time rate of change in temperature given by

$$\frac{dT}{dt} = \frac{\frac{1}{2}\omega\varepsilon_o\varepsilon''\left|E\right|^2}{\rho_o c} \tag{65}$$

Solving for the average power dissipated within a dielectric of volume V results in the following, expressed in W/m^3:

$$P_{dis} = \frac{1}{2}\varepsilon_o\varepsilon'' V\omega\left|E\right|^2 \tag{66}$$

5.6.5 Surface formation and Curing process

Based on the data shown in Figure 56 for a perfect dielectric, it became evident that the frequencies that we would use for pushing particles to their equilibrium positions (gradient and scattering forces) can be widely separated from the frequencies that we use to heat up the surface once the shape is formed. This finding (which may not be true in all regimes of particle size, structure size and material properties) allows us to decouple the two fields from each other since they have different frequencies: one for shaping and the other for heating. A schematic showing a rough estimate of the frequency selection for both stages of the large-scale space structure construction

process is shown in Figure 57. The middle frequency band will be used for refine positioning of any stray particles that have drifted away. At these smaller wavelengths compared to the shaping field wavelength the forces are higher albeit very directional.

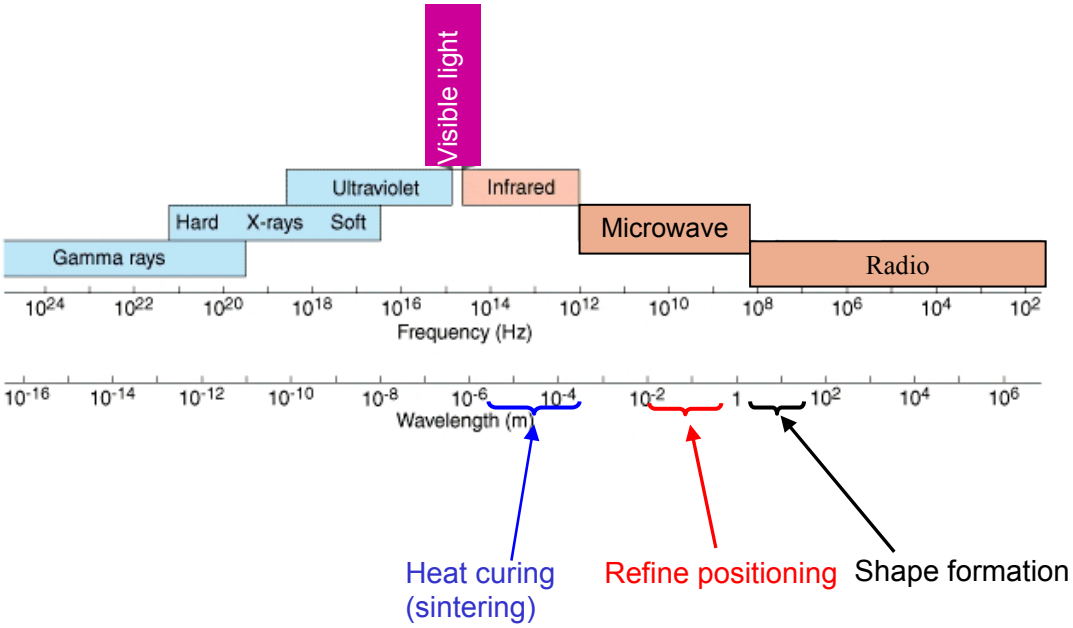

Figure 57 Frequency spacing of each step of the construction process

CHAPTER 6

ACOUSTIC – ELECTROMAGNETIC ANALOGY

The forces generated in both acoustic and electromagnetic fields have been shown in the previous chapters. These forces were classified into primary forces which collect the particles into the desired shapes, and secondary forces that act between the individual particles themselves, forming single-particle-thick surfaces that are complete with no gaps,. Comparing these forces between the fields it was clear that there exists a strong analogy between them. This analogy forms the subject of this chapter. Once the force fields are compared and the analogies highlighted, we discuss other observations made along the way.

6.1 Primary Forces

Recall that the primary acoustic forces are classified into traveling wave forces and standing wave forces. The electromagnetic primary forces consist of scattering and gradient forces. By examining these forces it becomes clear that the acoustic traveling force expression resembles the electromagnetic scattering force expression, and the acoustic standing wave force is very similar to that for the electromagnetic gradient force. In acoustics, the traveling wave force is a result of the momentum exchange that occurs when the wave collides with the particle and scatters off of its surface. This is a result of the difference in impedance between the host medium and the particle. It always points in the direction of the wave propagation for that reason. Clearly, these are the exact same characteristics of the electromagnetic scattering force. Thus, we conclude that these two forces are analogous. The standing wave acoustic force is also found to be strongly analogous to the electromagnetic gradient force. This is evident

when one considers what causes the force in the acoustic standing wave. As outlined in Chapter 3, this force is a result of the gradient in the Lagrangian energy density as derived by Gorkov. In electromagnetics the force comes about as result of the Lorentz force acting on the induced dipole, as was shown in Chapter 5. However, if we take the gradient of the potential energy U that a dipole p has in an electric field E, U=-p·E, we get F=(p·∇)E. In other words, the Lorentz force is also derivable from the gradient of the energy as we did in acoustics. Likewise, we conclude that the standing wave acoustic force is analogous to the electromagnetic gradient force.

All four forces are listed in the table below for comparison purposes. They are first given in Table 1 in the form presented in the previous chapters, then expanded , in Table 2 to a more general particle, i.e. not totally rigid in acoustics and not a perfect conductor in electromagnetics. In Table 3 the expressions are manipulated algebraically to have the same form, and then finally in Table 4 all the forces are generalized such that we achieve a unified force expression for both the energy gradient force and momentum transfer force.

Table 1 Summary of forces derived in previous chapters

	Acoustics	Electromagnetics
∇ energy density	$\mathbf{F} = -\frac{5\pi}{6}\frac{\mathbf{A}^2\mathbf{k}\mathbf{a}^3}{\rho_o \mathbf{c}_o^2}\sin 2\mathbf{k}\mathbf{X}$	$\mathbf{F} = \pi\varepsilon_o \mathbf{a}^3 \left(\frac{\varepsilon - \varepsilon_o}{\varepsilon + 2\varepsilon_o}\right)\nabla\lvert\mathbf{E}\rvert^2$
Momentum transfer	$\mathbf{F} = \frac{11\pi}{18}\frac{\mathbf{A}^2\mathbf{k}^4\mathbf{a}^6}{\rho_o \mathbf{c}_o^2}$	$\mathbf{F} = \frac{5}{3}\pi\varepsilon_o \mathbf{a}^2(\mathbf{k}_o\mathbf{a})^4\left(\frac{\varepsilon - \varepsilon_o}{\varepsilon + 2\varepsilon_o}\right)^2 \mathbf{E}_o{}^2 \sin^2(\mathbf{k}_o\mathbf{x})$

Table 2 Force expressions expanded to include general particles

	Acoustics	Electromagnetics
∇ energy density	$\mathbf{F} = -\frac{5\pi}{6}\frac{\mathbf{A}^2\mathbf{k}\mathbf{a}^3}{\rho_o\mathbf{c}_o^2}\left(\frac{5\rho - 2\rho_o}{2\rho + \rho_o} - \frac{\rho_o\mathbf{c}_o^2}{\rho\mathbf{c}^2}\right)\sin 2\mathbf{k}\mathbf{x}$	$\mathbf{F} = \pi\varepsilon_o\mathbf{E}^2\mathbf{k}\mathbf{a}^3\left(\frac{\varepsilon - \varepsilon_o}{\varepsilon + 2\varepsilon_o}\right)\sin 2\mathbf{k}\mathbf{x}$
Momentum transfer	$\mathbf{F} = \frac{11\pi}{18}\frac{\mathbf{A}^2\mathbf{k}^4\mathbf{a}^6}{\rho_o\mathbf{c}_o^2}\left(\frac{5\rho - 2\rho_o}{2\rho + \rho_o} - \frac{\rho_o\mathbf{c}_o^2}{\rho\mathbf{c}^2}\right)^2$	$\mathbf{F} = \frac{5}{3}\pi\varepsilon_o\left(\mathbf{k}^4\mathbf{a}^6\right)\left(\frac{\varepsilon - \varepsilon_o}{\varepsilon + 2\varepsilon_o}\right)^2\lvert\mathbf{E}\rvert^2$

Table 3 Force expressions manipulated to have the same form

	Acoustics	Electromagnetics
∇ energy density	$\mathbf{F} = \frac{5}{8}\mathbf{V}\left(\frac{5\rho - 2\rho_o}{2\rho + \rho_o} - \frac{\rho_o\mathbf{c}_o^2}{\rho\mathbf{c}^2}\right)\nabla\left(\frac{\mathbf{A}^2}{\rho_o\mathbf{c}_o}\right)$	$\mathbf{F} = \frac{3}{4}\mathbf{V}\left(\frac{\varepsilon - \varepsilon_o}{\varepsilon + 2\varepsilon_o}\right)\nabla\left(\varepsilon_o\mathbf{E}^2\right)$
Momentum transfer	$\mathbf{F} = \frac{11\pi}{18}\left(\mathbf{k}^4\mathbf{a}^6\right)\left(\frac{5\rho - 2\rho_o}{2\rho + \rho_o} - \frac{\rho_o\mathbf{c}_o^2}{\rho\mathbf{c}^2}\right)^2\frac{\mathbf{A}^2}{\rho_o\mathbf{c}_o^2}$	$\mathbf{F} = \frac{5}{3}\pi\varepsilon_o\left(\mathbf{k}^4\mathbf{a}^6\right)\left(\frac{\varepsilon - \varepsilon_o}{\varepsilon + 2\varepsilon_o}\right)^2\lvert\mathbf{E}\rvert^2$

Table 4 Unified force field expressions

	Acoustics	Electromagnetics
∇ energy density	$\mathbf{F} = \mathbf{V}\Theta\nabla\xi$	
Momentum transfer	$\mathbf{F} = \left(\mathbf{k}^4\mathbf{a}^6\right)\Theta^2\lvert\xi\rvert$	

In the above unified force expressions, V is the volume of the particle, Θ is the ratio of impedance between the particle and host medium as given previously by the bracketed terms in the full force expressions in Table 2 and Table 3, and ξ is the energy density of the field. For resonant acoustic fields Θ is given by $P^2/\rho c^2$ and εE^2 in electromagnetics. For each field the energy gradient force and the momentum transfer force can be expressed using the simple unified expressions given in Table 4. The only difference between them is a linear coefficient that was omitted for the purpose of illustrating the unified force field concept. However, there is no loss of information as this coefficient can be included in the Θ term.

An interesting observation was made by (Rayleigh 1871) in describing light scattering and explaining why the sky looked blue. If we consider a sound scattering

particle much smaller than the wavelength, with a compressibility not too far from that of the host fluid such that we can neglect the monopole term, we obtain a scattering behavior that resembles that of a pure dipole (which as explained above is usually the case in electromagnetics). We can write the displacement of the particle as it is entrained in the oscillating fluid and assuming harmonic motion of the fluid,

$$\zeta = Ae^{j\omega t} \tag{67}$$

Then the acoustic particle velocity can be written as,

$$v = j\omega Ae^{j\omega t} \tag{68}$$

And the acoustic particle acceleration is

$$a = -\omega^2 Ae^{j\omega t} \tag{69}$$

This is the acceleration on the fluid elements of the host medium. Since the scattering particle has a different density than the host medium (let us denote that difference by $\Delta\rho$), then it will also experience an acceleration that is proportional to the density difference (Mo 1993). The force on the particle then becomes

$$F = -(\Delta\rho V)\omega A^2 e^{j\omega t} \tag{70}$$

where V is the particle volume. This force on the particle by the fluid must have an equal and opposite reaction exerted by the particle on the fluid according to Newton's third law. It is this force from the particle on the host fluid that radiates the scattered wave. Since it results from an oscillatory motion, the scattered field resembles that of a pure dipole. The point made by Rayleigh from the above simple analysis, is that the amplitude of the scattered wave is proportional to the product of volume and frequency squared ($V\omega^2$). Thus the scattered power is proportional to the square of the particle volume and to the fourth power of frequency, i.e. k^4a^6. This explains the origin of the main difference between the scattering (or traveling acoustic) force and the gradient (or standing acoustic) force.

For the purposes of comparing equal quantities between acoustic and electromagnetics we perform the following comparison. In Figure 58 the energy density was calculated for acoustic and electromagnetic fields that would produce forces ranging from 1 μN to 1 N onto a 1.5 cm diameter silicon dioxide sphere. The field wavelength was fixed at 42 cm, and the properties of silicon dioxide at these frequencies were used in the calculations. The equations used in these calculations were obtained from Table 5. The field intensities were calculated for the energy densities calculated in figure 58 and are shown in Figure 59. Both the energy densities and the field amplitudes are summarized in Table 5.

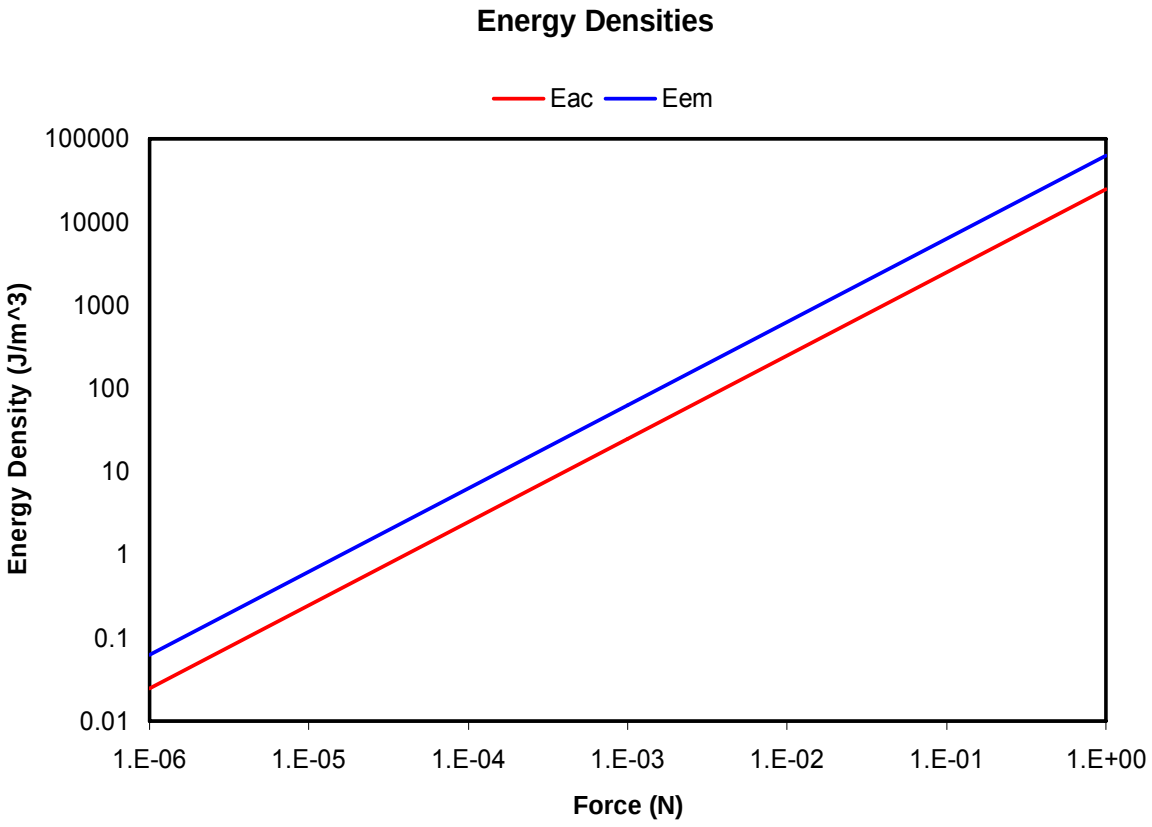

Figure 58 Acoustic and electromagnetic energy densities for fields needed to produce forces ranging 1μN to 1N onto a 1.5 cm diameter silicon dioxide sphere. Field wavelength is fixed at 42cm.

Table 5 Energy densities and field amplitudes needed to produce forces ranging from 1μN to 1 N

Force	**Energy Density needed (J/m^3)**		**Field Amplitude needed**	
	Acoustic	Electromagnetic	Acoustic (Pa)	Electromagnetic (V/m)
1 μN	0.025	0.063	60	1.2 x 10^5
1 mN	25	63	2,000	3.7 x 10^6
1 N	25,000	63,000	60,000	1.2 x 10^8

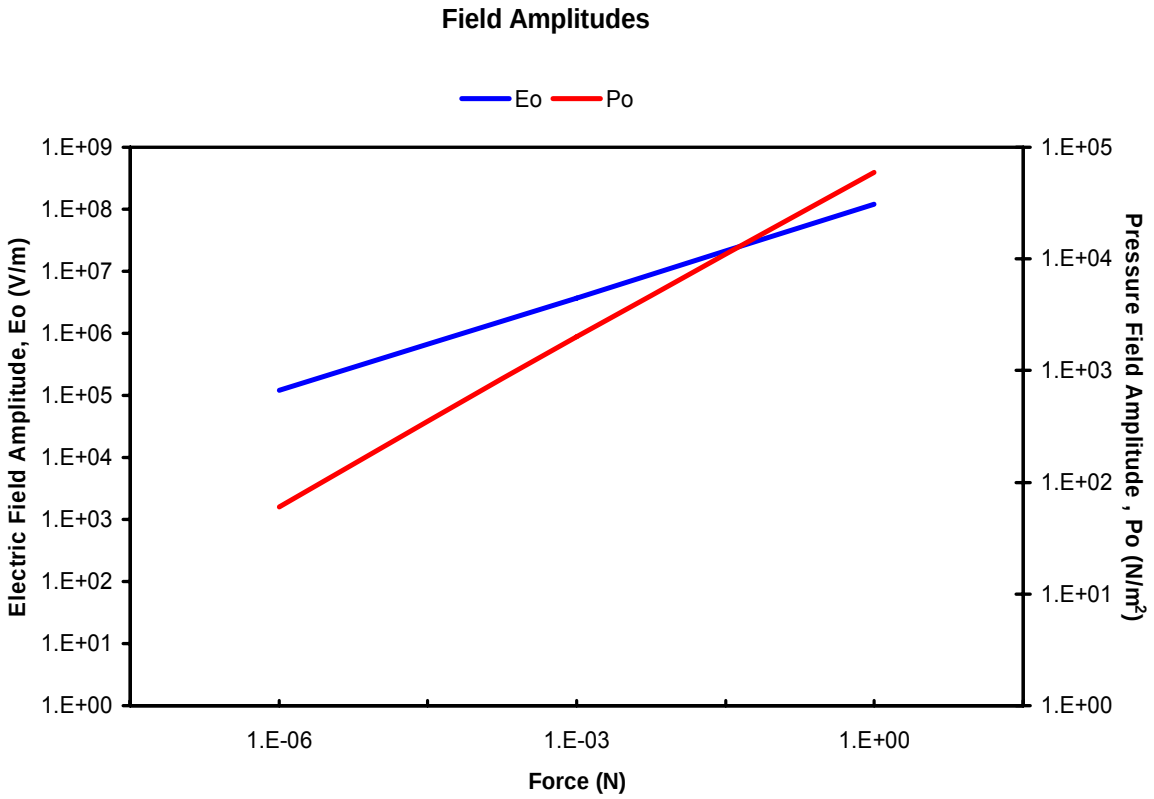

Figure 59 Acoustic and electromagnetic field amplitudes that correspond to the energy densities calculated in Figure 58.

6.2 Secondary Forces

In like manner to the primary forces we observed that the secondary forces also resemble each other in the two fields in 2D. In acoustics, the force of interaction between two dipoles goes as the square of the pressure amplitude (i.e. acoustic energy density), inversely proportional to the separation distance to the fourth power. In electromagnetics, the force of interaction between two electric dipoles is proportional to the electric field amplitude squared (i.e. electric energy density) and inversely proportional to the separation distance to the fourth power. Clearly, both secondary forces are analogous, and this stems from the fact that they are both dipole-dipole

interaction forces. The main difference between acoustic and electromagnetic dipoles comes in the regions of attraction and repulsion. In acoustics, the attraction regions are along two dimensions and repulsion along the 3rd, whereas in eletromagnetics there is only one dimension that experiences attraction, and the other two are repulsion. This behavior in acoustics and electromagnetics is illustrated in Figure 60 below. In Figure 60 everything inside the cones in acoustics is repelled and everything outside the cones attracted to the particle, whereas in electromagnetics the opposite is true, anything inside the cones is attracted and everything outside the cone repelled. This is due to the vector nature of the electric fields and is better understood when streamlines in acoustics is contrasted to electric field lines in electromagnetics, which is done in Figure 62 - Figure 65. The net result of this on the structures formed is that in acoustics we can achieve complete surfaces that vary in 3D space by exciting one resonant mode.

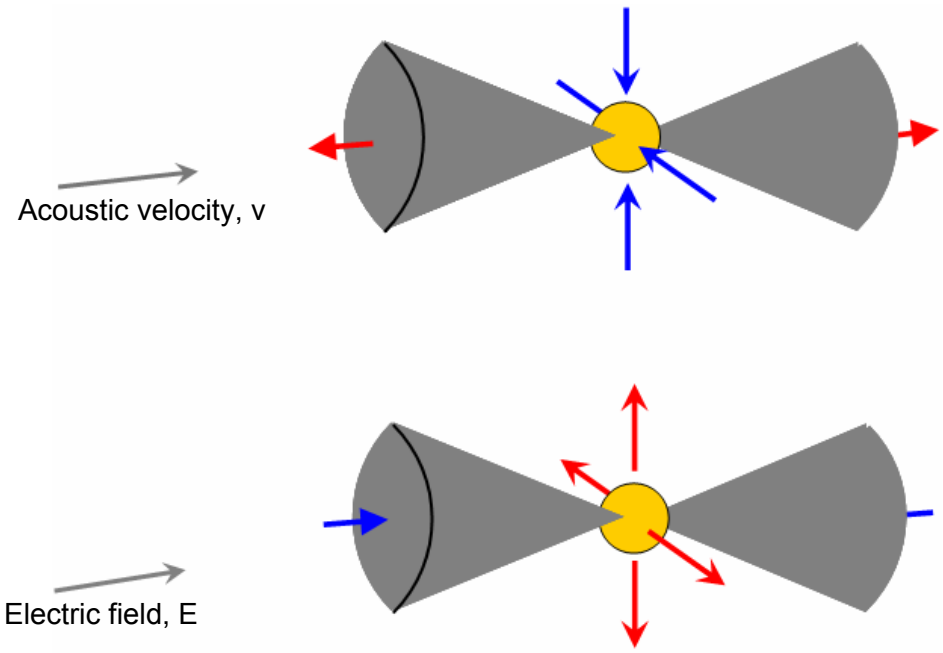

Figure 60 Attraction and repulsion zones in 3D in acoustic fields (top) and electromagnetic fields (bottom). Attraction denoted by blue arrows and repulsion by red arrows.

In electromagnetics we predict that since there is attraction along one dimension only, then the resulting structures are chains and not complete surfaces. These chains vary in 3D space depending on the resonant mode of excitation. To achieve complete surfaces in electormagnetics we hypothesize that a second mode needs to be excited once chains have formed and cured to force the chains to coagulate and then cure them into complete surfaces. Another difference between the two secondary force fields comes when the acoustic force has a nonzero monopole term. This is proportional to the ratio of the compressibility of the particle to the host fluid. In electromagnetics we do not see a mechanism for this to occur as long as the dielectric particle with which we are dealing does not have any net charge, and thus no electric monopole term.

It should be noted that the dipole equivalence of the behavior of a sound scattering particle in acoustics and a dielectric particle in electromagnetics, has been demonstrated experimentally, verified numerically, and shown analytically. Experimentally, we showed that the forces of interaction between two suspended particles in a sound field attract along one axis and repel along the other. This is characteristic of dipole-dipole interaction forces. Numerically, we solved for the field around a sound scattering sphere and a dielectric in FEMLAB and showed that the field around both spheres resembled that of a dipole. Finally, we showed that analytically, the interaction between two spheres in both fields have very analogous behavior. This is mainly due to the fact that they are both regarded as dipoles in their respective fields. This is the basis of the strong analogy between the two fields. Table 6 lists the interaction forces in acoustic and electromagnetic fields between two small particles. Figure 61 shows the potential energy of interaction, which when operated on by the gradient operator, yields the interaction forces in Table 6. The interaction energy potentials and the normalized force angular behavior are shown in Figure 61.

Table 6 Dipole-dipole interaction force in both fields

Acoustics	Electromagnetics
$\mathbf{F_s} = 4\pi \mathbf{a}^6 \left[\frac{(\rho - \rho_o)^2 (3\cos^2\theta - 1)}{6\rho_o \mathbf{r}^4} \mathbf{v}^2 \right]$	$\mathbf{F_s} = \frac{\mathbf{p}_1 \cdot \mathbf{p}_2}{\mathbf{r}^4} \left[1 - 3\cos^2\theta \right]$

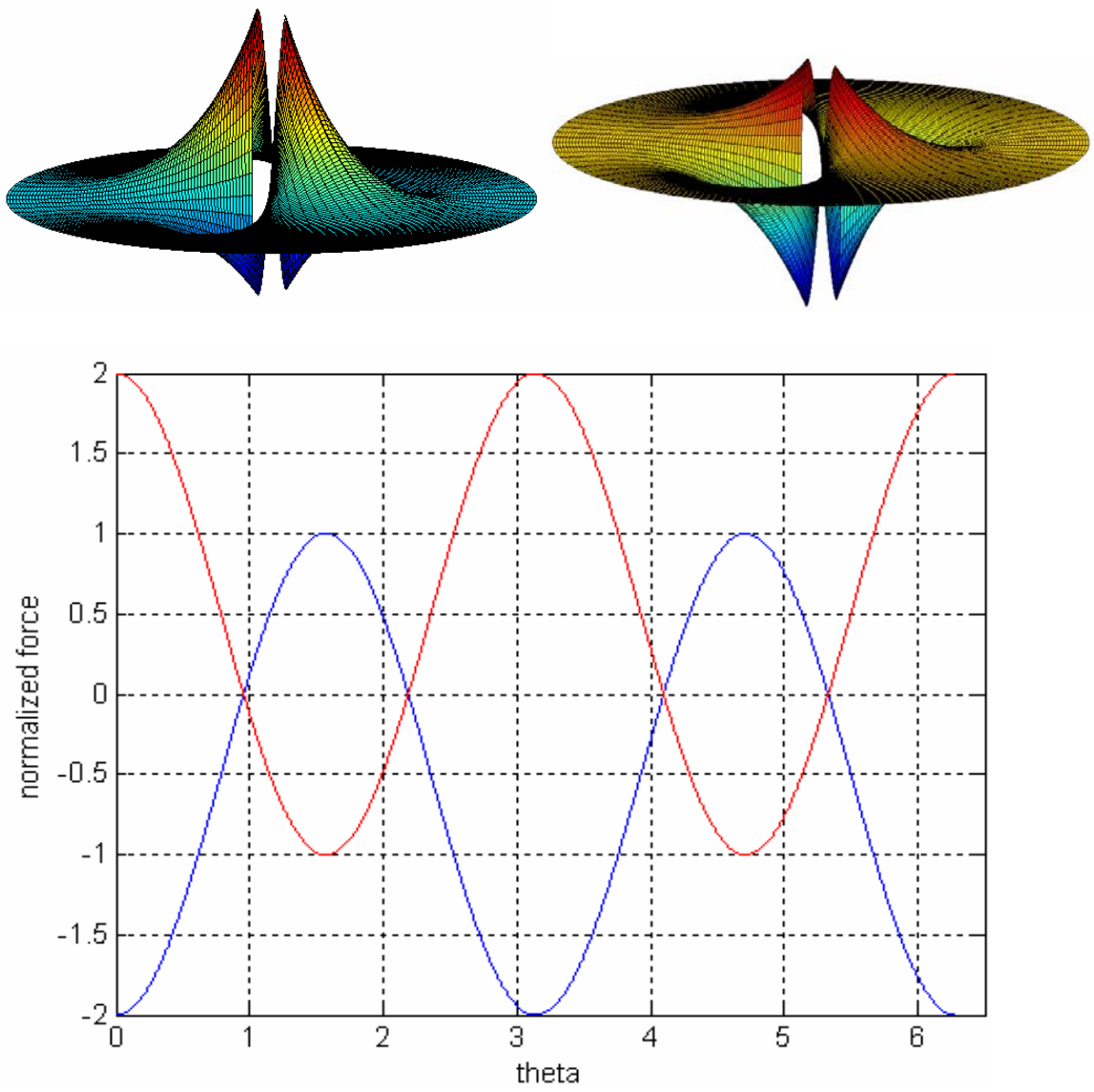

Figure 61 Top: Interaction potential energy in acoustics (right) and electromagnetics (left). Bottom: plot of normalized interaction force vs azimuth angle in acoustics (red) and electromagnetics (blue).

Clearly, both fields have very analogous interaction forces in regards to their dependency on particle separation distance, particle radius, and azimuth angle θ. The interaction force in electromagnetics has stronger attractive forces than repulsive forces and the opposite occur in acoustics, see Figure 61.

6.2.1 Alternative view of interaction forces using field lines

Another way to view the interaction of two spheres in both fields is to use elementary flows appropriate for each field type. In acoustics, the particles collect at the pressure nodes, which correspond to velocity anti-nodes. Thus, for acoustics, we use doublets as the appropriate singularities since we know that the nature of the interaction forces arises due to hydrodynamic effects. In fluid flow, a solid sphere is modeled as a doublet due to the zero normal velocity at the surface. To understand the behavior of the forces we observe the velocity streamlines, and knowing that pressure increases as the streamlines diverge, and vice versa, it is clear that particles that are located such that their line of centers is perpendicular to the wave direction, i.e. direction of acoustic wave velocity, the streamlines contract and thus the force is attractive, see Figure 62. The opposite occurs when the line of centers is turned 90^{o}, see Figure 63.

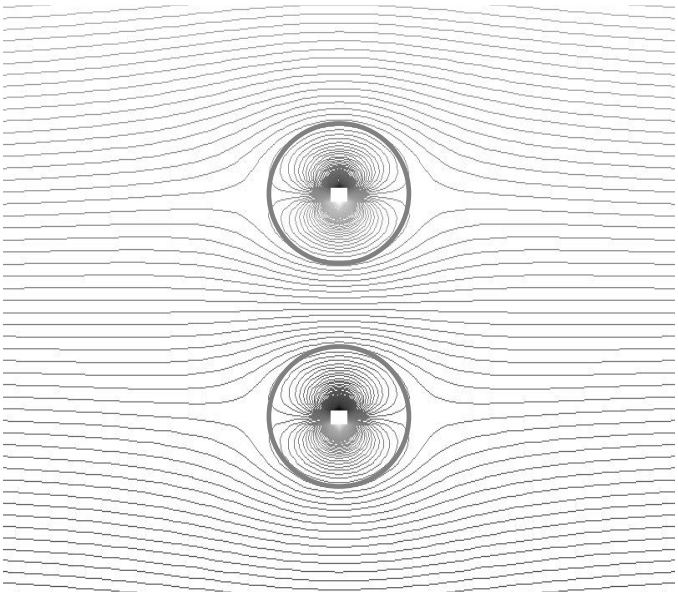

Figure 62 Acoustic particle velocity streamlines between two spheres, modeled as doublets, with their line of centers perpendicular to the wave direction.

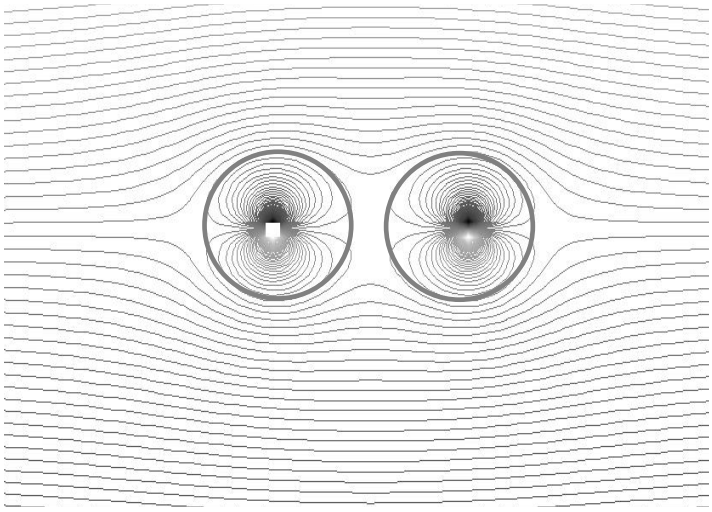

Figure 63 Acoustic particle velocity streamlines between two spheres, modeled as doublets, with their line of centers parallel to the wave direction.

In electromagnetics, a small dielectric can be modeled as a dipole. The difference between dipoles and doublets is the location of the positive and negative charges relative to the incoming field. This is what causes the electric field lines to converge ahead of and behind the particle, and diverge on top of and under the particle, as seen in Figure 64 and Figure 65. Clearly, in the configuration shown in Figure 64 the effect of the second dipole on the first is that it causes the electric field lines to converge between the two, indicating that the interaction force is attractive. In Figure 65 the electric field lines between the two dipoles diverge from each other which indicates that the effect of one particle onto the other causes a repulsion force in that configuration.

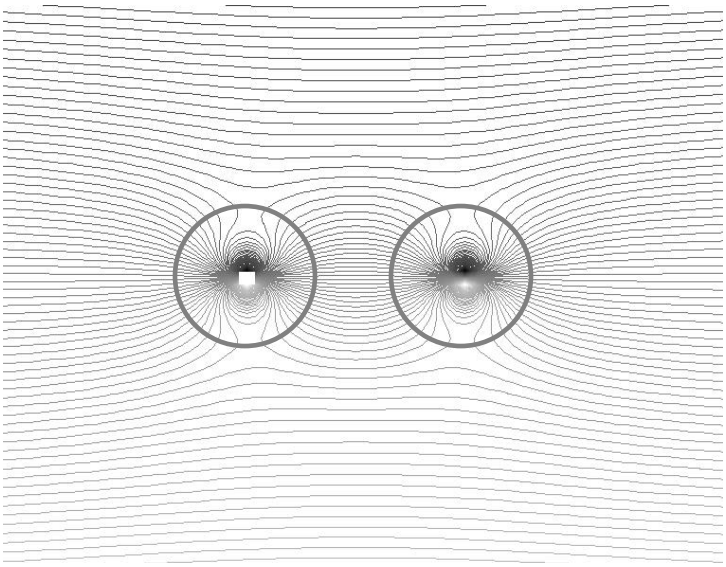

Figure 64 Electric field lines for two dielectric spheres, modeled as dipoles, with the line of centers parallel to the external electric field.

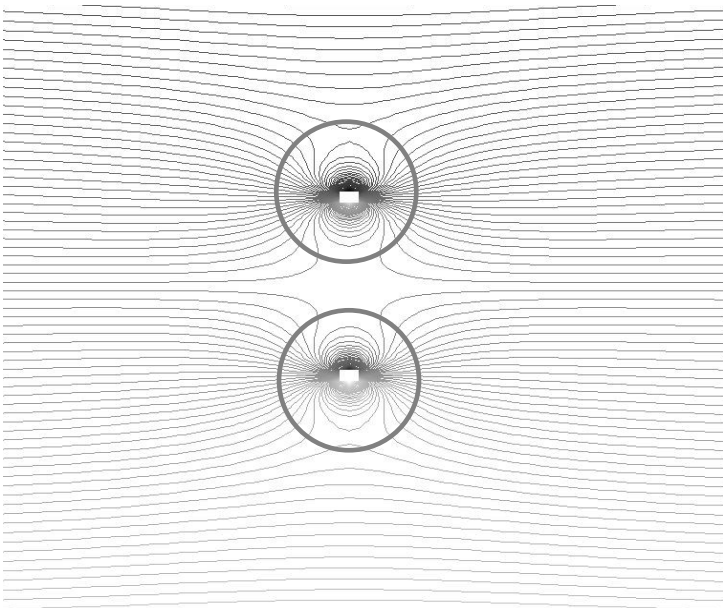

Figure 65 Electric field lines for two dielectric spheres, modeled as dipoles, with the line of centers perpendicular to the external electric field.

6.3 Boundary Conditions

The boundary conditions are strongly analogous, yet the nature of the boundary conditions is physically different for each field. The boundary conditions reveal a possible explanation for the behavior of particles close to the wall. This observation has been made experimentally in acoustic fields. It is based on the physics of the boundary conditions and the analogy. We extrapolate to electromagnetics and predict that similar behavior is expected. An experimental demonstration of wall formation in an electromagnetic resonator would confirm this hypothesis.

6.3.1 Acoustics

The rigid walls of the acoustic resonator yield a zero acoustic particle velocity at the walls and a zero pressure gradient (in standing waves pressure is in quadrature with velocity both in space and time). The behavior of a small rigid sphere near the wall can

be explained using the method of images. If we continue regarding the rigid sphere as an effective dipole in the sound field, then placing it close to a rigid wall becomes equivalent to solving the problem of having a mirror image the same distance behind the wall, which radiates in phase, and removing the wall, as seen in Figure 66. The reason the image is in phase is due to the rigid wall boundary condition.

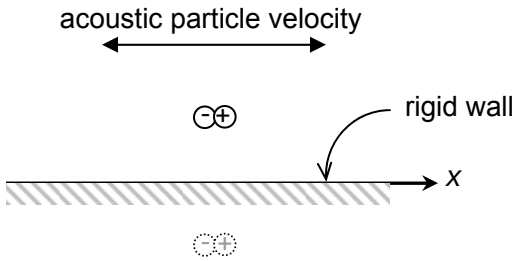

Figure 66 Schematic of rigid sphere (dipole) in front of a rigid wall and corresponding image same distance behind wall and in-phase.

The orientation of the dipole axis relative to the wall was determined from knowledge of the direction of the acoustic particle velocity in the field. For the simple case of a plane standing wave such as that formed in mode 1 0 0, the acoustic velocity is parallel to the x-axis. This implies that the configuration shown in Figure 66 is for a wall that has a normal vector pointing perpendicular to the x-direction. Clearly, from the boundary conditions it is clear that the acoustic velocity will always be parallel to any wall very close to it and thus the above schematic applies to more complex mode shapes as well.

The interaction between the dipole and the wall can now be determined qualitatively by studying the interaction between two dipoles that are in phase and point in the same direction. This is identical to what occurs between two particles in the cavity The interaction is thus attractive along the plane perpendicular to the acoustic velocity axis as shown in Chapter 4. Thus, the particle will be attracted to the wall and this is indeed what we observe in experiments.

6.3.2 Electromagnetics

Based on the strong analogy found between acoustic force fields and electromagnetic force fields, we can follow the same logic used above in determining what will happen when a dielectric sphere is placed close to the walls of an electromagnetic resonant cavity. The walls are assumed to be perfectly reflective to any incident wave which is to say, a perfectly conducting wall. The electric field is always normal to the wall and the magnetic field is always tangential. This is the same thing as saying that the tangential component of the electric field vector is analogous to the acoustic particle velocity, whereas the magnetic field vector is analogous to the pressure profile in acoustics. It is clear that one of the main differences between acoustic fields and electromagnetics is the fact that both the electric and magnetic fields are vector quantities and in acoustics the velocity is a vector, while the pressure is a scalar. In the electrostatics case where $\nabla \times E = 0$ and in acoustics we usually assume irrotational flow, $\nabla \times V = 0$, a potential function can be defined such that the electric field and the velocity field can be computed by simply taking its gradient. It is also true that in resonance, the electric field is in quadrature with the magnetic field.

Using the knowledge in Chapter 5 the behavior of a small dielectric particle in an alternating electric field, such as that in a resonator, can be replaced with an equivalent oscillating electric dipole. Thus, it is feasible to use the method of images to model the behavior of a dipole near a perfectly conducting plane. The orientation of the dipole is always parallel to the electric field vector. This can be easily shown by looking at the potential energy U of a dipole p in an electric field E; $U = -p \cdot E$. So for minimum energy both p and E are to be parallel, this was explained in detail in Chapter 5. For perfect conductors, the electric field lines are always perpendicular to the surface. This would

indicate that the only way for the E-field lines to be perpendicular to the surface is for the image to be out of phase by ½ cycle, as is shown in Figure 67

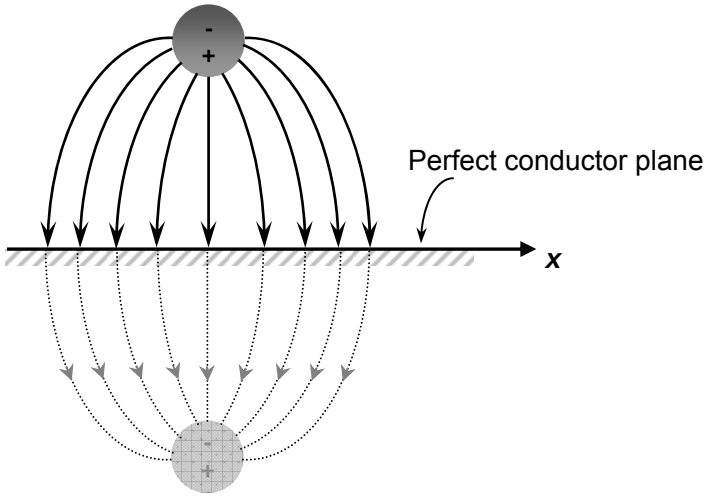

Figure 67 Electric dipole near a perfectly conducting plane

It is therefore, expected that the behavior of a dielectric sphere near a perfect conductor wall will be that of a dipole-dipole interaction force as discussed in Chapter 5. Again, in analogy to the acoustics case, the dipole will interact in such a way that it would with other dipoles in the field and thus should be attracted to the walls.

Clearly, although the physics behind the boundary conditions and the formation of dipoles within the particles in acoustic and electromagnetic fields is very different, their behavior in the two types of fields is strongly analogous. This finding confirms that the analogy holds up to the level of particles interacting with the walls of the resonant cavity.

6.4 Force derived from Energy

In an effort to extend TFF's capability, the analogy between acoustic and electromagnetic waves was studied. In fact, Lord Rayleigh, the first one to study

acoustic radiation pressure, approached it by searching for an acoustic counterpart to the pressure induced by an electromagnetic wave. Starting from the basic energy conservation equations we see a similarity in the form of the expressions involved in each term:

$$\frac{\partial}{\partial t}\left(density\ of\ \ quantity\right)+\nabla\bullet\left(\ flux\ of\ \ quantity\right)=\text{sources}-\text{sinks}$$

$$\frac{\partial}{\partial t}\left(\frac{1}{2}\frac{p^2}{\rho_o c^2}+\frac{1}{2}\rho_o u^2\right)+\nabla\bullet\left(pu\right)=work$$

$$\frac{\partial}{\partial t}\left(\frac{1}{2}\varepsilon_o E^2+\frac{1}{2}\frac{B^2}{\mu_o}\right)+\nabla\bullet\left(\frac{E\times B}{\mu_o}\right)=work$$

The first equation serves as a general conservation expression. The second equation governs the conservation of energy in acoustic fields. The first term is a measure of the acoustic potential energy density and the second the kinetic energy density. Comparing this to the third equation governing the conservation of electromagnetic energy reveals that similarly the first term is the potential energy stored in the electromagnetic field and the second term is a measure of its kinetic energy, see energy description below. For both equations the third term is the corresponding intensity and finally the terms on the RHS are the work done on the particles by the fields.

A brief look at the energy associated with electric currents reveals that this type of energy is not potential but kinetic in origin. The reason is because this energy is due to moving charges. Thus, currents are a measure of the kinetic energy of the field since they involve moving charges. The magnetic fields that are produced as a result of this current are therefore a measure of the kinetic energy of the field. That is why in the above expressions the magnetic field is analogous to the velocity in acoustic equation.

From classical mechanics (and the second law of thermodynamics) it is well known that a system will move in a direction such as to increase its kinetic energy (and disorder) and lower its potential energy (order). Maxwell pointed out that the energy associated with charges is potential in nature. When a material is polarized it has a higher potential energy than when it was at rest, and that increase in energy is at the expense of work done by the field onto the particle in polarizing it. The polarized material can now perform work and lower its potential energy in accordance with the path of minimum energy (dictated by the Lagrangian of the system). This is fundamental to the interaction of electromagnetic fields with dielectrics and is the governing factor to the formation of dipoles and ultimately polarization of materials.

Recall in Chapter 3 that Richter used energy methods to derive the forces induced onto a small particle in a standing acoustic wave, which is based on the Lagrangian energy density.

CHAPTER 7

SPACE CONSTRUCTION

7.1 Application to space Based Construction

In the zero gravity environment of space small forces produced by waves can achieve significant results. The acoustic wall formation process studied in the preceding chapters has been validated by reduced-gravity flight experiments as discussed early in this thesis. This process can be applied in a straightforward manner to building components of structures in zero gravity. However, the requirement to use acoustic fields implies use of a medium, which can be liquid or gaseous, and hence a pressurized enclosure. The dimensions of this enclosure will be limited by the wavelengths that can be generated, and the mass of the enclosure and medium. Thus acoustic manufacturing in Space is projected to be attractive mainly for forming smaller objects, rather than massive structures. In the late 1990s, our group started developing space flight experiments to demonstrate hardening of a wall of particles using epoxy resins in microgravity. A Student Experiments in Microgravity (SEM) module (NASA 2006) and a Get Away Special (GAS) module (NASA 2006) were being prepared for flight on the Space Shuttle, but these projects were abandoned after the Columbia tragedy. At the inaugural meeting of the Space Resources Roundtable (Komerath 1999), a presentation of acoustic shaping as a manufacturing concept for use inside future space habitats, generated interest in the larger problem which was to build the habitat shell itself.

In the early 1970s, NASA and ASEE (NASA 2005) did a detailed study of habitat construction, following the architecture set out by Gerard O'Neill (O'Neill 1977). The needs for effective radiation shielding and artificial gravity are currently the primary

biological obstacles to developing long-term human habitats (or spaceships, which are basically habitats with high propulsive thrust). Artificial gravity is best induced by rotating the habitat around an axis where humans would stay along the periphery. To keep the rotation rate below a level at which many people become disoriented (the limit is believed to be 1 revolution per minute), and still obtain a substantial fraction of terrestrial gravity, the station dimensions become large, on the order of 1 kilometer radius. An alternative is to build it out of modules connected by tensile elements. Even in the latter case, the module structure must be able to take radial acceleration on the order of 1-G, i.e., 9.8 m/sec2.

The problem of radiation shielding rules out low-mass structures for human habitats. Radiation in the solar system consists of particles, gamma rays and X-rays from the sun, along with high-energy particles such as cosmic rays (NOAA 2006). Typical low-mass aerospace vehicle shells made of metal, pose severe hazards due to secondary particles generated by the impact of high-energy particles. At present, there are concepts for inflatable multi-layer walls carrying hydrogen and/or water, polymer substances that stop certain parts of the radiation spectrum, strong electrostatic fields that surround the habitat and deflect radiation (Malik 2005), and combinations of the above. Hydrogen, water and polymers must be shipped from Earth, which increase the launch mass required which in turn translates into higher and higher launch costs. An attractive option, if feasible, is to use material from extraterrestrial, low-gravity sources, with minimal processing, and simply provide a thick, dense layer of mass that stops all forms of radiation. The thumb rule is that a layer of soil roughly two meters thick would provide complete protection. Ideally, the construction process would not require human presence for long durations. The NASA-ASEE studies showed that a spinning cylinder would be suitable to build colonies capable of self-sustainment, which is projected to house 10,000 to 100,000 inhabitants. The mass constraint narrowed the optimal shape

(NASA/ASEE 1975) down to a spinning torus, and a non-spinning shell was proposed around the spinning torus. However, the studies still failed to solve the problem of how to ship enough material from either the Earth or the Moon, and how to build the station without exposing the builders to radiation and micro-G for extended periods.

In 2000, our group proposed a systematic approach to building a 2km diameter, 2km long closed cylinder, radiation-shielded to two meters wall thickness, at the Earth-Moon L-2 point, for later transport to Earth-Moon L-4 (Komerath 2001). The approach was to combine proposed concepts for lunar-based robotic construction of a large solar power plant using in-situ resources (Ignatiev 2000), and a lunar-based electromagnetic launcher, as a coordinated long-term effort to build infrastructure and a space-based economy. It was argued that this would set the context for a large habitat justifying a large population, by enabling and providing markets for several long-term business cases. The construction of the cylinder was shown to be conceptually feasible entirely through automatic, repetitive operations, with at most telepresence supervision and control from Earth (Komerath 2001). The construction would start with a wire cage of lunar-manufactured cables launched in lunar-built railroad freight-car by a large electromagnetic launcher. A set of small “Shepherd” spacecraft equipped with electromagnets would perform the rendezvous / positioning operations for the initial phases, with robots attaching small thrusters to spin the cable loops up to sufficient rotational speed to maintain the loop shape. Regolith-filled metal containers would follow. It was shown that these could be maneuvered into position inside the cable loops, and fixed in place, using one or more robotic construction arms, interacting with the electromagnets on the “Shepherd” craft.

Another example of using electromagnetic forces in space is found in (Miller 2002). Here a sparse aperture telescope is conceptualized, where multiple spacecraft form elements of the telescope maintain relative orientation and spacing by creating a

dipole in each spacecraft and controlling the relative orientation and strength of each dipole. The field is created by onboard power of each craft, so that they are active dipoles. In our assembly concept, the metal containers would be welded together after they attach to the large rotating grid. The entire process of building such a shell was calculated to take 10 years of automatic operation, with a launch rate matched to power generation on the Moon.

The concept was studied further under a 6-month NIAC Phase 1 grant (Komerath 2003) until the problem was reduced to engineering design steps. At this point, attention was shifted to the more extensive challenge of using unsteady fields to produce steady force fields that can be used to automatically form structures. In the preceding chapters it was shown how tailored force fields (TFF) provide a means of collectively manipulating matter into organized structures. Specifically, acoustic and electromagnetic waves were discussed in some detail. Other fields (i.e. other type of wave motion) are expected to produce analogous results due to the wave nature of these fields but are not studied in this dissertation. The generality of wave type enables a wide selection of material types to be used, whereas the size and shape scalability of system is achieved through wavelength modulation.

7.2 Force-Fields for Space-based Construction

In this chapter the application of electromagnetic force fields to space-based construction is discussed. In order to size the power requirements of a full-scale construction system, an estimation method had to be devised for the forces that could be generated in fields large enough to be applied in large-scale construction. The key issue is to see what power levels are needed in order to achieve a given acceleration level on solid particles of a given size, using a given wavelength. The wavelength is dictated by the mode shape needed to construct walls of a given curvature. For a full-scale habitat

module, the module size was estimated to be a cylinder 50 m in diameter and 50 m long. Four of these modules tied with tensile tubes to a fifth module at the center, would form a habitat station with artificial gravity in the outlying modules, and zero gravity inside the center module. The particle size needed for construction is chosen to be practical for material handling and to keep the formation time of the module within reasonable limits. As long as the acceleration caused by the field is larger than that due to the other random or systematic "g-jitter" in the construction region, then it may be assumed that the field will be successful in driving the particles to stable regions and holding them there until they are fused in position. If the power required to achieve this acceleration is feasible to develop, then the construction scheme can be developed further.

7.2.1 Sizing Metric: Acceleration per Unit Intensity

The discussion starts with a comparison of the forces that can be generated from acoustic, optic, and microwave force fields. To compare these forces, a substance must be found that can be manipulated using acoustic, optical, and longer-wave electromagnetic fields. As an order of magnitude comparison, the acceleration per unit intensity was calculated for both acoustic and electromagnetic fields at optic and microwave bandwidths, as seen in Figure 68. We used the following logic to enable a direct comparison of different types of waves and particles, drawing upon each application area. Optical tweezers usually use visible wavelengths and work found in the literature often deals with glass beads (which are mostly silicon dioxide) in water. Microwaves can propagate through and polarize a silicon dioxide particle and acoustic shaping works with most materials as long as the particles become effective dipoles and scatter incident sound waves due to their impedance mismatch with the host fluid. This enabled us to choose material of the same density (roughly 2000 kg/m^3), and assume the refractive index of glass relative to vacuum for both the optical and microwave cases.

A common metric was given by estimating the acceleration per unit intensity on a silicon dioxide particle that is in the Rayleigh scattering regime. The diameter of the particle was set to one-tenth of the wavelength and the acceleration per unit intensity is plotted against particle diameter. The corresponding pressure field amplitude and electric field amplitude was then calculated respectively. This is seen as a way to compare the field quantities in both acoustic and electromagnetic fields that would produce the same results. It is important to note that these calculations were made for silicon dioxide and its electric properties at these frequencies dictate the electric field force.

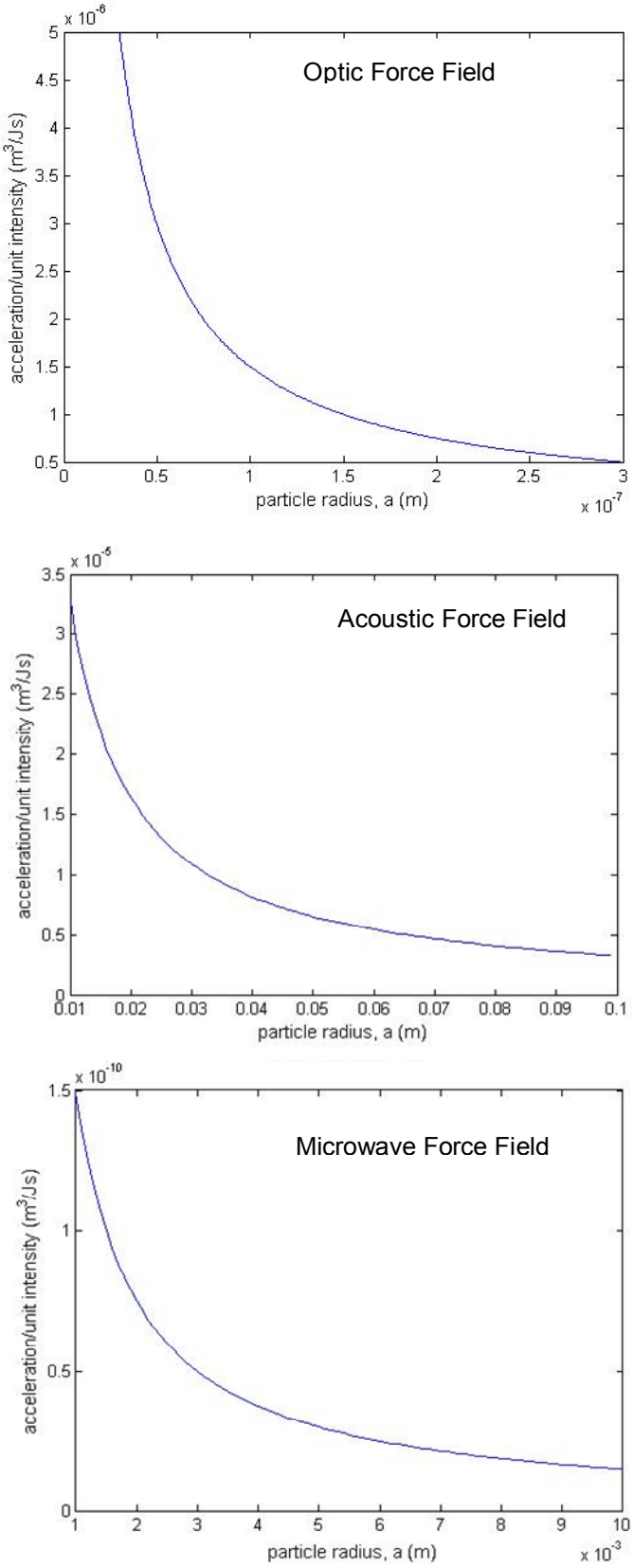

Figure 68 Acceleration per unit intensity for three force fields

The force per unit incident radiation intensity is divided by the mass of a particle to obtain the acceleration per unit intensity. The abscissa is the particle radius. For each particle radius, it is assumed that the wavelength used is 20 times the particle radius to stay within the Rayleigh regime. The acceleration in each case depends inversely on particle radius.

The above results indicate that high microwave intensities would be required to move particles. It is a good rule of thumb that intensities achievable inside resonators can reach 3 orders of magnitude higher than source beam intensity. Our experiments on acoustic shaping as discussed in Chapter 2 show that 1.3 kW/m2 corresponding to the 151dB resonant field shown in Wanis (1999) is adequate for forming walls from ceramic materials in acoustic resonators. Microwave beam intensities up to 8MW /m2 have been demonstrated in ground based laboratory experiments (Beauvais 1997). It thus appears reasonable that microwave or radio-induced electromagnetic shaping using raw materials such as silicon dioxide (primary component of lunar regolith) is feasible in prototype experiments.

7.2 Construction Phases

The manner in which structures could be constructed in space using TFF is as follows:

a. The construction material is broken up into appropriate size range particles.
b. The unsteady potential field best suited for the size scale of the object is selected.
c. A resonant field is setup by adjusting the field source frequency or the dimensions of the boundaries or some combination of the two.
d. The construction material particles now respond to the radiation pressure imposed on them by scattering the incident wave and, altering the wave's momentum path. They thus react by moving to force nodal locations within the

field. In other words, the particles are attracted to points of minimum potential in order to minimize the total energy of the system.

e. Once stable, a suitable curing method is employed to fuse the particles together forming a permanent structure. Since chains form in electromagnetic force fields this may be repeated several times in order to obtain a solid surface out of the chains formed in the initial shaping process.

f. If the final object consists of many smaller objects, i.e. span a large size scale, then individual structures could be fabricated using this force field method and final assembly would occur externally via any appropriate means, such as a robot.

7.3 Estimate of Power Requirements

A particle size of 20 cm diameter was chosen for the construction material, and it was tentatively assumed to have properties similar to silicon dioxide. An acceleration level of 1 micro-G was selected as being adequate to dominate over background forces such as g-jitter due to the solar wind and all other forces at the orbit of Earth around the Sun (1 A.U.), but sufficiently far away from Earth. The Earth-Sun L-4 region was selected as a representative location for a long-term habitat. This level of acceleration was found to be sufficient to drive the particles to the contours of a 50m diameter cylinder and thus form the cylinder within one hour of operation. The scaling relationships for the forces were used to back out the field intensity required to cause the required forces. It was assumed that a resonator Q factor of 10,000 could be achieved, and this was used to estimate the continuous input power required to the resonator. In turn, the size of the solar arrays needed to capture sufficient sunlight, at an assumed conversion efficiency of 10% was estimated. Initially this came out to be on the order of 2 square kilometers. Later, the design was refined to use large-area collectors made of solar-sail material,

focusing sunlight on to a much smaller array of high-temperature, high-intensity solar cells. The cavity was formed of four radio-wave resonators operating at 100m wavelengths. With this design it was found that the mass of each of the four resonator walls, with its attendant solar sail/collector, power conversion system, maneuvering thrusters and a 58 micron resonator wall thickness, could be held to 25,000 kilograms. This was considered to be well within the capabilities of heavy-lift launchers from earth (Wanis 2005).

To extract 20cm blocks, a "Rockbreaker" spacecraft was conceptualized. This is described in (Vanmali 2005). Again, it was seen that solar energy available at L-4 was sufficient to power the craft to break up enough mass of 20cm-blocks, to form a cylinder within the equivalent of 19 Earth days. In the case of both the TFF craft and the Rockbreaker craft, the sail/collector size was dictated by the propulsion requirement from Earth, and hence power was not the limiting factor.

7.4 Issues in space construction using TFF system

While much has been learned about the development of a Space construction system using Tailored Force Fields, several technical issues remain requiring careful engineering. Some of these are summarized below.

Resonant cavity: A resonator with as high a Q-factor as possible is needed to keep the power levels of the source antenna reasonable. Ideally a perfect solid wall made of a good conductor, is needed. In practice it could be a wire mesh layer such that the hole size (defect) is 2 orders of magnitude smaller than the wavelength, as is the case in microwave oven doors. With 100m wavelength, the mesh size can be quite large.

Source (antenna): Estimates show that current-off-the-shelf solar cells are adequate to power the antenna assuming a Q of 10,000. Calculations by PSI Corp (Wanis 2005) show that the Q can be as high as 300,000 with modern resonator designs; however, the various sources of loss such as absorption by the particle cloud, and leakage lobes at the top and bottom are expected to reduce this value substantially. An appropriate electromagnetic waveguide coupler must be designed to input the forcing field power from the antenna into the resonant cavity is needed (i.e. source experiences a totally resistive load – no reactive component). Current state-of-the-art work done on direct conversion of solar energy using optical rectannae could replace the solar cell approach (Corkish 2002). This would negate the need for solar cells to power the antenna because the forcing frequency would come from a direct conversion of optical energy from the sun.

Wall formation: As mentioned earlier in chapter 1 once a wall starts to form in the resonator the field is altered. This effect needs to be modeled in the current simulation tool to understand the form of frequency adjustment needed to maintain a stable well for the particles. Alternatively, given that the results show that chains are more easily formed in electromagnetics, the effects of a finite number of chains of particles on the field must be estimated.

Heating effects: As outlined in chapter 5 it is plausible to polarize the construction particles (i.e. induce forces) at one frequency and heat them at another frequency, thereby uncoupling the two processes. The exact frequency for each effect is to be measured empirically.

Other forces on construction particles: Previous work (Komerath 2004) has shown that other forces in the region as at least 2 orders of magnitude lower than the electromagnetic force on the particles.

7.5 Other uses of TFF

a. Separation of resource extracted particles: Pulverized material extracted from in-situ resources can be sorted out based on their dielectric properties. Different material will polarize differently depending on its relative permittivity and thus scatter the electromagnetic field differently. This leads to varying forces on different materials and thus different stable locations within the resonant field are obtained.

b. Nuclear reactor shielding: In similar reasoning to demanding radiation shields for prolonged human presence in space nuclear shielding will be necessary with the increased demand for nuclear propulsion for space travel.

c. General space flexible fabrication tool: As described in chapter 1, the selection of the field type (acoustic of electromagnetic) is made in response to the demand for space-construction. Smaller scale fabrication of pressure vessels for example could be readily accomplished in an acoustic tailored force field. In the acoustics case, wall hardening could be done either through chemical means (epoxy curing) or through melting/sintering. Within the same TFF system several shapes are plausible by simply controlling the excitation frequency.

d. Hazardous Material Fabrication: Handling of dangerous materials such as beryllium and other ceramic components where machining generates hazardous

dust could be handled in a TFF system with no human presence, with the objects formed, and the residue removed.

e. Self replicating machines: Since the size scale of the TFF system dictates the frequency allowable, then for smaller and smaller manufacturing systems higher and higher frequencies are to be used. For example nano-components could be assembled in an ultrasonic TFF and the resulting shape could be used to make another TFF system of another geometry.

7.6 Decision making flowchart

A simple list of questions was formulated to determine which force field is better suited to perform the surface shaping and curing processes. The sample case study was used as a test case to run through the list. It was determined after answering all of the questions that it is best to use electromagnetic waves in the radio frequency region of the electromagnetic spectrum and for the construction site to be close to the region where the material will be extracted from. This was mainly based on the fact that the final product is to reside in space and the launch costs involved in sending large amounts of material into orbit is enormously high.

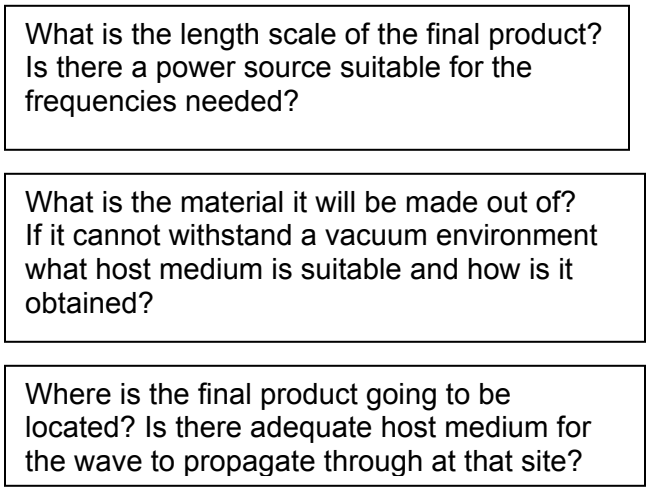

Are there any host medium requirements? If so, what are they?

What are some of the background force expected to be present in that host medium selected above?
e.g. solar wind, Brownian motion, gravity, etc.

Is the force field at least one order of magnitude higher than the background force field present? If no, can you change the: host medium, location of facility, or the wave type to achieve a suitable ratio?

What are the requirements for curing the surface?

CHAPTER 8

CONCLUSIONS AND RECOMMENDATIONS

8.1 Summary of findings and Discussion

The findings in this thesis are summarized into six general areas listed here and described in some detail below.

I. *Proof-of-concept experiments* achieved using acoustic force fields.

II. *Acoustic-electromagnetic analogy* studied to determine if electromagnetic waves can achieve similar results

III. *Optic tweezers* studied in order to determine origin of forces in optical fields

IV. *Wavelength extension to radio waves* by careful examination of the force expressions and their derivation in optic tweezers

V. *Space construction* studied as an example to identify major challenges to this technology

VI. *Unification of force fields* by generalizing the force expressions in both fields and studying the physics of each force generation mechanism

8.1.1 Proof of concept experiments

A series of experiments were devised to investigate the hypothesis of shaping structures using acoustic-generated forces. The experimental setup consisted of a compression-type speaker mounted to a rectangular acrylic cavity that served as the sound resonator. The speaker was driven by a function generator though a power amplifier. The frequency was adjusted using the function generator and a few normal modes of the

cavity were excited. A large number of small particles, on the order of hundreds, were placed in the cavity in no specific distribution and were found to respond to the pressure field generated by standing acoustic waves within the cavity. These experiments were successful in demonstrating surface formation using acoustic force fields.

The shape was tailored by controlling the resonant mode pattern at which the chamber was being excited Single-particle thick surfaces show great promise for flexible fabrication applications. The fact that the forces are exerted onto the particles without contact is of great use to researchers who are interested in high purity grade material-processing where even the walls of the container could contaminate the sample. While the use of acoustic forces to manipulate a single particle throughout a volume of interest has been demonstrated by others in the past, the principle of using sound waves to manipulate a large number of particles and shape them into a desired shape of interest is novel.

Since every mode shape is characterized by its own 3D pressure distribution, a MATLAB script was coded with the solution to the unforced Helmholtz equation; with rigid boundary conditions at the walls, to predict the pressure distribution of any mode. The code could handle multiple modes, which can be harmonics, where the user inputs any mode numbers and their relative magnitudes. This prediction capability was validated by a 2D pressure-sensitive-paint experiment that measured the global surface pressure on one of the cavity walls.

8.1.2 Acoustic-Electromagnetic Analogy

Based on the success of the acoustic shaping proof-of-concept experiments, potential applications were considered that could utilize such phenomenon. Realizing that the forces generated in acoustic fields are relatively small, when compared to other conventional contact-type molds and presses, led us to investigate whether it was

feasible to apply this concept to the problem of space fabrication, where gravity was cancelled by the orbital motion, or greatly reduced by distance from massive objects. The requirement of a fluid to host the sound waves poses a problem since this means additional weight has to be included in the equipment to be launched from earth. This becomes more of a problem as the structure to be built becomes large. As was noted in Chapter 2, nonlinear phenomena were observed when finite amplitude sound waves interact with air, which inhibits the wall formation. This is what motivated the study of the acoustic-electromagnetic analogy. An electromagnetic counterpart to acoustic shaping was sought out mainly because electromagnetic waves can propagate freely through the vacuum of space and thus do not require a fluid host. This translates to huge savings in the mass to be launched from earth.

8.1.3 Optical Tweezers

A literature review was performed on forces generated from electromagnetic waves. Optic tweezers were found as the optical counterpart to our work in acoustics albeit on a much smaller scale (about 10^3 to 10^6 times smaller). The expression for the force on a small dielectric particle in an optical field which had a gradient in its energy density was found analogous to the force on a small rigid particle in a sound field that had gradients in its energy density. Thus, this study revealed that the forces from light are strongly analogous to the forces induced by sound. This led to the investigation of whether it was physically possible to extend the theory from optical wavelengths to radio wavelengths while still using the same expression to express the force.

8.1.4 Wavelength extension from optic to radio waves

A close study of the origin of optical forces revealed that it in most optic tweezers, it was the electrical component of the light waves that was inducing the forces. It was clear that, for optically small particles, the electric field was polarizing the particle and thus inducing a dipole moment within its volume. The field radiated by the polarized particle is responsible for generating scattering forces which arise as a result of the momentum exchange that occurs when the radiated field from the particle alters the energy density of the, otherwise unperturbed, incident wave. The gradient forces are generated as a result of the Lorentz force acting on the induced dipole. Going through these force expressions and their derivations revealed that there was nothing specific about the optical bandwidth within the electromagnetic spectrum. The forces come about from the fact that energy is transferred from the wave and to the particle. As long as the particle dimension is smaller than the wavelength such that it is in the Rayleigh scattering regime then the force expressions hold for any wavelength in the spectrum. This key finding enabled us to extend the theory of optic tweezers to much larger wavelengths.

8.1.5 Space construction application case study

As the application of space construction was the main driving motivation behind this research, a sample space structure problem was formulated which was outlined in Chapter 7. This enabled us to identify as much of the challenges that would need to be addressed before such a concept could be advanced to a technological level. The decision flowchart provided a useful mechanism by which we identified the key issues that are pertinent to this case study. The most challenging component was found to be the power source requirement. However, this estimate was done with an assumed Q-factor of 10,000 for the resonator quality. This value can be greatly increased as advances continue to be made in superconductors. In fact, a superconductor Q-factor of

10^{11} at radio frequencies has already been demonstrated (Palmieri 2004). The main requirements of the force field for achieving a solid surface are found to be satisfied from the current work. The primary forces are responsible for manipulating the individual particles into the shape of interest. The secondary forces between the particles are attractive in nature such that single particle thick walls are formed. Both primary and secondary forces have been addressed. For typical materials, heating of the surface so as to hold the shape in place once the field is switched off was found to not interfere with the shaping field.

8.1.6 Unification of both force fields

The primary goal of this research was to generalize acoustic and electromagnetic force fields such that a unified description of the force fields is available. This enabled us to perform simple and cheap experiments using acoustic fields to understand behavior that would occur in electromagnetic fields. The idea that acoustics and electromagnetics are analogous was introduced as far back as Lord Rayleigh in 1878. However, a generalized description of forces generated by these fields onto a multitude of particles had never been done to the best knowledge of the author. In Chapter 6 this observation was shown and a generalization of the force expressions was made. Each term in the generalized expression is expressed differently for each field, i.e. in parameters specific to that field, but describes the same physical property, such as energy density, wave speed, and impedance ratio of particle to host medium. This was done for both the primary forces (scattering and gradient forces) and the secondary forces (dipole-dipole interaction forces).

8.2 Future Work

8.2.1 Electromagnetic Secondary Forces Experiment

Based on the data obtained from NASA JPL which confirms our predictions for microwave forces induced on a small dielectric sphere placed in a resonator, we proposed to perform an experiment to test out our hypothesis of the nature of secondary forces in electromagnetic force fields. The NASA Langley High Intensity Radiation Lab (HIRL) facility appears to be a suitable venue for such an experiment. The HIRL is an environment where a diffuse electromagnetic field can be setup. The entire room is a metallic cavity and is usually used to test electromagnetic interference (EMI) on aircraft components. In a typical experiment we would excite a low order mode of the room and place a wooden grid that suspends two dielectric spheres and measure the change in displacement between them.

8.2.2 Real time simulation of particles moving within field

One necessary step is to produce a prediction code that simulates the evolution of the particles in a force field in time. It will calculate the forces at each time step and predict the new location for the next time step. It will march in time until equilibrium is reached, which in this case is defined when the net forces are zero on every particle.

APPENDIX A

FIELD AROUND A DIELECTRIC SPHERE IN AN ALTERNATING ELECTRIC FIELD

Since a dielectric material when placed in an electric field polarizes then we can regard the response as a superposition of a somewhat more complicated collection of dipoles. Considering a neutral dielectric sphere of radius R placed in a uniform field E_o we solve Laplace's equation in spherical coordinates. Poisson's equation was reduced to Laplace since we are solving for the field in charge-free regions.

$$\nabla^2\phi = \frac{\partial^2\phi}{\partial r^2} + \frac{z}{r}\frac{\partial\phi}{\partial r} + \frac{1}{r^2}\frac{\partial^2\phi}{\partial\theta^2} + \frac{1}{r^2}\frac{\cos\theta}{\sin\theta}\frac{\partial\phi}{\partial\theta} = 0$$

Letting ϕ_i and ϕ_e be the potential inside and outside the sphere respectively, we have the following form of the solution

$$\phi_i = \left(\frac{A}{r^2} + Br\right)\cos\theta \text{ and } \phi_e = \left(\frac{C}{r^2} + Dr\right)\cos\theta$$

The field intensity must remain finite at the sphere surface thus fi must equal fe at the surface. For no surface charge to exist the normal component of the dielectric displacement must be continuous. Therefore, at the surface ($r = R$) the following holds

$$\phi_i = \phi_e$$

$$\varepsilon_i' \frac{\partial \phi_i}{\partial r} = \varepsilon_e' \frac{\partial \phi_e}{\partial r} \qquad \text{(a)}$$

We also require that at relatively large distances from the sphere the external field remains undisturbed, i.e. at r = ∞

$$\phi_e = -E_o r \cos\theta = -E_o z \cos\theta \qquad \text{(b)}$$

and lastly, we need to restrict the potential to remain finite at the sphere center, at *r* = 0

$$\phi_i = \textit{finite} \qquad \text{(c)}$$

From the boundary conditions (a)-(c) we obtain the following coefficients for the potential solutions:

$$A = 0$$

$$B = -\frac{3\varepsilon_e'}{\varepsilon_i' + 2\varepsilon_e'} E_o$$

$$C = \frac{\varepsilon_i' - \varepsilon_e'}{\varepsilon_i' + 2\varepsilon_e'} R^3 E_o$$

$$D = -E_o$$

Therefore, the potential inside and outside the sphere becomes

$$\phi_i = -\frac{3\varepsilon'_e}{\varepsilon'_i + 2\varepsilon'_e} E_o z$$

$$\phi_e = \left(\frac{\varepsilon'_i - \varepsilon'_e}{\varepsilon'_i + 2\varepsilon'_e} \frac{R^3}{r^3} - 1 \right) E_o z$$

Solving for the field strength inside the sphere

$$E_i = -\nabla \phi_i = \frac{3\varepsilon'_e}{\varepsilon'_i + 2\varepsilon'_e} E_o$$

This shows that the field is constant inside the sphere. The E-field lines are parallel to the original external field E_o. For $\varepsilon'_i > \varepsilon'_e$ the field inside is smaller than E_o (and for $\varepsilon'_i < \varepsilon'_e$ larger than E_o) by

$$E_o - E_i = \frac{\varepsilon'_i - \varepsilon'_e}{\varepsilon'_i + 2\varepsilon'_e} E_o$$

The polarization vector previously defined now becomes

$$P = \left(\varepsilon'_i - \varepsilon'_e\right) E_i = \frac{\varepsilon'_i - \varepsilon'_e}{\varepsilon'_i + 2\varepsilon'_e} 3\varepsilon'_e E_o$$

inside the sphere, also known as the *Clausius-Mosotti* equation. This is what links the microscopic behavior (polarizability) to the macroscopic response (permittivity). By its definition this is the dipole moment per unit volume, therefore the sphere appears to the outside world having the following dipole moment

$$\mu = (vol) \times P = \frac{4\pi}{3} R^3 P = 4\pi R^3 \varepsilon_e' \frac{\varepsilon_i' - \varepsilon_e'}{\varepsilon_i' + 2\varepsilon_e'} E_o$$

located at the center of the sphere. Figure 69 shows the superposition of E_o and the dipole field (of the polarized sphere).

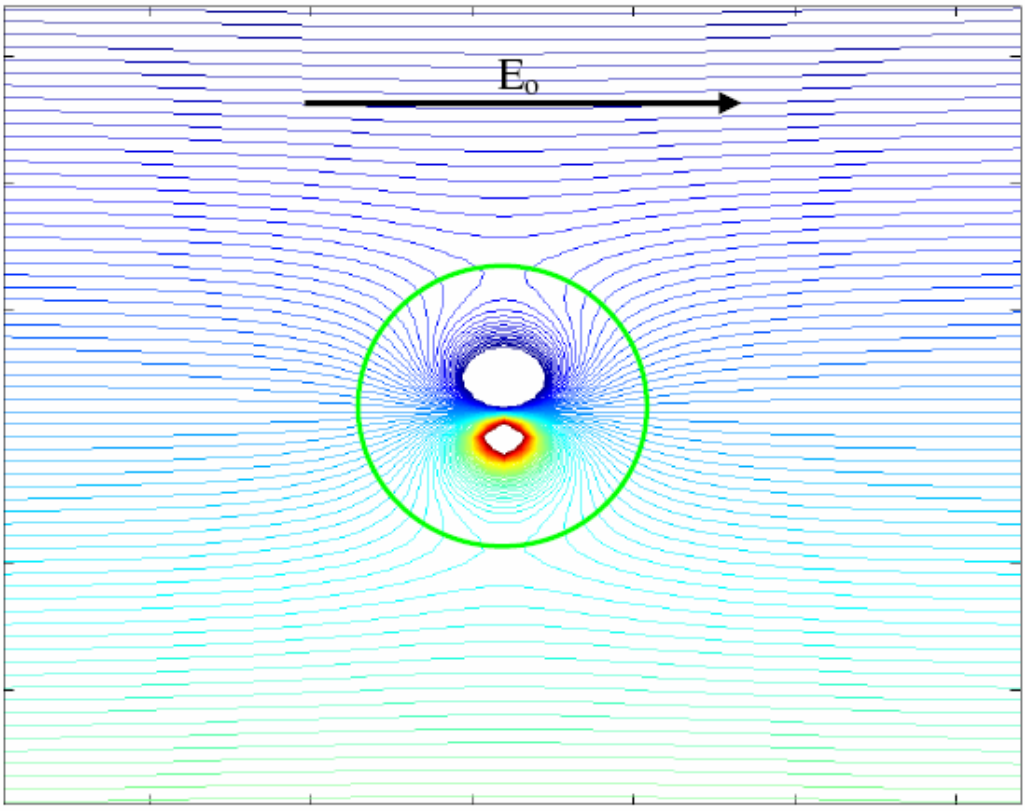

Figure 69 Total field due to dielectric sphere in a uniform electric field. Green circle added to show approximate sphere surface boundary.

For non-uniform electric fields a translational force will be present just as in the case of a single dipole explained earlier. This force will act on the sphere in a direction pushing it to regions of higher field intensity for $\varepsilon'_i > \varepsilon'_e$ and to regions of lowest intensity for $\varepsilon'_i < \varepsilon'_e$.

$$F = \mu \cdot E_o = 2\pi R^3 \varepsilon'_e \frac{\varepsilon'_i - \varepsilon'_e}{\varepsilon'_i + 2\varepsilon'_e} \nabla\left(E_o^2\right)$$

Note that in deriving this we have considered an electrostatic field (i.e. $\nabla \times E_o = 0$). In the case of electrodynamics, i.e. an alternating electric field, the same expressions will come out as long as the particle is much smaller than the wavelength. This ensures that the wave is much longer than the spacing between the atoms and molecules that make up the sphere. A rule of thumb is particle diameter about ten times smaller than the wavelength.

APPENDIX B

EXPERIMENTAL VIDEO CLIPS

The following appendix contains video clips showing experiments described in the dissertation. The table below lists each file with a description of each clip.

Table 7 Description of video clips and corresponding file names

clip	Description of clips	File name (*.mpg)
1	**Figure 70** Low gravity flight test using mode (1,1,0) to shape many Styrofoam pellets into curved surfaces	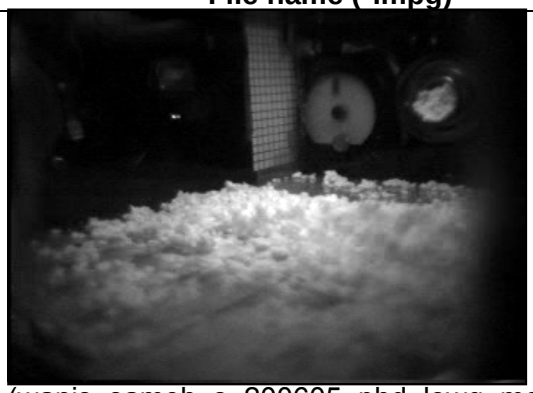 (wanis_sameh_s_200605_phd_lowg_mode110_1.mpg, 3.28M)
2	**Figure 71** A repeat of clip 1 from another camera view angle	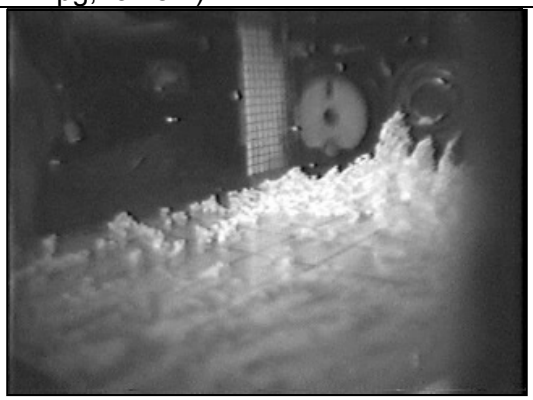 (wanis_sameh_s_200605_phd_lowg_mode110_2.mpg, 1.18M)

3	**Figure 72** Secondary attraction forces evident between Styrofoam pellets levitated in mode (0,1,0)	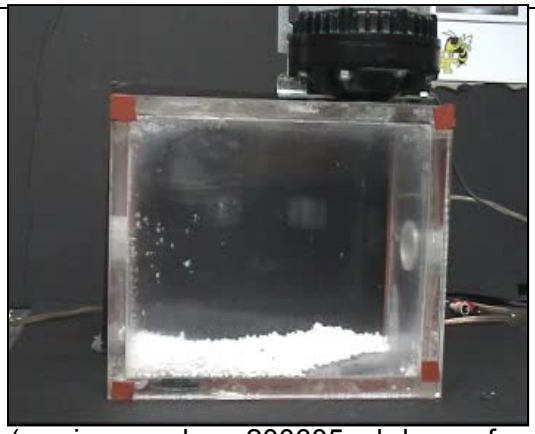 (wanis_sameh_s_200605_phd_sec_frces_styro.mpg, 5M)
4	**Figure 73** Secondary attraction forces and wall attraction evident between Styrofoam pellets levitated in mode (0,1,0)	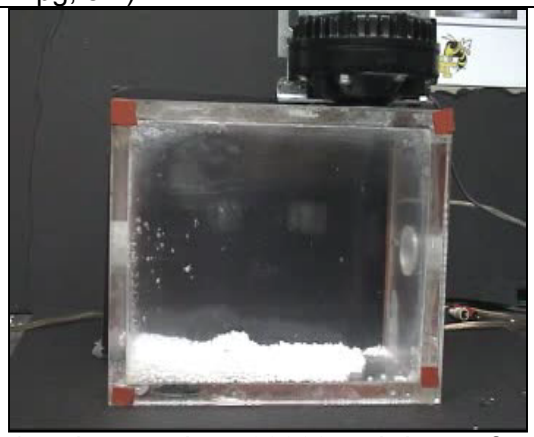 (wanis_sameh_s_200605_phd_sec_frces_styro_wall.mpg, 2.3M)
5	**Figure 74** Secondary attraction forces between two suspended particles	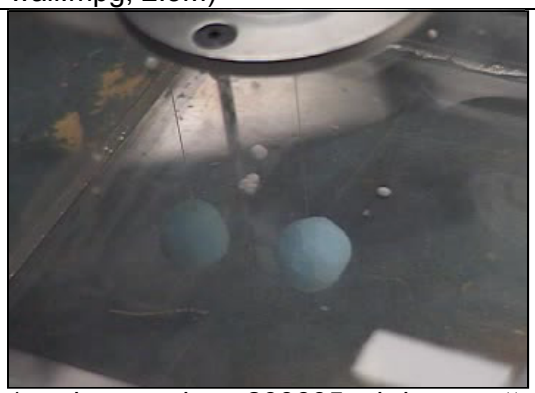 (wanis_sameh_s_200605_phd_sec_att_frces_2_prtcls.mpg, 605k)

6	**Figure 75** Secondary repulsion forces between two suspended particles	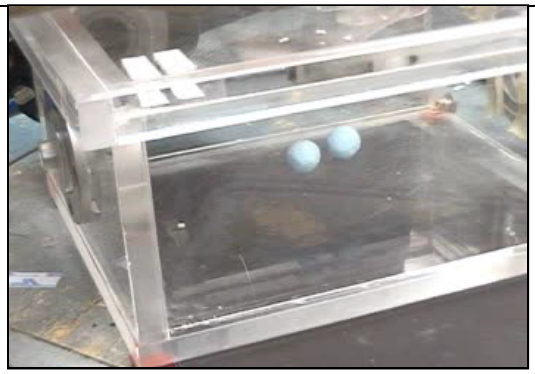 (wanis_sameh_s_200605_phd_sec_rpl_frces_2_prtcls_1.mpg, 1.5M)
7	**Figure 76** A repeat of clip 6 with a zoomed in camera view	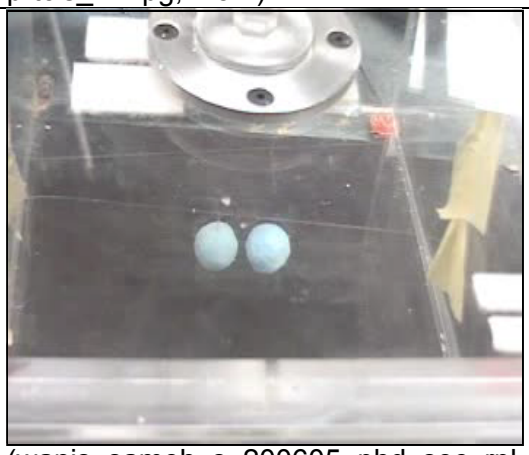 (wanis_sameh_s_200605_phd_sec_rpl_frces_2_prtcls_2.mpg, 2.63M)
8	**Figure 77** Primary and secondary forces acting on multiple particles in mode (0,1,0)	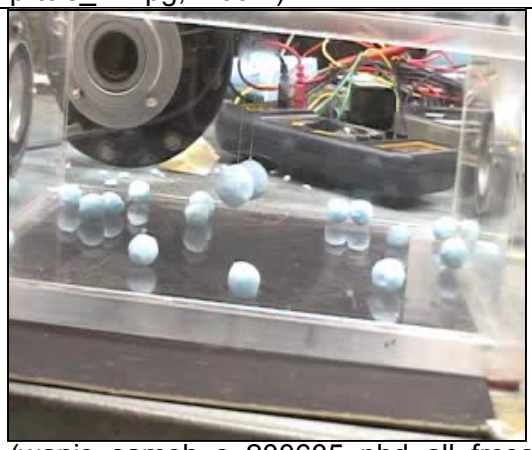 (wanis_sameh_s_200605_phd_all_frces_multple_prtcls.mpg, 2.02M)

REFERENCES

Abramowitz, M., and Stegun, I. (1965). Handbook of Mathematical Functions. New York, Dover.

Altberg, W. (1903). Ann. Phys. (Leipzig) 2: 405.

Ashkin, A. (1986). "Observation of a single-beam gradient force optical trap for dielectric particles." Optics Letters 11(5).

Ashkin, A. (2000). "History of Optical Trapping and Manipulation of Small-Neutral Particles, Atoms, and Molecules." IEE Journal of Selected Topics in Quantum Electronics 6(6): 841-856.

Barlow, J., Rae, Jr., and Pope, A. (1999). Low-Speed Wind Tunnel Testing. New York, John Wiley & Sons.

Barmatz, M. (1982). Overview of Containerless Processing Technologies, Elsevier Science Publishing Co.

Barmatz, M. (1983). System for controlled acoustic rotation of objects. USPO. USA.

Barmatz, M. (1984). Acoustic agglomeration methods and apparatus. U. P. Office. USA.

Barmatz, M., Granett, Lee, M. (1985). Vibrating chamber levitation systems. USPO. USA.

Barmatz, M., and Allen, J. (1988). Single mode levitation and translation. USPO. USA.

Barmatz, M., Aveni, G., Putterman, S., Rudnick, J. (1990). Acoustic positioning and orientation prediction. USPO. USA.

Blackstock, D. (2000). Fundamentals of physical acoustics. New York, John Wiley & Sons, Inc.

Burns, M., Fournier, J., Golovchenko, J. (1989). "Optical Binding." Phys. Rev. Let 63(12).

Chu, S. (1986). Phys. Rev. Lett. 57: 314.

COMSOL (2006). COMSOL Multiphysics (FEMLAB). Electromagnetics Module.

Crum, L. (1971). "Acoustic force on a liquid droplet in an acoustic stationary wave." J. Acoust. Soc. Am. 50(1): 157-163.

Danley, T., Rey, C. (1989). Horn loaded transducer for acoustic levitation. U. P. Office. USA.

Debye, P. (1909). Ann. Phys. 30(4): 57.

Doinikov, A. (1994). "Acoustic radiation pressure on a compressible sphere in a viscous fluid." J. Fluid Mech. 267: 1.

Embelton, T. (1962). "Mutual interaction between two spheres in a place sound field." J. Ac. Soc. Am. 34(11).

Galajda, P., and Ormos, P. (2001). "Complex micromachines produced and driven by light." Appl. Phys. Lett. 78: 249-251.

Goforth, R., and Ohkawa, T. (1995). Acoustic barrier separator. USPO. USA.

Gorkov, L. P. (1962). "On the forces acting on a small particle in an acoustic field in an ideal fluid." Sov. Phys. Dokl. 6: 773-775.

Gregory, J., Sullivan, J, Wanis, S., and Komerath, N. (2006). "Pressure-sensitive paint as a distributed optical microphone array." J. Acoust. Soc. Am. 119(1): 251-261.

Grier, D. (2003). "A revolution in optical manipulation." Nature 424: 810-816.

Griffiths, D. (1989). Introduction to electrodynamics. New Jersey, Prentice-Hall, Inc.

Groschl, M. (1998). "Ultrasonic separation of suspended particles - Part I: Fundamentals." Acustica 84: 432-447.

Guign, J., Barmatz, M., Jackson, H., Koptenko, S. (1996). Acoustic beam levitation. USPO. USA.

Haake, A. a. D., J. (2005). "Contactless micromanipulation of small particles by an ultrasound field excited by a vibrating body." J. Acoust. Soc. Am. 117(5): 2752-2760.

Hallock, A., Redmond, P., and Brus, L. (2005). "Optical forces between metallic particles." PNAS 102(5): 1280-1284.

Hanock, A., Insana, M., and Allen, J. (2003). "Microparticle column geometry in acoustic stationary fields." J. Acoust. Soc. Am. 113(1): 652-659.

Harada, Y. a. A., T. (1996). "Radiation forces on a dielectric sphere in the Rayleigh scattering regime." Optics Communications 124: 529-541.

Herrick, J. (1958). Pearl-chain formation. Proceedings of the second tri-service conference on biological effects of microwave energy, Virginia.

Hoffmann, T. a. K., G. (1996). "Visualization of acoustic particle interaction and agglomeration: Theory and experiments." J. Acoust. Soc. Am. 99(4): 2130-2141.

Hunter, R. (2001). Foundations of colloid science. New York, Oxford University Press Inc.

Hussey, M. (1975). Diagnostic Ultrasound. London, Blackie & Son Limited.

Ignatiev, A., Freundlich, A., Duke, M., Rosenberg, S. (2000). New Architecture for Space Solar Power Systems: Fabrication of Silicon Solar Cells Using In-Situ Resources, NIAC 2nd Annual Meeting.

Iida, T. a. I., H. (2003). "Theoretical study of the optical manipulation of semiconductor nanoparticles." Phys. Rev. Lett. 90(7): 057403.

Karpov, S., Slabko, V., and Chiganova, G. (2002). "Physical principles of the photostimulated aggregation of metal sols." Colloid Journal 64(4): 425-441.

Kerker, M. (1969). The scattering of light and other electromagnetic radiation. New York, Academic.

King, L. V. (1934). "On the acoustic radiation pressure on spheres." Proc. Roy. Soc. A147: 861.

Komerath, N., Matos, C., Coker, A., Wanis, S., Hausaman, J., Ames, R., Tan, X. (1999). Acoustic Shaping: Enabling Technology for a Space Based Economy. First Space Resources Roundtable, Colorado School of Mines.

Komerath, N. (2003). NASA Institute for Advanced Concepts Phase 1 report. Atlanta, GA.

Komerath, N. (2003). Tailored force fields for space based construction. Atlanta, NASA Institute of Advanced Concepts.

Komerath, N., Wanis, S. (2004). Radio Waves for Space-Based Construction. Space Technology and Applications International Forum, NM, AIP Conference Proceedings.

Komerath, N. et al. (2001). Electromagnetic construction of a 1km radius radiation shield in orbit. Space Manufacturing, Space Studies Institute.

Kundt, A., Lehmann, O. (1874). "Longitudinal vibrations and acoustic figures in cylindrical columns of liquids." Annalen der Physik und Chemie (Poggendorff's Annalen) 53: 1.

Lee, C. (1983). Acoustic suspension system. USPO. USA.

Lee, C., and Wang, T. (1993). J. Acoust. Soc. Am. 93: 1637.

Leung, E., Man, K. (1994). Plasma heating for containerless and microgravity materials processing. USPO. USA.

Malik, T. (2005). Lunar Shields: Radiation Protection for Moon-Based Astronauts. SPACE.com.

Meyer (1972). Physical and applied acoustics. New York, Academic.

Mie, G. (1908). Ann. Phys. (Leipzig) 25: 377.

Miller, D. (1976). An instrument for microscopical observation of the biophysical effects of ultrasound, University of Vermont. Ph.D.

Miller, D., Sedwick, R., Kong, E., Schweighart, S. (2002). Electromagnetic Formation Flight for Sparse Aperature Telescopes. 2002 IEEE Aerospace Conference, Big Sky, MT.

Misawa, H., Sasaki, K., Koshioka, M., Kitamura, N., and Masuhara, H. (1993). "Laser manipulation and assembling of polymer latex particles in solution." Macromolecules 26: 282-286.

Mo, L. a. C., R. (1993). Theoretical models of ultrasonic scattering in blood. Boca Raton, CRC Press, Inc.

Mulser, P. (1985). "Radiation pressure on microscopic bodies." J. Opt. Soc. Am. B 2: 1814-1829.

NASA. (2005). "Building the Colony and Making it Prosper." Space Settlements, Chapter 6 Accessed September 21, 2005, from http://lifesci3.arc.nasa.gov/SpaceSettlement/75SummerStudy/Chapt6.html#EST.

NASA. (2006). "Shuttle Small Payloads Project." Accessed April 7 2006, from http://sspp.gsfc.nasa.gov/about/index.html.

NASA. (2006). "Space Experiment Module." Accessed April 7 2006, from http://sspp.gsfc.nasa.gov/sem/about.html.

NASA/ASEE (1975). Space colonization. N. A. R. Center. Mountain View, CA, NASA Ames Research Center.

NOAA. (2006). "A Primer on Space Weather." Accessed April 4, 2006, from http://www.sec.noaa.gov/primer/primer.html.

Nyborg, W. (1967). "Radiation Pressure on a Small Rigid Sphere." J. Acoust. Soc. Am. 42(5): 947-952.

Nyborg, W. (1978). Physical mechanisms for biological effects of ultrasound. Public Health Service, Food and Drug Administration report. E. Dept. of Health, and Welfare.

Nyborg, W. a. G., A. (1974). Microsonation of cells under near-threshold conditions. Second World Congress on Ultrasonics in Medicine, Rotterdam, Amsterdam.

Ohkawa, T. (1994). Plasma processing apparatus for controlling plasma constituents using neutral and plasma sound waves. USPO. USA.

O'Neill, G. (1977). Space-Based Manufacturing from Nonterrestrial Materials, AIAA.

Oran, W., Berge, L., Reiss, and Johnson, J. (1980). Method and apparatus for shaping and enhancing acoustical levitation forces. USPO. USA.

Park, C. a. R., R. (1998). Mater. Sci. Eng. A 257: 295-311.

Putterman, S., Rudnick, J., Barmatz, M. (1989). "Acoustic Levitation and the Boltzmann-Ehrenfest principle." J. Acoust. Soc. Am 85(1): 68-71.

Rayleigh, L. (1871). "On the light from the sky, its polarization and colour." Phil. Mag. J. Sci. CCLXXI: 107.

Rayleigh, L. (1905). "On the momentum and pressure of of gaseous vibrations, and on the connexion with the virial theorem." Phil. Mag. 10: 364-374.

Rey, C. (1981). Acoustic levitation and methods for manipulating levitated objects. USPO. USA.

Richter, G. (1940). Z. Physik 115: 97.

Rohrbach, A., and Stelzer, E. (2001). "Optical trapping of dielectric particles in arbitrary fields." J. Opt. Soc. Am. A 18(4): 839-852.

Rozenberg (1971). High-Intensity Ultrasonic Fields. Moscow, USSR, Acoustics Institute Academy of Sciences of the USSR.

Rudnick, I. (1951). J. Acoust. Soc. Am. 23: 633.

Satoh, N., Hasegawa, H., Tsujii, K., and Kimura, K. (1994). "Photoinduced coagulation of Au nanocolloids." J. Phys. Chem. 98: 2143-2147.

Smith, G. (1997). An introduction to to classical electromagnetic radiation. New York, The Press Syndicte of the University of Cambridge.

Spengler, J., Jekel, M., Christensen, K., Adrian, R., Hawkes, J., and Coakley, W. (2001). "Observation of yeast cell movement and aggregation in a small-scale MHz-ultrasonic standing wave field." Bioseparation 9: 329-341.

Svoboda, K., Block, S. (1994). "Biological applications of optical forces." Rev. Biophys. Biomol. Struct 23: 247-285.

ter Haar, G. a. W., S. (1978). "Blood cell banding in ultrasonic standing wave fields: a physical analysis." Ultrasound in Med. & Biol. 4: 111-123.

Terray, A., Oakey, J., and Marr, D. (2002). "Fabrication of linear colloidal structures for microfluidic applications." Appl. Phys. Lett. 81: 1555-1557.

Torr (1984). "The Acoustic Radiation Force." American Journal of Physics 52(5): 402-408.

Vanmali, R., Li, B., Tomlinson, B., Wanis, S., Komerath, N. (2005). Conceptual Design of a Multipurpose Robotic Craft for Space Based Construction. AIAA Space 2005, AIAA.

Visscher, K., Brakenhoff, G. (1992). "Theoretical study of optically induced forces on spherical particles in a single beam trap I: Rayleigh scatterers." Optik 89: 174-180.

Wang, T., and Lee, C. (1998). Radiation Pressure and Acoustic Levitation, Academic Press.

Wanis, S., Akovenko, J., Cofer, T., Ames, R., Komerath, N. (1998). Acoustic Shaping in Microgravity. AIAA Aerospace Sciences Meeting & Exhibit, Reno, NV, AIAA.

Wanis, S., Sercovich, A., Komerath, N. (1999). Acoustic Shaping in Microgravity: Higher Order Surface Shapes. AIAA Aerospace Sciences Meeting & Exhibit, Reno, NV, AIAA.

Wanis, S., Matos, C., Komerath, N. (2000). Acoustic Shaping: Application to Space Based Construction. AIAA Aerospace Sciences Meeting & Exhibit, Reno, NV, AIAA.

Wanis, S., Komerath, N. (2005). Advances in Force Field Tailoring for Construction in Space. International Astronautical Congress, Fukuoka, Japan, International Astronautical Federation.

Weiser, M. a. A., R. (1984). "Interparticle forces on red cells in a standing wave field." Acustica 56: 114-119.

Whymark, R. (1975). "Acoustic Field Positioning for Containerless Processing." Ultrasonics: 251-262.

Williams, G. a. T., D. (1998). "Phenomenological and molecular theories of dielectric and electrical relaxation of materials." Application Note Dielectrics 3: 1-28.

Woodside, S., Bowen, B., and Piret, J. (1997). "Measurement of Ultrasonic Forces for Particle-Liqiud Separations." AICHE Journal 43(7): 1727-1736.

Wu, J., and Du, G. (1990). J. Acoust. Soc. Am. 87: 997.

Yosioka, K., and Kawasima, Y. (1955). Acustica 5: 167.

Zemanek, P., Jonas, A., Sramek, L., Liska, M. (1998). Optics Communications 151(Elsevier Science): 273-285.

Zhan, Q. (2003). "Radiation forces on a dielectric sphere produced by highly focused cylindrical vector beams." J. Opt. A: Pure Appl. Opt. 5: 229-232.